Master Thesis CODEN: LUTMDN/(TMMV-5298)/1-134/2018

LUND UNIVERSITY
Lund Institute of Technology

Performance and Wear Behavior of Ultra-Hard Cutting Tools during Machining of Titanium Alloy

Rebecka Lindvall

2018

DIVISION OF PRODUCTION AND MATERIALS ENGINEERING
DEPARTMENT OF MECHANICAL ENGINEERING
LUND UNIVERSITY, FACULTY OF ENGINEERING

Author:	Rebecka Lindvall
Examiner:	Jan-Eric Ståhl, Professor Division of Production and Materials Engineering, Department of Mechanical Engineering, Faculty of Engineering, Lund University
Supervisor:	Volodymyr Bushlya, Ass. Professor Division of Production and Materials Engineering, Department of Mechanical Engineering, Faculty of Engineering, Lund University
Assistant supervisor:	Henrik Persson, M. Sc. Division of Production and Materials Engineering, Department of Mechanical Engineering, Faculty of Engineering, Lund University
Company supervisor:	Dr. Rachid M'Saoubi Seco Tools AB, Sweden

Keywords:
Metal cutting
Machining performance
Titanium machining
Ti6Al4V
(α + β)-alloy
Tool wear
Wear mechanisms
Cost efficiency
Colding analysis
Cemented carbide
PCD
pcBN
TEM

Abstract

Since the 1950's, a wide range of titanium alloys has been developed. Attractive titanium properties are the high strength-to-weight ratio, resistance towards corrosion, low thermal conductivity and low thermal expansion. Properties that make titanium alloys difficult-to-machine materials are those of low thermal conductivity, chemical reactiveness and the high strength, requiring low cutting data, resulting in low material removal rate and therefore high manufacturing costs. This implicates the importance of solutions for high speed machining and knowledge about wear mechanisms and machining performance.

The most commonly used cutting tool for machining in titanium alloys are those of cemented carbide with sharp edges. The study includes a range of cutting tool materials: cemented carbides (coated and uncoated), PCD and cBN, to compare and analyze with regard to wear mechanisms and chemical reactions in the cutting tool.

This study investigates the machining performance and wear mechanisms during high speed machining in ($\alpha + \beta$)-alloy Ti6Al4V, the most commonly used titanium alloy. The cutting data are for finishing operations, where tolerances and surface roughness are essential result parameters. The machining is performed with longitudinal continuous turning under application of high-pressure coolant.

Cutting tools of interest (PCD and pcBN) are subjected to in-depth microscopic analysis with FIB-SEM and TEM. Selected cutting tools are subjected to cost-efficiency to present the results regarding machining performance and cutting tool cost in context.

The pointed cutting tools shows that UCC 2 has a better cost efficiency compared to CCC 1. For the higher values of the cutting speed for UCC 2 and PCD 8, PCD 8 is superior regarding cost efficiency compared to UCC 2. PCD 8 has got a better cost efficiency compared to cBN 2.

The chemical analysis with TEM on PCD 8 and cBN 2 is somewhat difficult to read. There are small boundary areas between the cutting tool material and the adhered workpiece material. Probably, there are formations of titanium carbides or diffusion of carbon into the workpiece material in the cutting tool PCD 8. Between the diamond grains, there seems to have been titanium working its way down into the cutting tool material. Regarding cBN 2, the boundary area between the cutting tool material and the adhered workpiece material are somewhat sharp. There might be formations of titanium nitrides in this boundary area or possibly diffusion of boron or nitride into the workpiece material. Leftover elements from the cutting tool manufacturing process are noted.

Preface

The master thesis is funded by the European Union's Horizon 2020 Research and Innovation Program under the Flintstone2020 project (grant agreement No 689279), anticipating to accumulate knowledge on the machining performance, wear mechanisms and cost efficiency during machining of titanium alloys. The project was performed in collaboration with Seco Tools AB and was executed at the Division of Production and Materials Engineering, Department of Mechanical Engineering, Faculty of Engineering at Lund University.

The master thesis was accomplished during the time period of 8th January to 15th June 2018, the final course (30 credits) before graduating as a mechanical engineer. The performance of the master thesis was of both practical and theoretical character; machining tests with different cutting tools, wear mechanisms analyzed with optical stereo microscopes, FIB-SEM and TEM, as well as theoretical studies is performed.

I would like to thank the examiner, Jan-Eric Ståhl, for your door always being open. Supervisor Volodymyr Bushlya, thank you for your guidance during the process and for you sharing your knowledge in the metal cutting area, I have learned a lot from you. Assistant supervisor, Henrik Persson – thank you for always helping me out in both practical and theoretical issues and for your advices in both the machining and writing process – it is all about making the cut.

Rachid M'Saoubi, it has been great to have you as a supervisor – thank you for your guidance and ideas in how to manage this project. Filip Lenrick, your efforts and guidance for the in-depth microscopy studies have been excellent – now I have a FIB-SEM license! Thank you for your patience and taking time to thoroughly explain the mechanisms in the FIB-SEM and TEM.

I would like to thank the personnel at the division of Production and Materials Engineering, for help and support during the master thesis performance.

Finally, I would like to thank my family and friends for listening, supporting and encouraging.

Lund, June 2018

Rebecka Lindvall

Table of Contents

1 Introduction 1
1.1 Problem description 2
1.2 Purpose 2
1.3 Scope 2
1.4 Limitations 2
2 Theory 3
2.1 Turning 3
2.1.1 Cutting forces 4
2.1.2 Cutting data 5
2.1.3 Engagement distance 5
2.1.4 Material removal rate 6
2.1.5 Surface roughness 6
2.1.6 Cutting fluid 6
2.1.7 High speed machining 7
2.2 Cutting tools 8
2.2.1 Geometry 8
2.2.2 Compositions 8
2.2.3 Coatings 11
2.3 Tool wear 12
2.3.1 Wear types 12
2.3.2 Plastic deformation 16
2.3.3 Breaking or cracking 17
2.3.4 Material transformations 17
2.4 Tool life criterion and tool wear criterion 18
2.5 Workpiece material machinability 20
2.5.1 Strain hardening 20
2.5.2 Adhesiveness 20
2.5.3 Thermal conductivity 21

2.5.4 Ductility 21
2.5.5 Hardness 21
2.5.6 Multiphased materials 22
2.5.7 Chemical reactiveness 22
2.5.8 Porosity 22
2.5.9 Manufacturing process effects 22
2.6 Titanium alloys 23
2.6.1 α- and near-α-alloys 24
2.6.2 (α + β)-alloys 24
2.6.3 β-alloys 24
2.7 In-depth microscopic analysis 26
2.7.1 FIB-SEM 26
2.7.2 TEM 27
2.8 Cost efficiency 29
3 Experimental method 31
3.1 Workpiece material 31
3.2 Cutting tools 32
3.3 Turning 33
3.3.1 High-pressure coolant and tool holders 34
3.3.2 Force acquisition 36
3.3.3 Rig 36
3.3.4 Cutting data 37
3.4 Surface roughness measurement 38
3.5 Microscopy 38
3.5.1 Flank wear measurement 38
3.5.2 Rake wear measurement 39
3.5.3 FIB-SEM 39
3.5.4 TEM 41
3.6 Cost efficiency 42
4 Results 45

4.1 Tool life, surface roughness and material removal rate 45
4.1.1 Coolant pressure test 47
4.2 Tool wear 47
4.2.1 UCC 2 48
4.2.2 CCC 1 54
4.2.3 PCD 8 57
4.2.4 cBN 2 60
4.2.5 cBN 3 63
4.3 SEM 65
4.3.1 UCC 2 65
4.3.2 PCD 8 66
4.3.3 cBN 2 67
4.4 TEM 68
4.4.1 PCD 8 68
4.4.2 cBN 2 74
4.5 Cutting forces 80
4.6 Cost efficiency 80
4.6.1 UCC 2 81
4.6.2 CCC 1 81
4.6.3 PCD 8 82
5 Discussion 83
5.1 UCC 2 83
5.2 CCC 1 84
5.3 PCD 8 85
5.4 cBN 2 86
5.5 cBN 3 87
5.6 Cost efficiency 88
6 Conclusions 89
7 Further work 91
8 References 93

9 Appendix A – Tool life, surface roughness and material removal rate 95
9.1 UCC 2 95
9.2 CCC 1 97
9.3 PCD 8 99
9.4 cBN 2 101
9.5 cBN 3 103
10 Appendix B – Flank wear curves 105
10.1 UCC 2 105
10.2 CCC 1 110
10.3 PCD 8 113
10.4 cBN 2 116
10.5 cBN 3 119
11 Appendix C – Cutting forces 121
11.1 UCC 2 122
11.2 CCC 1 126
11.3 PCD 8 128
11.4 cBN 2 130
11.5 cBN 3 132

Nomenclature and Symbols

A list of symbols, the respective meaning and unit is presented below.

Symbol	Meaning	Unit
a_p	Cutting depth	mm
b_1	Chip width	mm
D	Workpiece diameter (cut surface)	mm
e_T	Engagement distance	m
f	Feed rate	mm/rev
F_c	Main cutting force	N
F_f	Feed force	N
F_p	Passive force	N
MRR	Material removal rate	cm^3/min
n	Rotation/spindle speed	rev/min
R_a	Surface roughness	µm
r_β	Edge radius	µm
r_ε	Nose radius	µm
T	Tool life	min
VB	Flank wear	mm
v_c	Cutting speed	m/min
K	Colding constant	-
H	Colding constant	-
M	Colding constant	-
N0	Colding constant	-
L	Colding constant	-

Greek symbols

α	Clearance angle	°
β	Wedge angle	°
γ	Rake angle	°
ε	Included angle	°
κ	Major cutting edge angle	°
κ_b	Minor cutting edge angle	°
λ	Inclination angle	°

Abbreviations

A list of abbreviations and the respective meaning is presented below.

Abbreviation	Meaning
BUE	Built-up edge
BUL	Built-up layer
cBN	Cubic Boron Nitride
CCC	Coated Cemented Carbide
FIB	Focused Ion Beam
HAADF	High-angle annular dark-field
pcBN	Polycrystalline cubic Boron Nitride
PCD	Polycrystalline Diamond
SEM	Scanning Electron Microscopy
TEM	Transmission Electron Microscopy
TPL	Tool protection layer
UCC	Uncoated Cemented Carbide

1 Introduction

Titanium emerged as a 'wonder material' in the 1950's and since then, a wide range of alloys has been developed. Titanium alloys have a high strength-to-weight ratio, resistance towards corrosion, low thermal conductivity and thermal expansion – attractive properties for applications in the aerospace industry. As an element, titanium shows strong chemical reactivity, leading to poor surface quality on the workpiece and to chemical and diffusion wear in the cutting tool [1]. Properties that makes titanium alloys hard-to-machine materials are the low thermal conductivity, chemical reactiveness and the strength – demanding low cutting data and hence low material removal rate, leading to high manufacturing costs. This stipulates the importance of solutions for high speed machining which gives a faster throughput. The solutions for high speed machining includes suitable cutting data, process parameters such as high-pressure cutting fluid and cutting tool materials. To find these solutions, one must understand the wear mechanisms and the chemical reactions.

In the manufacturing industry, there are many factors to consider in order to balance the manufacturing costs. The total cost of manufacturing is connected to factors such as tooling, workpiece material, process parameters, employees and organization, maintenance, equipment indirectly connected to the process and factors that are special or even unknown. The machining cost is connected to the type of wear the cutting tool is subjected to and at which speed the wear progresses. The selected cutting data affects the production speed of the cutting process and the course of wear subjected on the cutting tool – directly affecting the cycle time of the machining operation. The machining time, the rejection rate and the tool replacement interval are some of the parameters determining the machining cost and they are affected by how well functioning the cutting tool is [1].

In industrial manufacturing, there is a need to balance the process time cost to the tooling cost, depending on for example the manufacturing system and the part geometry. The process time cost can include factors such as the material removal rate and need of tool changes requiring a pause in the process. The tooling cost is linked to the tool life of the cutting tool edge, e.g. how many parts or fractions of a part's geometry a cutting tool edge can produce before being considered worn out, in relation to the price of the cutting tool [2].

When balancing the process time cost and the tooling costs, optimization of the cutting data is required. Then, it is important to consider the tool wear, especially when optimizing the cutting speed. Generally, the cutting speed has the main impact on the tool life. To get a relation between the tool life, the cutting data, the wear mechanisms and the acquired surface quality, laboratory tests are carried out. The results from the tests can be used in for example the Colding tool life model and for optimization of manufacturing costs. The tool life models are used for cutting data recommendations in different web applications, provided by tool manufacturers [2].

1.1 Problem description

What will the machining performance and surface quality be, and how will the chosen titanium alloy affect the selected cutting tool materials during high speed machining under application of high-pressure coolant?

1.2 Purpose

The purpose of the study is to accumulate knowledge on the basic performance, wear mechanisms and cost efficiency of selected cutting tool materials and workpiece material. This knowledge enables selection support for suitable cutting tools and cutting data to a certain workpiece material.

The results refers to be a part of the ongoing research in the metal cutting area. The results will primarily be used by the contracted company, be a part of the examples in the courses at the department at which the master thesis is performed and be a base for other master theses or doctoral dissertations.

1.3 Scope

Workpiece material: (α + β)-alloy Ti6Al4V (grade 5).

Cutting tool materials:

- Uncoated cemented carbide
- Coated cemented carbide
- PCD
- pcBN

1.4 Limitations

For selected cutting tools, cost efficiency is executed to present the machining performance in relation to the tool cost. In cases of interest, the worn tools are subjected to in-depth microscopic analysis of chemical wear mechanisms, using FIB-SEM and TEM.

The standard wear criterion when turning (ISO 3685) used is 0.3 mm [3].

Hardness of the machined surface, considering deformation-hardened layers, is not performed, because of the already time consuming tests.

2 Theory

The following chapter deals with the theory for turning operations including high speed machining, cutting forces, cutting data, engagement distance, material removal rate, surface roughness, process additives in the form of cutting fluids, and how to calculate the equivalent chip thickness. The chapter includes the basics on cutting tool geometries, compositions and coatings used in the study. Definitions of tool life and wear criterions and the types of tool wear are included. This chapter presents the workpiece machinability and information about titanium as a workpiece material. The Colding tool life model as well as the cost efficiency, followed by basic theory about the microscopy methods used in the study are introduced. The chapter is written in a manner for the reader not being accustomed to metal cutting processes.

2.1 Turning

Turning as a manufacturing method is defined as when a rotational-symmetrical workpiece turns around its axis, and a movable cutting tool is pressed against the workpiece. The stagnation point enables the chipping process and the shearing of the workpiece material. Normally, the workpiece is fastened in both ends, by a chuck on one side and a tailstock on the other side. Typically, the turning is continuous, and will be in the following study, but it might also be intermittent. In an intermittent process, the cutting tool is cyclically active – the cutting tool edge periodically engages and disengages into and out of the workpiece. Intermittent processes occurs when the workpiece is discontinuous, for example when having a keyway of splines [1]. Figure 2-1 illustrates the turning setup with holder and workpiece.

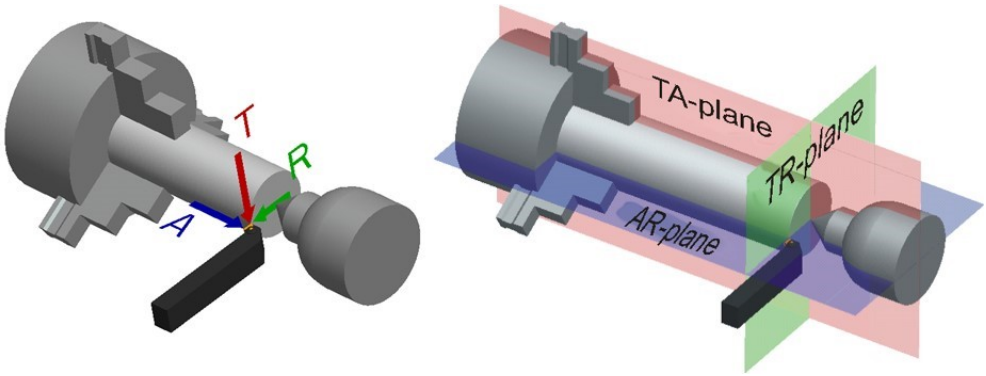

Figure 2-1. Turning setup, showing the planes for the T-, R- and A-directions [1].

Figure 2-2 displays the cutting tool geometry when turning including applicable angles. Two of the angles are independent of the tool holder, the wedge angle, ε, and the included angle, β. A larger wedge angle and included angle gives a stronger edge and improved heat removal from the cutting tool edge. The nose radius, r_ε, rounds the wedge angle and in relation to the feed creates the theoretical surface integrity [1].

The rake angle, γ, is dependent on the tool holder; a positive rake angle results in smaller cutting forces but a weaker tool edge, and a negative rake angle results in higher cutting forces but a stronger tool edge. The inclination angle, λ, affects the cutting forces and the chip breakage. A negative inclination angle results in better load conditions on the cutting tool edge, but directs the chips towards the workpiece, increasing the risk of damaging the surface [1].

The major cutting edge angle, κ, and the minor cutting edge angle, κ_b, are dependent on the tool holder geometry and installation. The major cutting edge angle affects the theoretical chip thickness, h_1, and its relation to the theoretical chip width b_1 [1].

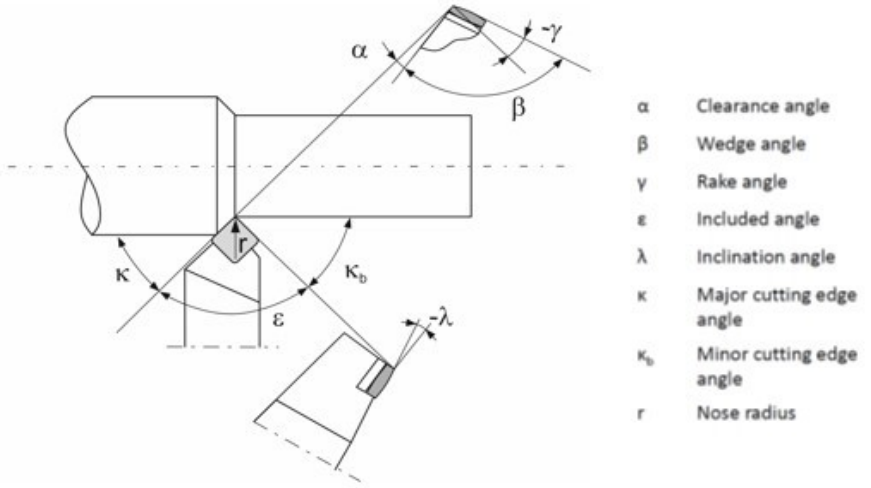

Figure 2-2. Turning geometry [1].

2.1.1 Cutting forces

As can be seen in Figure 2-3, the cutting force, F, can be divided into three orthogonal force components during a turning operation; the main cutting force, F_c, the feed force, F_f, and the passive force, F_p.

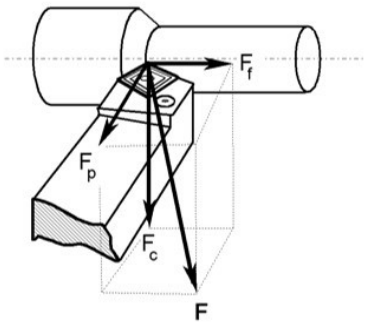

Figure 2-3. Cutting forces in a turning process [1].

2.1.2 Cutting data

The cutting speed, v_c, is defined as the relative speed between the cutting tool and the workpiece surface. The cutting speed depends on the diameter, D, and the spindle speed, n, see Equation 2-1. The feed rate, f, is defined as the axial distance that the tool moves per revolution. The cutting depth, a_p, is the radial depth at which the cutting tool is moved to before the feed movement starts. See Figure 2-4 for an illustration of a_p and f.

$$v_c = \frac{n \cdot \pi \cdot D}{1000} \qquad \textit{Equation 2-1}$$

Figure 2-4 displays the chip area parameters in turning when using cutting tools with a nose radius. The chip width is calculated with Equation 2-2.

$$b_1 \approx \frac{a_p}{sin(\kappa)} \qquad \textit{Equation 2-2}$$

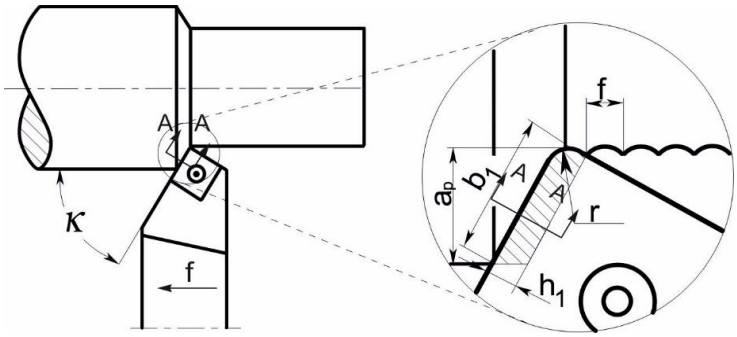

Figure 2-4. The major chip area parameters in turning, shown in the AR-plane [1].

The selection of cutting data depends on if the application is for roughing or finishing operations. For roughing operations, the surface quality is of minor importance. Then, the selection of cutting data is to maximize for what the machine, the workpiece material and the tool allows regarding material removal rate. For finishing operations, there are other aspects to consider, such as surface quality and to meet dimension requirements. To meet these requirements it is common to use low feeds and cutting depths together with a relatively high cutting speed [1].

2.1.3 Engagement distance

The engagement distance, e_T, is the spiral distance when turning. Equation 2-3 displays the tool engagement distance for one cutting edge. The equation is applicable when the cutting data is constant for the whole tool life [1].

$$e_T = v_c \cdot T \qquad \textit{Equation 2-3}$$

2.1.4 Material removal rate

The chip volume flow, dV/dt, also known as the material removal rate, MRR, is calculated with Equation 2-4 when turning. A in the below equation represents the chip area [1].

$$\dot{V} = \frac{dV}{dt} = A \cdot v_c \approx a_p \cdot f \cdot v_c \qquad \textit{Equation 2-4}$$

2.1.5 Surface roughness

The international standard for describing the deviation of a surface from a perceived average level is the Center-Line Average, R_a. The surface roughness when using the Center-Line Average is calculated using Equation 2-5. L_m is the measured length, y is the depth of the surface integrity and x is the direction of L_m [1]. The cons of using the R_a-value is that it does not describe the surface characteristics since the value is independent on which side of the average line the depth is [4].

$$R_a = \frac{1}{L_m} \cdot \int_0^{L_m} |y| \cdot dx \qquad \textit{Equation 2-5}$$

In practical situations, the above Equation 2-5 can be difficult to calculate exactly. Instead, a simplified equation is commonly used, see Equation 2-6 [1].

$$R_a \approx 0.77 \cdot \left[1 - \frac{\frac{f}{2 \cdot r_\varepsilon}}{\arcsin\left(\frac{f}{2 \cdot r_\varepsilon}\right)}\right] \cdot r_\varepsilon \qquad \textit{Equation 2-6}$$

Empirically obtained values for the surface roughness are often inferior compared to the values computed theoretically. Factors affecting the Center-Line Average are side flow, formation of built-up edges, vibrations and damages to the edge line, which are explained in 2.3 Tool wear and 2.5 Workpiece material machinability [1].

2.1.6 Cutting fluid

Cutting fluids are mainly used for the below purposes [1]:

- Cooling of the machining zone and the immediate surroundings.
- Transporting chips from the machining zone.
- Binding of chip dust.
- To some degree improve the tribological conditions, e.g. function as a lubricator in the cutting process.

When a workpiece material requires process additives in the form of cutting fluids in order to be machinable, it implies that the particular workpiece material is less

machinable compared to other workpiece material that does not require process additives in the form of cutting fluids. Cutting fluids are hard to dispose of appropriately and are often expensive to handle; they might also cause allergies and skin irritations. If various alloys such as Cr, Ni and Mo are machined, the cutting fluid can be contaminated; increasing the risk of allergic reactions. Although the human risks exists when using cutting fluids, these can also be used to improve the working environment by encapsulating dust and chip fragments that otherwise would be more harmful [1].

The cooling medium should penetrate into or come as close as possible to cutting zone to effectively use the cooling system. One type of cooling system use high-pressure methods, applicable for the increasing use of high speed machining, i.e. high cutting speeds. For high speed machining, the heat generation in the machining becomes an important factor for the tool wear. HPDC systems (High Pressure Directed Cooling) are especially effective by delivering the cutting fluid via nozzles aiming a powerful jet of coolant directly into the cutting zone [5]. The pressure of the cutting fluid breaks the chips into smaller pieces, minimizing the risk of problems connected to longer chips. By aligning the stream towards the cutting edge, the tool life, chip breaking and surface roughness can be improved [6].

2.1.7 High speed machining

For higher productivity and throughput, one key manufacturing technology is high speed machining. High speed machining is not easy to define because of the actual cutting speed achieved depends on factors such as workpiece material, type of cutting operation and cutting tool. Therefore, the definition of high speed machining depends on the technology used. For high speed machining in titanium alloys, high speed machining is according to the current source between approximately 120-1000 m/min in cutting speed, with a transition region of 80-120 m/min. [7].

The advantages of high speed machining are, in addition to an increased productivity or throughput, for example [7]:

- Machining accuracy increase.
- Improved surface quality and a reduction of the damaged layer.
- Reduced burr formations.
- Improved chip disposal.

In difficult-to-machine materials, such titanium alloys, high speed machining is suggested for finishing operations since the improved surface quality, compared with those acquired with conventional methods, can reduce the time for sub-sequent final processes such as grinding. Disadvantages with high speed machining is that the cutting speed is limited by the tool wear in difficult-to-machine materials, such as titanium alloys [7].

2.2 Cutting tools

2.2.1 Geometry

In cutting tool manufacturing processes, edge treatment can be carried out. Along the edge line, the edge is rounded off to create the desired edge radius. The treatment method employed differ in the exact edge-line profile created. The edge radius, r_β, usually differs between 10-80 µm. The edge radius on cutting tools for roughing operations is often larger compared to the edge radius on cutting tools for finishing operations, because of the higher edge strength needed in roughing operations. The edge treatment is often carried out with abrasive methods such as brushing, blasting or barrel finishing. Cutting tools with chip breakers are used to control the chip formation by breaking the chips into smaller pieces as they are generated [1].

Figure 2-5 presents the cutting tool geometries used in the study. The shortages for the cutting tool type is the first letters and –F1 stands for finishing operations degree 1, used by the manufacturer to name the cutting tool type.

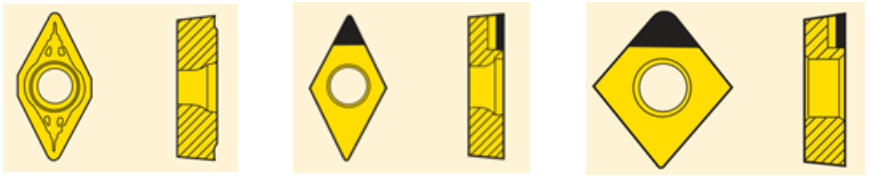

DCMT-F1 DCMW CCMW

Figure 2-5. Geometry for cutting tool type DCMT –F1 (left), DCMW (middle) and CCMW (right) [6].

2.2.2 Compositions

The absolute requirement for cutting tools in order to function well is that the cutting tool needs to be harder than the machined material. The cutting tool material should contain materials such as particles, fibers or other compositions that are sufficiently hard [1].

The simplest cutting tool material has a single-phase structure, consisting of heat-treated and tempered martensite (a specific phase in carbon steel), in order to meet the requirements and balance between the toughness and hardness. Cutting tools that are multi-phased can be acquired by adding alloy elements to carbon steel, and for example letting the new phases contain hard particles. When a cutting tool is multi-phased and containing one or more alloy elements, the following is required for the manufacturing process [1]:

- The alloy elements should be readily soluble in the material's principles phase.
- Segregation tendencies and dendrite formation should be controlled.
- The grain size and the size of the phases precipitated, for example in carbide forms, should be controlled.

- The base material is given the hardness, the residual stress state and the geometric form desired.

The above requirements can result in certain limitations, for example regarding the proportion of hard phases that the basic material contains. The limitations can be reduced or overcome by using powder metallurgy techniques. With powder metallurgy techniques, the individual phases of desired size and required characteristics are mixed and pressed together, followed by a sintering process. This technique are used to manufacture all types of cutting tool materials. The three major components in a powder-based cutting tool material are mainly [1]:

- Hard phases – providing wear resistance.
- Binding phases – can also be a matrix, holding the hard phases together.
- Process additives – facilitates or controls the manufacturing process.

More phases can be added, for example to increase the thermal conductivity. Additionally, fibers can be added to increase the flexural strength [1].

The functional requirements applying to a cutting tool can be achieved by an appropriate selection of the following [1]:

- Bulk material and its specific characteristics.
- The macrogeometry (the cutting tool major geometric characteristics).
- The microgeometry (primarily the cutting edge form or edge line).
- The gradient characteristics.
- Provided coating.

2.2.2.1 Cemented carbide

Cemented carbides represent a group of composite materials that is manufactured with powder metallurgy techniques. High wear resistance and high levels of hardness and strength characterize cemented carbides. Usually, cemented carbides consist of hard particles of one or more types, sintered together by a relatively tough binding metal. The most important hard phase is tungsten carbide, WC, but either carbides, carbonitrides or nitrides of titanium, niobium, vanadium or chromium can also be present. These are generally quite hard but has a limited toughness. The most used binding metal is cobalt; other elements such as nickel and iron, as well as alloys of these, can be present too. The binding metal/-s are tasked to provide the composite material with better toughness and a solid consistency without pores, to achieve a sought after balance of hardness, wear resistance and toughness. Today, most types of cemented carbides are provided with a hard, brittle and chemically resistant ceramic coating [1].

2.2.2.2 Diamond

The world's hardest and most wear resistant material is diamond. The characteristics of diamond tool materials are either monocrystalline or polycrystalline. In addition, diamond-silicone composites, D+SiC, are produced. Chemical vapor deposition, CVD, or ultra-high temperatures and pressure synthesis can be used as

manufacturing methods for each class of diamond materials. The most popular form of diamond tool material is polycrystalline diamond, PCD. PCD is synthesized by using ultra high temperatures and pressures. The diamond particles are in the size of 1-30 μm, sintered together with a cobalt catalyst present. The stable region of the diamond is controlled during the sintering process in order to create the extremely hard and abrasion resistant structure [1].

During machining, the cutting tool is subjected to high temperatures and pressure. This means that the cutting tool need properties which enables resistance towards plastic deformation, fracture, abrasive and chemical wear resistance, while a sharp cutting edge is maintained for an extended period of time. The most basic requirement to be met is the hardness, where diamond is unique. Other requirements are a suitable degree of toughness, thermal stability and thermal shock resistance. Monocrystalline diamond has the highest thermal conductivity of all known materials. Regarding toughness, thermal stability and thermal shock resistance, monocrystalline diamond are greater compared to other diamond materials [1].

Cemented carbides are generally tougher than diamond materials, but the incorporation of cobalt and the associated diamond-to-diamond intergrowth, regarding UHPT-synthesized material, gives high values of toughness and strength and only a negligible loss in hardness and abrasion resistance. CVD-PCD materials compared to monocrystalline diamond and polycrystalline diamond are intermediate regarding the values of thermal conductivity and abrasion resistance. CVD-PCD materials without a cobalt binder are more prone to chipping during impact loading, but can be compensated by use of a stronger edge geometry, compared to those generally used for PCD [1].

Finer grains in PCD grades shows better strength compared to grades with coarser grains, but generally has lesser abrasion resistance. Recent PCD-development with one-micron sized particles are designed to an optimal combination of strength, wear resistance and machinability performance [1].

The use of PCD are mainly for machining in non-ferrous metals, alloys, composites and reinforced plastics. The largest area of application is for machining in aluminum-silicon alloys for the automotive industry. The machining with PCD is limited to operating temperatures lower than or equal to 730 °C. PCD has been successful in machining in cast irons and is gaining in popularity for milling and turning of titanium alloys and in precision finishing of grey and high-strength cast irons [1].

2.2.2.3 Cubic Boron Nitride

Cubic Boron Nitride, cBN, is purely man-made material and is not found in any form in nature. Only diamond is harder than cBN, and at elevated temperatures the hardness is retained for cBN. Also, cBN is inert to iron. These characteristics makes cBN an ideal cutting tool material for machining both hard and abrasive ferrous workpiece materials [1].

Polycrystalline cubic Boron Nitride, pcBN, consists of cBN grains that are bound together by a ceramic, metallic or wBN binder under ultra-high pressure and high temperatures, in order to form a homogenous material. Wurtzite Boron Nitride, wBN, is another super hard BN phase which is metastable. wBN has lesser hardness than cBN but has higher toughness, therefore suitable in interrupted machining operations. The metallic or wBN binder in pcBN holds the hard grains together. Depending on the type and amount of binder, the pcBN materials are graded as [1]:

- Low-cBN (LcBN) – content material with a ceramic binder.
- High-cBN (HcBN) – content material with ceramic or metallic binder.
- Binderless cBN (BcBN).

pcBN provides the most extreme combination of properties such as hardness (needed for it to resist plastic deformation and abrasion), a moderate to relatively high level of strength and toughness (to resist fracture), and a moderate to very high level of thermal conductivity (enabling heat dissipation). Specific grades of pcBN are designed to be highly resistant to reactions with ferrous materials and limits the chemical wear mechanisms. This design makes pcBN favorable when machining for example hardened alloy steels and high-temperature super alloys. The uses of pcBN for turning in super alloys are a small but growing area [1].

2.2.3 Coatings

Cutting tools can be provided with a coating in order to increase the wear resistance. Usually, coatings consist of ceramics and sometimes diamond or diamond-like substances. Coatings with ceramics include oxides, nitrides and carbides. The typical ceramic characteristics are stability at high temperatures, chemical inertness, extreme hardness and brittleness. The thin coating with ceramics on cutting tools enables the use of their characteristic without needing to suffer from the brittleness. The coating is usually built up based on several layers of materials that has different characteristics [1].

Coatings are 1-20 µm thick and depends on the application method. The physical vapor deposition, PVD, technique applies a coating 1-5 µm thick; the chemical vapor deposition, CVD, technique applies thicker coatings of 4-20 µm. A typical CVD coating is built up by a sub-layer of Ti(C, N), covered by a layer of Al_2O_3. The PVD technique allows more possibilities of varying the composition of the coating material, with a large number of combinations of different materials. The most common materials for this technique are Ti, Al, Cr, Si, N, O and C. The CVD-technique allows lesser variations in the materials system employed compared to the PVD-technique. Ti(C,N), TiN and Al_2O_3 are the major coating materials used today [1].

2.3 Tool wear

The wear-based tool deterioration depends largely in the form of wear on the cutting-edge surfaces that are in contact with the workpiece. The wear character can be uniform or non-uniform. There are non-wear-related deterioration of the cutting tool, for example crack formation, plastic deformation and deterioration caused by chemical processes. The tool deterioration is closely related to mechanical and thermal loads exposed to the cutting tool. The thermal load accelerates tool deterioration, such as chemical reactions and diffusion. Combined cutting tool deterioration, including simultaneous flank wear and plastic deformation, increases the importance of the development of new and improved tool materials and coatings. The types of tool deterioration are listed below [1]:

- Wear – changes in tool geometry caused by continual loss of cutting tool material.
- Plastic deformation – changes in the geometric form without loss of cutting tool material.
- Breaking or cracking – parts of the cutting tool breaks, break off or are removed at a given point in time.
- Material transformations – changes in characteristics and in structure, primarily based on chemical processes such as diffusion or chemical reactions in the cutting tool.

2.3.1 Wear types

Wear on the cutting tool results in geometrical changes by a continual loss of material, affecting machining results such as tolerances and surface quality, and the cutting tool performance. Geometric changes such as flank wear, crater wear and notch wear caused by abrasive and adhesive wear are described below. A cutting tool can be affected by one or several wear mechanisms and the total tool wear is a sum effect of the relevant wear mechanisms [1].

2.3.1.1 Abrasive wear

Abrasive wear occurs if the workpiece material contains hard inclusions that grinds the cutting tool. If there is an absence of hard inclusions, the wear is called erosive. Chromium and vanadium as alloy components forms carbides that increases the abrasive wear [1].

2.3.1.2 Adhesive wear

Adhesive wear occurs when there is a micro-welding of the workpiece material to the cutting edge, resulting in micro-chipping of the cutting edge. One way is that there is a high contact pressure between the chips and the cutting tool, resulting in a pressure-welding of the workpiece material on the tool or formations of built-up edges, BUE, on the cutting tool. Later, the adhered layer is sheared off and removes parts of the tool material [1]. At a process temperature of 600-700 °C, combined with a high pressure, a thin layer of the workpiece material is welded on the cutting tool

edge. The built-up edge consists of highly deformed workpiece material which is considerably harder than it was originally. Consequences of built-up edges can be that the surface quality is reduced when the built-up edge is ripped off the cutting tool, or that the cutting tool geometry is changed in a way that the size of the edge radius is reduced and the edge line becomes irregular in form [8]. See Figure 2-6 for the schematics of the formation and removal of built-up edges, affecting the machined surface.

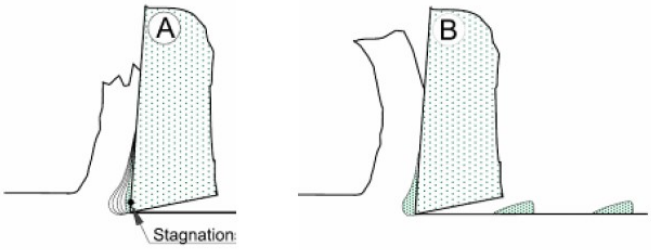

Figure 2-6. Schematics of the formation of built-up edges (A) and the removal of them (B) [1].

Built-up layers, BUL, always precede the formation of built-up edges and is a formation of a workpiece material layer on the cutting edge. The amount of material adhering to the cutting edge can remain constant if the machining temperature is sufficiently high. Compared to when built-up edges occur, the substitution of material under formation of built-up layers are considerably less. A tool protection layer has a positive influence on the tool life; see Figure 2-7. A tool protection layer consists of workpiece material or reaction products between the tool, workpiece and/or the environment [8].

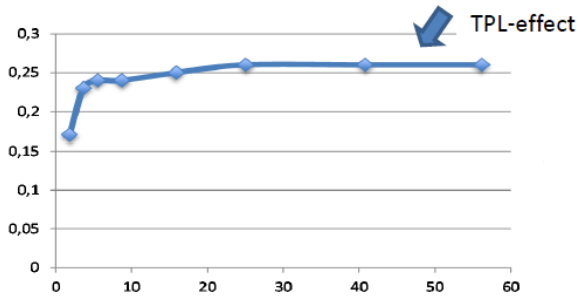

Figure 2-7. The flank wear plotted as a function of the engagement time (Y-axis: VB [mm], X-axis: engagement time [min]) – note that the tool life stabilizes at approximately VB = 0.26 mm, an effect of tool protection layers. The workpiece material for the presented test is the steel AISI 4340 [9].

2.3.1.3 Flank wear

Flank wear creates a wear surface parallel to the cutting speed direction, resulting in the cutting edge becoming increasingly blunt and the clearance angle approaching zero. An increase in flank wear results in an increase in the shear forces and the normal forces; as a result, there is an increase in heat generated and in the cutting

resistance. An increase in the flank wear leads to a shift in the relation of the edge line to the workpiece, leading to changes in the dimension of the produced part unless compensated for. See Figure 2-10 for examples of the flank wear and the relation of a worn and new tool to the dimension of the workpiece; Figure 2-9 and Figure 2-12 also presents the flank wear. As the flank wear progresses and the cutting forces increases, the tool holder, the workpiece or the machine might result in being bent or deflected. The flank wear is often dependent on the temperature and is most affected by deformation zone ε_{III}, see Figure 2-8 [1].

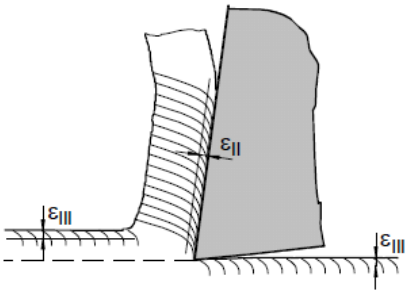

Figure 2-8. Deformation zones [1].

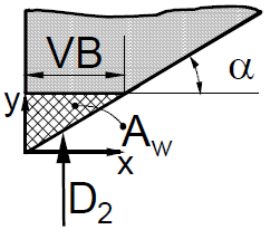

Figure 2-9. An idealized view of the flank wear in a cutting process. A_W is the wear surface of the cutting tool removed during the machining process and D_2 is a constant in the axial direction used for calculating the feed force [1]. A_W and D_2 are not used in this study.

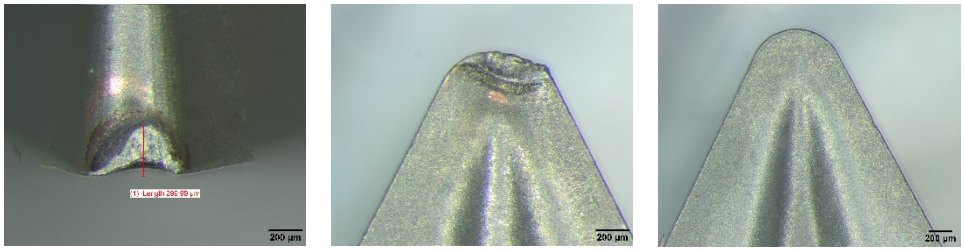

Figure 2-10. Example of the flank wear in the C-zone (left); cutting tool that has reached the tool wear criterion, shown from the rake side (middle), compared to a new cutting tool (right) – showing the degradation in the diametric direction and why it must be compensated for to remain the dimensions of the produced part.

Figure 2-11 presents typical wear curves in metal cutting in five tests with different cutting data, to show how the flank wear curve might look like.

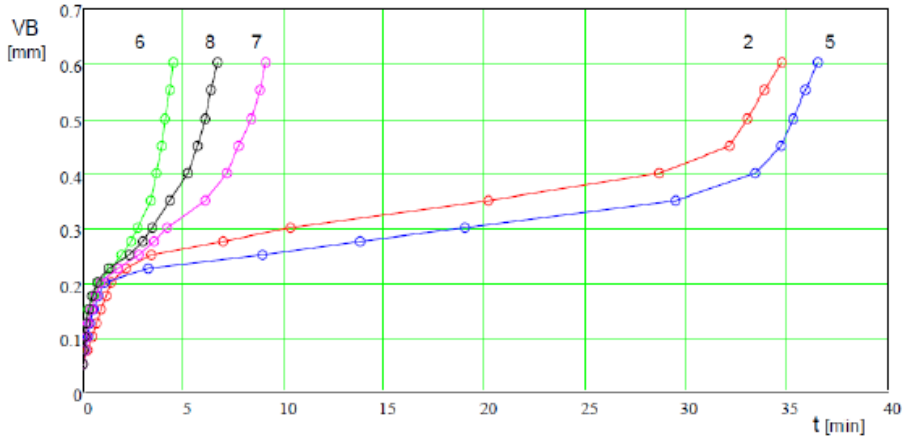

Figure 2-11. Typical wear curves in metal cutting (workpiece material SS2541) [9].

2.3.1.4 Crater wear

Crater wear is located on the rake face of the cutting tool, usually not directly on the edge line, see Figure 2-12 for an example. In short chipping material, the crater wear might reach the edge line. The initiation of crater wear is located on the rake face where the cutting temperatures are the highest, which has been shown by experimental studies. Hence, the crater wear is brought about by the energy consumption level, primarily in deformation zone ε_{II}, see Figure 2-8. The crater wear has the largest effect on the edge strength since the wedge angle decreases and therefore weakens the cutting edge. Crater wear also leads to an increased positive rake angle, slightly decreasing the cutting forces. When the crater wear increases, it is common that the chip breaking is improved [1].

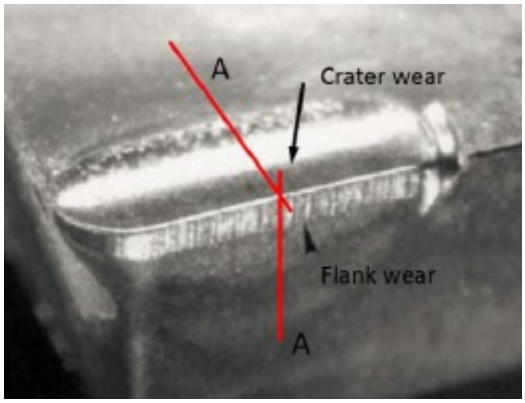

Figure 2-12. Example of crater wear and flank wear. Notch wear can be observed at the upper right part, where the flank wear and crater wear ends [1].

2.3.1.5 Notch wear

Notch wear normally occurs on the clearance face of the cutting tool, in the same height as the previously cut surface. The notch wear occurs when there is a deformation hardened layer that has been created or if the cutting tool is oxidized in the area where air is present [1]. Notch wear can be observed in Figure 2-12.

2.3.2 Plastic deformation

Plastic deformation depends on the mechanical and thermal loads developing during the cutting process, as well as the geometric form of the cutting tool. As the tool wear progresses, the load-bearing capacity increases for a time when geometric changes on the cutting tool develops. During the same time, the thermal and mechanical loads increases. An increase in mechanical loads can result in a more favorable stress level within the cutting tool, as there is a balance between the increasing wear and the plastic deformation developing on the cutting tool. Eventually, the balance can be followed by a very rapid plastic deformation, leading to it failing to perform [1]. See Figure 2-13 for a cutting tool being plastically deformed.

Figure 2-13. Example of plastic deformation close to tool failure [8].

Under rather frequently occurring conditions, there is a successive plastic deformation taking place whereas there is a change in the cutting tool geometry that compensates the continuing flank wear. This leads to an increase in the clearance angle, α, between the workpiece and the wear-exposed surface of the cutting tool, tending to prolong the tool life. This is referred to as a temperature-dependent plastic deformation, where the absolute stress level either remains constant or slightly falls, because of the edge strength increases as the cutting temperature increases. The increase in cutting temperature leads to a decrease in the cutting tool's deformation resistance. The successive increase in plastic deformation results in an increasingly negative rake angle and inclination angle that can have a negative effect on the topography of the cut surface [1].

A reduction or avoiding of plastic deformation on the cutting tool can increase the cutting efficiency and is achieved by selecting a larger cutting tool, so that the volume of material in the cutting tool is increased [1].

2.3.3 Breaking or cracking

2.3.3.1 Edge chipping

Edge chipping is a tool wear that involves local breakage along the edge line accompanied with loss of material, see Figure 2-14 for an example. Edge chipping can be caused by many different factors, for example loss of material between different sets of cracks or chip hammering. The edge line damage caused by edge chipping can affect the surface quality. The consequences are rather limited in roughing operations, but in finishing operations, the edge chipping can lead to a higher probability of rejection of the product due to a rougher generated surface [1].

Figure 2-14. Example of edge chipping [10].

2.3.4 Material transformations

2.3.4.1 Diffusion

Diffusion occurs when there is a transport of material between the cutting tool and the workpiece material at an atomic level. Diffusion results in a decline of the cutting tool material characteristics in the parts of the cutting tool where the diffusion occurs. This wear type is strongly dependent on temperature. A marked deformation of the workpiece material occurs in a temperature interval of 800-1100 °C for cemented carbide grades, leading to a complete contact between the cutting edge and the established chips. The strong concentration gradients between the materials of the cutting tool and the workpiece material are favorable for diffusion taking place [1].

In metal cutting, there is a shearing process of the workpiece material at a high velocity. The relative velocity of movement can be low between the cutting tool and the workpiece as well as between the cutting tool and the chips. The workpiece material typically deforms in the region closest to the cutting tool where the relative velocity is approaching zero, just as for laminar flows. The contact surface there intensifies the diffusion process, resulting in a decline of the cutting tool material characteristics and an acceleration in various types of wear. To prevent diffusion occurring, the cutting tool can be provided with a coating [1].

2.3.4.2 Chemical and electrochemical wear

Chemical and electrochemical wear can for example occur in cemented carbide grades, since it oxidizes at temperatures of 800 °C. In continuous cutting processes, there is a small chance that gases penetrate into the space between the workpiece and the chips created, leading to a slim chance for oxidation to occur. In intermittent processes, oxidation can occur because of the contact with the environment in the work-free phase [1].

2.4 Tool life criterion and tool wear criterion

A tool wear criterion and a tool life criterion are not to be equated. A tool life criterion represents the point at which the cutting tool fails to function as it is supposed to in a given application. A tool wear criterion represents the point when the cutting tool needs to be replaced to avoid the risk of it failing to function. There is a certain margin towards how long it will be possible to use the cutting tool when applying a tool wear criterion. The selection of a tool wear criterion depends on the probability that the produced part meets the desired quality, for example permitted tolerances and surface quality. In a robust process, the tool wear criterion corresponds to the maximum engagement time permitted to reach the tool wear criterion. In practice, the tool might be replaced before the tool wear criterion has been reached. The need of tool change might be concerns in changes of the produced part, workplace shift changes or changing the cutting tool before a lunch break [1].

For roughing operations, damages on the edge line can be accepted even though it might cause defects on the cut surface. For finishing operations, damages on the edge line are more critical. This is because the topography of the cut surface can be critical for meeting the requirements. Spontaneous tool failure is unusual if the tool wear has been uniform. A uniform flank wear increases the load carrying capacity and a reduction in the principal stress of the cutting tool. Regarding localized wear and crater wear, both wear types can lead to abrupt tool failure. If there are notch damage on both the main and minor cutting edge, a lower value of the tool wear criterion needs to be employed to avoid tool failure. If the notch damage is accompanied with crater wear, the load bearing capacity decreases and therefore increases the risk of tool failure. Cutting tools with a smaller nose angle are more prone to have geometrical changes caused by crater wear. If advanced coatings have been applied to the cutting tool, both localized wear and plastic deformation can occur, called composite deterioration [1].

The tool wear is not only dependent on the selection of cutting data, workpiece material, use of coolant and coolant pressure, but also on the stability of the machine and/or other individual factors for the specific manufacturing system. These factors can affect the tool life largely from what is estimated [2].

When performing laboratory tests for analyzing the tool wear and the tool life, the tool wear criterion is VB = 0.3 mm, see Figure 2-15. The tool wear criterion may differ between roughing and finishing operations. In the real application system of

the cutting tool, the operator can judge if the cutting tool is worn out and when there is a need for a change of the cutting tool edge. The cutting tool edge might be used in several sub-operations with different cutting data, geometries and methods, leading to different contributions to the tool wear. Hence, the theoretical tool life for each sub-operation can therefore be difficult to predict [2].

Figure 2-15 presents a pointed cutting tool with crater wear and flank wear, the flank wear definitions of VB_A, VB_B, VB_C and VB_{max} and the worn part of the cutting tool divided into zones (A, B, C and N). The definitions of the zones are [3]:

- Zone C – the curved part of the cutting edge at the tool corner.
- Zone B – the remaining straight part of the cutting edge between zone A and zone C.
- Zone A – the quarter of the worn cutting edge length *b* farthest away from the tool corner.
- Zone N – the part extending beyond the area of mutual contact between the tool and the workpiece for approximately 1-2 mm along the major cutting edge. The wear is of notch type.

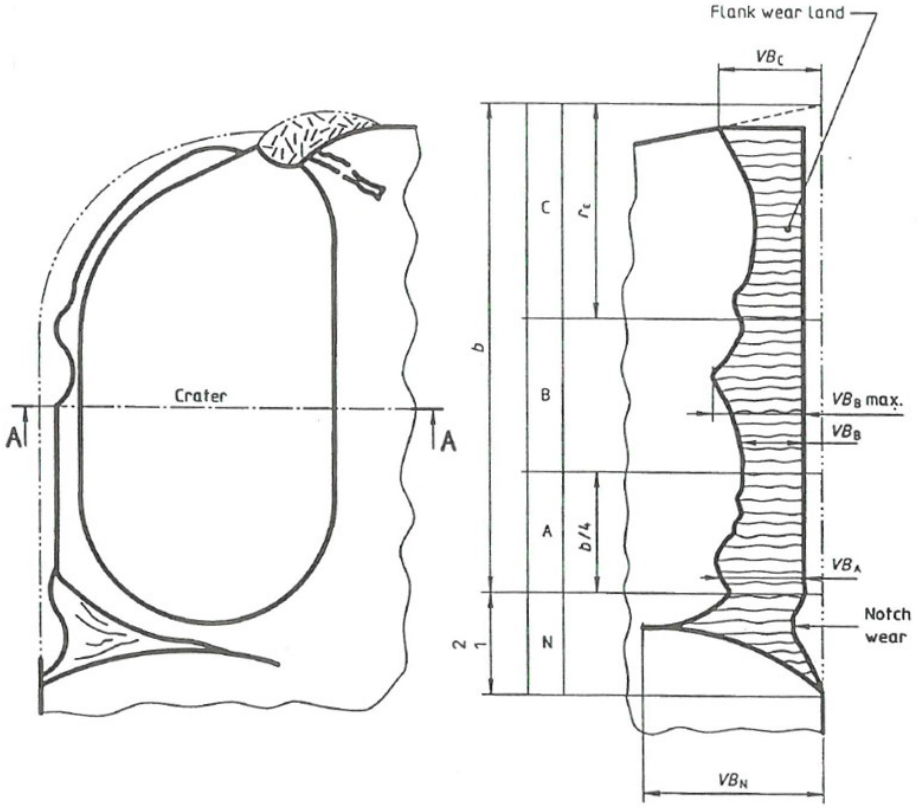

Figure 2-15. Crater wear and flank wear on a cutting tool, the flank wear definitions of VB_A, VB_B, VB_C, VB_{max} and the worn part of the cutting tool divided into zones (A, B, C and N) [3].

2.5 Workpiece material machinability

The overall level of machinability obtained is a result of a combination of material factors, cutting data, cutting tool geometry and characteristics of the cutting tool material. When choosing measures to achieve the highest level of machinability possible, the measures can be contradictive. Hence, when optimizing a cutting process, compromises in the workpiece material characteristics are needed. Listed below are factors affecting the cutting process and the workpiece material machinability [1]:

- Strain hardening.
- Adhesiveness.
- Specific heat and density.
- Variation in microstructure.
- Elongation after breakage.
- Deformation resistance.
- Bulk hardness and the distribution in bulk hardness.
- Phase size.
- Structure notch effects.
- Size, geometric relations, distribution and hardness between η and β phases.
- Effect of ε-phases.
- Chemical reactiveness.
- Porosity.

2.5.1 Strain hardening

Strain hardening of the workpiece material is an effect of machining and results in the outer surface being harder and possessing greater yield strength than the bulk material. A combination of low values for the theoretical chip thickness, h_1, (see Figure 2-4) and high values of the width of the deformed layer ε_{III} (see Figure 2-8) can lead to damages in the edge line. In order to machine less of the deformation hardened layer, the feed can be increased and a cutting tool with a smaller nose radius can be selected. To reduce the thickness of the deformation hardened layer ε_{III}, the edge radius, r_ε, can be reduced by selecting a sharper cutting edge. If the edge radius increases as the tool wear progresses, the problem with harder outer surfaces intensifies. For many workpiece materials, it is common that the deformation hardened layer ε_{III} is reduced when the cutting speed is reduced. If the cutting tool wear is increased, ε_{III} usually increases and therefore a selection of a lower wear criterion can be appropriate. Strain hardening in combination with low thermal conductivity can result in the machinability of the workpiece material to be rather low [1].

2.5.2 Adhesiveness

The workpiece material can adhere to the cutting tool in the cutting process, which is a complex occurrence and is often difficult to predict. The adhesiveness and the ductility of a workpiece material are related – a highly ductile material is often

adhesive to a cutting tool with a coating. Adhesiveness of a workpiece material can be both an advantage and a disadvantage; if the adhesiveness is rather high with a combination of the adhered layer being rather stable on the cutting tool, the adhered layer can protect the cutting edge and extend the tool life. A disadvantage of adhesiveness is if the adhered layer on the cutting tool is frequently removed, leading to rapid or progressive wear of the cutting tool as follows for built-up edges. The border between when these occur can be very narrow. Dramatic differences in the functioning in the cutting process can be caused by only slight differences of the workpiece material characteristics. The adhesiveness of the workpiece material is a necessary condition for the deposition of material, built-up layers, on the cutting edge to occur. Deposition of material on the cutting edge increases the effective rake angle, resulting in a smaller chip radius that improves the chip control [1].

2.5.3 Thermal conductivity

A low level of thermal conductivity in the workpiece material results in the heat generated in the cutting process transmits to the cutting tool. The effect of a higher temperature in the cutting tool edge can result in plastic deformation of the cutting tool. The resistance to deformation limits the level of machinability achieved. To counteract, the amount of heat produced by the cutting process can be reduced by reducing the cutting speed and the feed, or to increase the heat removal by choosing a cutting tool that has the ability to conduct heat through it and its outer surfaces. A lowering of the feed also reduces the mechanical load on the cutting tool. To cool down the cutting process, process additives in the form of cutting fluid in rich amounts can be used to absorb the heat generated. If there are gaps between the cutting tool and the anvil, the cutting fluid can prevent these in the aspect of heat distribution. In order to reduce the energy developed, the cutting depth can be reduced. The thermal conductivity in the workpiece material and the heat generated in the cutting process can start phase transformations in the workpiece material that changes its machinability [1].

2.5.4 Ductility

The ductility of a workpiece material is a characteristic of the material being able to withstand a marked degree of plastic deformation without breaking. In turning of workpiece materials being highly ductile, the chips produced tends to hold together, i.e. chip breaking is difficult to achieve. These difficulties are especially immense if the material is strong, like for super-alloys including titanium [1].

2.5.5 Hardness

The hardness of a workpiece material is not a measure of its machinability; the exception would be if the material group and the materials included are very similar in the characteristics and composition. The hardness is a measure of resistance to plastic deformation, where the resistance towards plastic deformation is only one of many factors included in the machinability concept [1].

2.5.6 Multiphased materials

Multiphased materials often has different machinability in the respective phase. Often, one of the phases is more brittle compared to the others. The β-phase is usually more brittle and harder than the other phases. The hardness of a material is directly linked to the deformation resistance and therefore also the cutting resistance. The variation in hardness is partly connected to variations in the phase distribution. If the workpiece material has a varied hardness, it can be observed in variations in the cutting forces. In the condition that the removed material is in a harder phase, the chips produced tends to be short-chipping or showing a degree of segmentation. The geometric phase distribution that characterize a workpiece material can have a substantial effect on its machinability. A reinforcement phase with hard inclusions of other types, or outer surfaces of the material, are referred to as η-phases. Workpiece materials with phases or inclusions that promotes the lubricating effect in the machining process are referred to as machinability-promoting phases, ε-phase [1].

2.5.7 Chemical reactiveness

Workpiece materials that reacts chemically with the cutting tool is problematic if it changes the cutting tool's characteristics in a negative manner, i.e. shortens the tool life. This type of wear is referred to as chemical wear. When machining certain types of titanium, the occurrence of chemical reactions can be quite general and is largely dependent of the type of cutting tool involved [1].

2.5.8 Porosity

If there is porosity occurring in a workpiece material, it can lead to a decrease in machinability caused by the velocity increase with which the material in the deformation zones ε_{II} and ε_{III} is deformed. The porosity causes an effect of intermittence in which the cutting edge is subjected to frequent entry and exit phases [1].

2.5.9 Manufacturing process effects

When manufacturing a workpiece material, different methods can be used. A material can be hot-worked or cold-worked. Heat treatments can for example be full-annealing, soft-annealing, recrystallization annealing and stress-relieving annealing. Another heat treatment is normalization or hardening. The most important parameters affecting the material structure are the deformations under which it has been subjected, the manner in which the initial cooling took place and if heat treatment has been performed and then under the manners it was carried out. Any clear relationship between the condition of the workpiece material and its machinability are not yet found. That is why each case has to be analyzed individually, weighing the ductility and adhesiveness on one hand and the hardness and abrasiveness on the other hand [1].

2.6 Titanium alloys

The titanium industry has developed a wide range of alloys with different compositions since the emergence of titanium as a 'wonder material' in the 1950's. Titanium alloys are attractive for the aerospace industry for both engine and airframe components because of the high-strength-to-weight ratio, the good resistance to corrosion, the low thermal conductivity and thermal expansion [11]. The high corrosion resistance is a major factor for their use in chemical, petrochemical and offshore industries. Another application area is implants in for example jaws, knees and hips [1].

The machinability of all titanium alloys decreases when the alloy content increases. Also, pure and non-alloyed titanium is difficult to machine. The difficulties in machining titanium are the extremely low thermal conductivity and the marked tendency towards stress deformation. As an element, titanium is characterized by strong chemical reactivity, which can result in a layer of titanium or titanium alloys depositing on the surface of the cutting tool. This can lead to poor surface quality and the fatigue characteristics of it becoming worse. Therefore, it is common to use cutting tools of cemented carbide with sharp edges when machining titanium materials [1].

Alloying additions changes the temperature at which the α- to β-transition takes place. Titanium exists in the cph, close packed hexagonal, α-form up to 882 °C and then as bcc, body centered cubic, β-form up to the melting point. Alloying additions that raises the transition temperature are called α-stabilizers and those that lower the β-transition temperature are called β-stabilizers. For α-stabilizers, Al is predominant. Up to elevated temperatures of 550 °C, Al is also an effective α-strengthening element and is therefore a major constituent of most commercial alloys. The low density of Al is an advantage if the application requires lower weight. Sn and Zr as additions are α-strengthening and exhibit extensive solubility in both α and β titanium. Sn and Zr are considered as neutral additions since they have little influence on the β-transus. The β-stabilizers are either β-isomorphous or β-eutectoid as elements. The β-isomorphous are completely soluble in β-titanium and has a limited α-solubility; commonly used additions are Mo, V and Nb. In a solid solution, titanium will take interstitial solutes where H is a β-stabilizer, while C, N and O are strong α-stabilizers. Manufacturing costs are high in order to minimize the gas in titanium. The heat treatment requires vacuum or inert gas conditions and freedom from refractory contact [11].

The commercial titanium alloys are usually heat-treated. To optimize the mechanical properties, the transformation of the β- to the α-phase is controlled and the extent is governed by the alloy composition and the cooling rate. No matter what the cooling rate is, the α-alloys can transform completely from the β- to the α-phase. Treatments as the latter has a negligible effect on the properties – α-alloys tends to be used in the annealed state [11].

When describing titanium alloys, it is conventional to classify them after the microstructural phase [11]:

- α-alloys.
- near-α-alloys (predominately α phase with a small volume of β phase).
- (α + β)-alloys.
- β-alloys.

Figure 2-16 presents the typical microstructures for α-, (α + β)- and β-alloys. The microstructure shows variations in the morphological development in the α- and the β-phase. The variations are dependent on the alloy chemistry, prior work, temperature from which the workpiece is cooled and at which rate. The microstructures presented in Figure 2-16 are anticipated to be representative, although they are not all-inclusive, because of the prior described variation dependent factors [12].

2.6.1 α- and near-α-alloys

The α-alloys contain alloying elements in particular of Sn and Al, used in applications requiring high creep-strength [1]. Near-α-alloys have increased the strength and the volume of the more creep-resistant cph α-phase at the expense of the bcc β-phase, importing good low-temperature strength and forgeability [11]. See Figure 2-17 for the phase diagram of CP (commercially pure) Ti grade 2.

2.6.2 (α + β)-alloys

The (α + β)-alloys can be precipitation-hardened and the by far most common of these alloys are Ti6Al4V (6 % Al and 4 % V), representing approximately half of the titanium alloy material produced [1]. It contains alloying additions, which strengthen both phases. These alloys are processed thermomechanically to control the size, shape and distribution of both α- and β-phases. Ti6Al4V can be used in temperatures up to 350 °C and has good forging and fabrication properties [11]. See Figure 2-18 for the phase diagram of Ti6Al4V grade 5.

2.6.3 β-alloys

The β-alloys contains V, Nb and Mo as alloy elements, and can be precipitation-hardened [1]. β-alloys contain enough β-stabilizing elements to maintain the bcc β-phase at room temperature. Bcc β-alloys are prone to embrittlement. β-phased alloys have potential as airframe construction materials and offers high strength and toughness in relatively thick cross-sections. β-phased alloys possesses superior hot-working characteristics which are attractive in expensive forging operations [11].

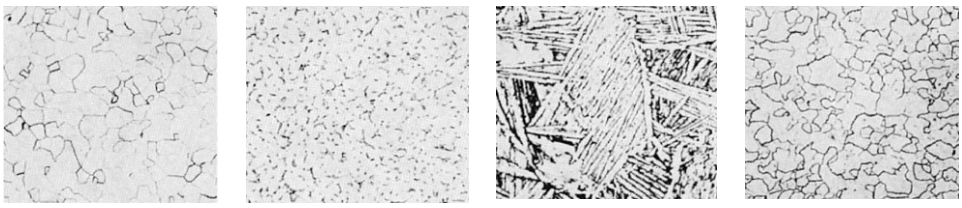

Figure 2-16. The typical microstructures of α-, (α + β)- and β-alloys. Equiaxed α in unalloyed Ti after 1 h at 699 °C (left), Equiaxed (α + β) and acicular (α + β) in Ti6Al4V (two middle), Equiaxed β in Ti13V11Cr3Al (right) [12].

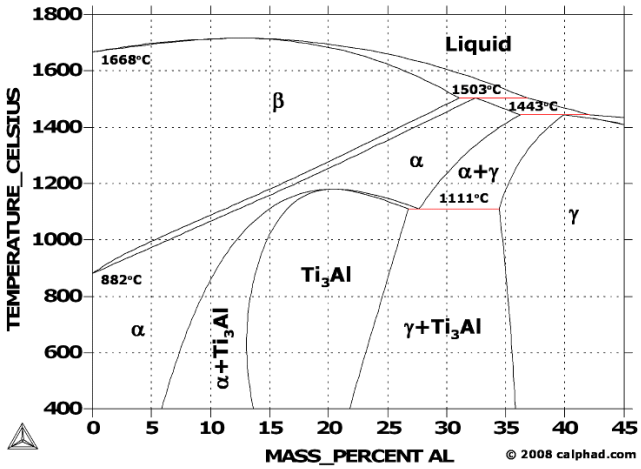

Figure 2-17. Phase diagram for CP Ti grade [13]. Use 0 % Al. The transition temperature from α- to the β-phase s 882 °C.

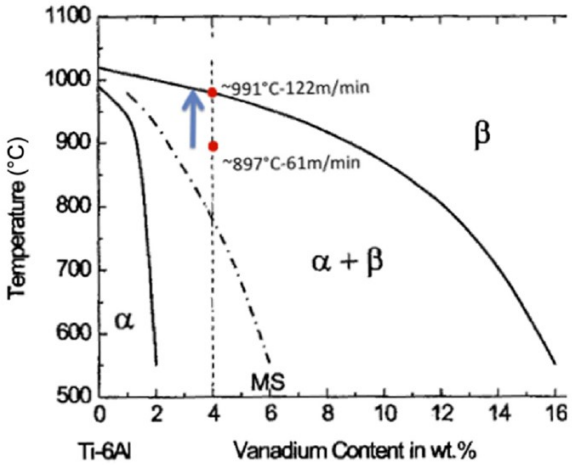

Figure 2-18. Phase diagram for Ti6Al4V (grade 5) [14]. Use 4 % V. The reference source was turning in dry conditions, therefore is the temperatures for the corresponding cutting speeds not applicable for this study.

2.7 In-depth microscopic analysis

The basics about Selective Electron Microscopy (SEM), sample preparation with Focused Ion Beam (FIB) for Transmission Electron Microscopy (TEM) are described below. One difference between SEM and TEM is that for SEM, secondary electrons and back-scattered electrons are used for imaging, see Figure 2-19 for the schematics of a FIB-SEM. When for TEM, the transmitted direct beam and forward scattered electrons are used to create images, see Figure 2-20 for the schematics of a TEM. For SEM and TEM, the electrons used in the beam originates from an electron gun that is mounted at the top of the microscope column [15].

2.7.1 FIB-SEM

SEM is commonly used as a tool to characterize and quickly inspect objects that are too small to be observed in an optical microscope. The image that is generated when scanning the electron beam over the sample is presenting the signal on another screen. Compared to a 'state-of-the-art' optical microscope, SEM generally has a much higher spatial resolution. Another advantage of SEM is the superior depth of focus. A SEM consists of an electron source, condenser lenses, apertures, scanning coils, an objective lens and a specimen chamber. Vacuum is used in the electron column to reduce unwanted collisions between electrons and air molecules, which can lead to scattering along the path to the sample and reduce the spatial resolution [16].

The two major sections for SEM are the illuminating system and the detection system. The illuminating system purpose is to form a well-focused, small probe. The sample used in a SEM is usually thick enough for no electrons to pass through it. Also, all electrons in the incident beam are going to interact with the sample. When the electrons meet the sample, some of the electrons will interact inelastically and some of their kinetic energy will be transferred to the sample. If the energy is transferred to an electron in the outer shells of an atom, the excited electron might gain enough energy to overcome the work function of the material and be ejected. The ejected electrons are called secondary electrons. To collect the low energy secondary electrons, an electric field is used to attract them into a detector. Secondary electrons that are ejected from surfaces tilted away from the detector might as well be spotted. Any surfaces tilted relative to the electron beam will appear brighter compared to surfaces perpendicular to the electron beam. This is the reason why it is possible to detect small topographical variations and roughness on a surface that is otherwise considered as flat. The beam probe size and the electron penetration depth governs the spatial resolution in a SEM. These are influenced by the acceleration voltage of the microscope; the penetration depth is also dependent on the sample material [15].

To create thin samples required for the TEM, there is use of a FIB. The FIB technique allows engraving or milling in the sample at very low dimensions, see section *2.7.2 TEM*. FIB allows 3D patterning of the target material by the use of a finely focused

pencil of ions having speeds of several hundreds of km/s at impact. The patterning made by the FIB can be achieved either by local surface defect generation by ion implantation or by local sputtering [17]. See Figure 2-19 for schematics of a FIB-SEM.

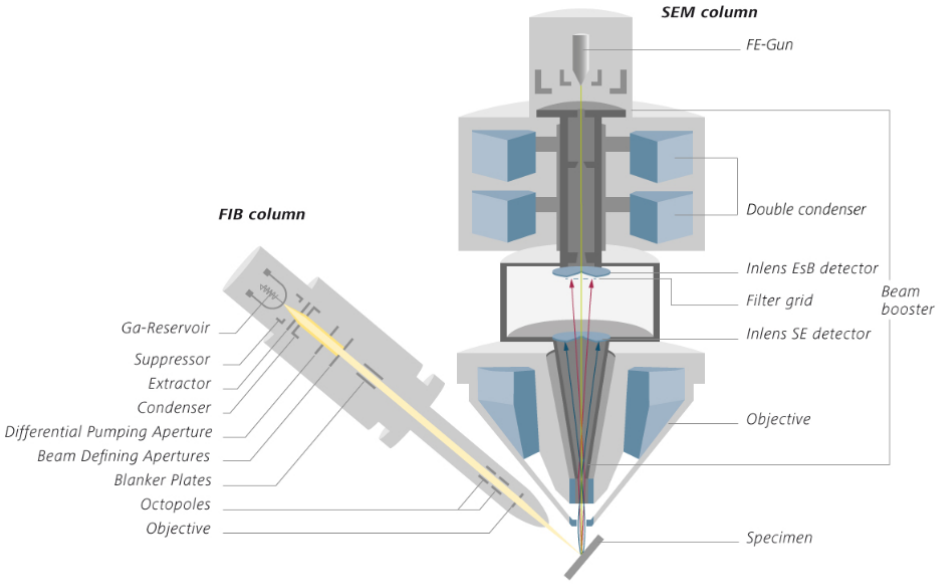

Figure 2-19. Schematics of a FIB-SEM [18].

2.7.2 TEM

The two major sections for TEM are the addition of an image formation system and a projection system compared with SEM. The illuminating system purpose is to form a parallel beam. A thin enough sample allows for an electron beam with high enough energy to pass through it [15]. As a rough number, the sample should be smaller than a hundred nanometer thick [16]. Elastically scattered electrons passing through the sample makes it possible to generate images, which is the basis of TEM. When the electron energy is increased, the probability for scattering is reduced. In comparison, a too high selection of electron energy can result in a knock-on damage so that the electrons displaces atoms in the sample [15].

A TEM is generally divided into four major sections: the illuminating system, the image formation system, the projection system and the detection system, see Figure 2-20 for the schematics of a TEM. The images recorded in a TEM can be divided in two categories and depends on the background contrast. The background will appear bright if unscattered electrons are used to form an image (bright field imaging). If only scattered electrons are used, the background appear dark (dark field imaging) [15].

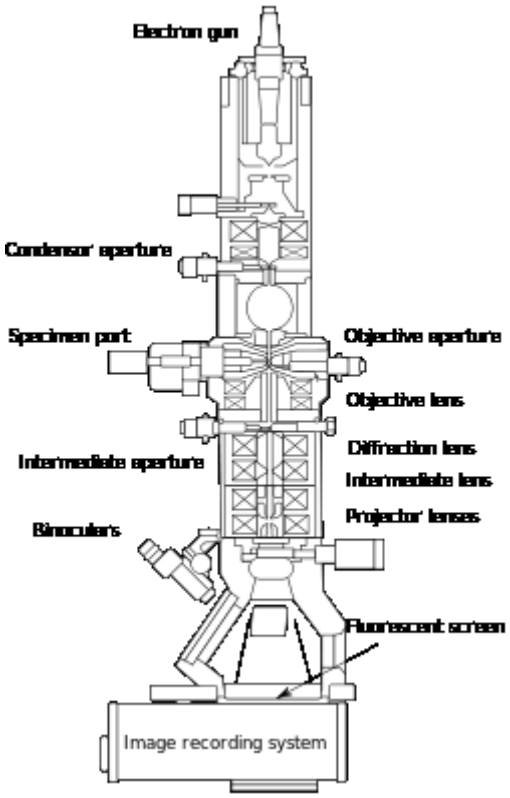

Figure 2-20. Schematics of a TEM.

2.8 Cost efficiency

The cost efficiency in this study is based on the integrated part cost model introduced by Ståhl. The difference in the integrated part cost model is that technical cutting arrangements are included compared to the standard model. The production cost of a part consists of varying elements [19]:

- K_A – tool cost per component
- K_{BQ} – the cost of workpiece material per rejected part
- K_{CP} – machine costs during production per part
- K_{CS} – machine costs during downtimes per part
- K_D – direct costs for personnel per part

The equations for the respective element is presented in Equation 2-7 to Equation 2-11 below. The total production cost is presented in Equation 2-12 and the cost per volume of removed material is presented in Equation 2-13. Table 2-1 presents and explains the factors in the integrated part cost equation [19].

$$K_A = \frac{k_A}{z} \cdot \frac{t_e}{T \cdot (1 - q_Q)} \qquad \textit{Equation 2-7}$$

$$K_{BQ} = \frac{k_B}{(1 - q_Q)(1 - q_B)} - k_B \qquad \textit{Equation 2-8}$$

$$K_{CP} = \frac{k_{CP}}{60} \cdot \frac{t_e}{(1 - q_{rem})(1 - q_{tct})(1 - q_Q)} \qquad \textit{Equation 2-9}$$

$$K_{CS} = \frac{k_{CS}}{60} \cdot \left(\frac{t_e \cdot q_S}{(1 - q_{rem})(1 - q_{tct})(1 - q_Q) \cdot (1 - q_S)} + \frac{T_{su}}{N_0} \right) \qquad \textit{Equation 2-10}$$

$$K_D = \frac{k_D \cdot n_{op}}{60} \cdot \left(\frac{t_e}{(1 - q_{rem})(1 - q_{tct})(1 - q_Q) \cdot (1 - q_S)} + \frac{T_{su}}{N_0} \right) \qquad \textit{Equation 2-11}$$

$$k = K_A + K_{BQ} + K_{CP} + K_{CS} + K_D \qquad \textit{Equation 2-12}$$

$$k_{cm^3} = \frac{k}{V} \qquad \textit{Equation 2-13}$$

Table 2-1. Factors in the integrated part cost equation.

Factor	Description	Unit
k_A	Tool cost	SEK/cutting tool
z	Cutting edges	-
t_e	Engagement time	min
T	Tool life	min
k_B	Workpiece material cost	SEK/part
q_B	Material waste rate	-
q_Q	Rejection rate	-
q_S	Downtime rate	-
q_{rem}	Time loss factor within cycle time	-
q_{tct}	Time loss factor related to tool change	-
k_{CP}	Hourly machines cost during production	SEK/h
k_{CS}	Hourly cost of machines during downtime and setup times	SEK/h
N_0	Nominal batch size	-
T_{su}	Setup time for a batch	min
k_D	Payroll expenses	SEK/h
n_{op}	Number of operators	-
V	Volume of removed material	cm^3

3 Experimental method

This chapter includes the experimental methods and the conditions in the study. The experimental method and the conditions include the workpiece material, the cutting tools tested, the turning equipment and method. The wear tests are performed by turning of the workpiece material with different cutting data. The surface roughness are measured during the machining operations. The microscopy methods used and the equipment are included. Thereafter, in-depth microscopic analysis of selected cutting tools are performed with FIB-SEM and TEM to gather information about chemical wear mechanisms. Theoretical models such as the cost efficiency is presented.

3.1 Workpiece material

The workpiece material used is (α + β)-alloy Ti6Al4V (grade 5). The bar was annealed, the cooling method is not included in the material specification. Table 3-1 presents the element amount according to the supplier material specification.

Table 3-1. Element amount in Ti6Al4V (grade 5) according to supplier material specification. The β-transform temperature is at 980-990°C.

Element	Maximum [%]	Result [%]
Fe	0.40	0.17
C	0.08	0.021
N	0.05	0.006
H	0.015	0.001
O	0.20	0.141
Y	0.005	< 0.005
Al	5.5 - 6.75	6.03
V	3.5 - 4.5	4.05
Residuals	0.10	< 0.10
Ti	Balance	Balance

3.2 Cutting tools

Table 3-2 presents the cutting tools used in the study with the respective geometry and shape, see Figure 2-5 for the geometry and shape. Uncoated cemented carbide, coated cemented carbide, PCD, pcBN are the cutting tool materials used. The cutting tool material content and manufacturing method are confidential, therefore referred to as the cutting tool material group and a number. The shortages used in the study for the cutting tool material are as follows:

- Uncoated Cemented Carbide UCC
- Coated Cemented Carbide CCC
- PCD PCD
- pcBN cBN

Table 3-3 presents the pointed cutting tools and their respective included angle, nose radius and clearance angle.

Table 3-2. Cutting tools used in the study and the corresponding geometry and shape.

Cutting tool	Geometry	Shape
UCC 2	DCMT-F1	Pointed
CCC 1		
PCD 8	DCMW	
cBN 2		
cBN 3	CCMW	

Table 3-3. Pointed cutting tools: included angle, nose radius and clearance angle.

Cutting tool	ε	r_ε [mm]	α
UCC 2	55 °	0.4	7 °
CCC 1			
PCD 8			
cBN 2			
cBN 3	80 °		

3.3 Turning

The machine used for turning is an SMT SAJO, 500 Swedturn, CC 4100, NC-turning machine.

Before starting the data collection, the workpieces were prepared. The workpieces used for pointed cutting tools was machined to achieve a groove close to the chuck, for a clean exit and to be sure of the tool holder not to crash into the revolving chuck. The groove was placed to be able to use as much material of the workpiece as possible. The vertical side towards the tailstock was machined to get a clean surface in order for the entry phase not starting with being intermittent because of a possible uneven surface. The surface in the longitudinal direction was machined in a couple of passes to enable continual machining. See Figure 3-2 for the workpiece machined with pointed cutting tools.

For every test with new cutting data, a new cutting tool edge was used in order to analyze the cutting tool afterwards and connect the wear mechanisms to the wear curve, the surface integrity and the cutting forces.

In order to set the diameter correctly of the workpiece in relation to the coordinates of the turning machine, the diameter was measured with a caliper with an accuracy of 0.05 mm. To correct the machine coordinates, the installed holder with the cutting tool was manually operated in the lathe, as the workpiece rotated with a low rotation speed of approximately 150 rev/min, and moved in the diametric direction to lightly touch the surface of the workpiece. The accuracy of the touching operation was 0.02 mm. Knowing the coordinates of where the cutting tool was touching the surface of the workpiece, the correct coordinates could be programmed.

To follow the flank wear development, the flank wear was measured with a stereo microscope. The photocopy was stored for later analysis. Regarding the machining with the pointed cutting tools, only the cutting tool was removed from the tool holder when the flank wear was measured. The tool holder was installed in a fix position and the cutting tool was installed in the same position due to the tool holder geometry for the cutting tool.

When performing the documented wear tests, the turning machine was programmed as to move down to the correct diameter to be machined considering the previous cut surface and the cutting depth. The feed at which the cutting tool was moved towards the workpiece was 0.1 mm/rev and for the last 1 mm before reaching the correct diameter, the feed was 0.005 mm/rev. This in order to not going to deep axially before the returned value of the reached diameter was sent to the control system, i.e. minimize effects of possible slow feedback. When the correct diameter was reached, the program continued to move with the selected feed in the axial direction. The cutting tool was programmed to move away from the workpiece in the diametric direction at a feed rate of 0.2 mm when the end coordinate was reached. The flank wear measurements were performed more frequently in the beginning of the

machining and at the end of the machining as the flank wear approached the wear criterion of VB = 0.3 mm.

The cutting speed was corrected in the program code of the lathe in order to have the exact spindle speed for the diameter to be machined, as the calculated value when using Equation 2-1.

3.3.1 High-pressure coolant and tool holders

The high-pressure coolant was applied and managed by the integrated system in the lathe. Table 3-4 presents the used coolant pressure for the cutting tool shape. A round shape of a cutting tools provides a better temperature distribution compared to a pointed cutting tool, where the heat generated during the cutting process is located in the nose of the cutting tool – leading to a faster tool deterioration, requiring better cooling and hence, a higher coolant pressure.

Table 3-4. Coolant pressure for the cutting tool shape.

Cutting tool shape	Coolant pressure [bar]
Pointed	90

The cutting fluid used during the machining with the pointed cutting tools contained 8 % oil.

Table 3-5 presents the used jetstream tool holders, the corresponding cutting tool type, cutting tool shape, major cutting edge angle, minor cutting edge angle, rake angle and inclination angle.

Table 3-5. Jetstream holders used, the corresponding cutting tool type, cutting tool shape, major cutting edge angle, minor cutting edge angle, rake angle and inclination angle.

Holder	SDJCL3225P11JET	SCLCL3225P09JET
Jetstream direction: Rake/flank	Yes/No	Yes/No
Cutting tool geometry	DCMT-F1 DCMW	CCMW
Cutting tool shape	Pointed	Pointed
κ	93°	95°
κ_b	32°	5°
γ	0°	0°
λ	0°	0°

One case was tested where the tool life and the corresponding surface roughness was measured for the same cutting tool and cutting data, see Table 3-6. This test was performed to get a sense of the effect from the high-pressure coolant on the specified cutting tool.

Table 3-6. The two different coolant pressures tested and the cutting tool with the corresponding cutting data.

Cutting tool	**a_p [mm]**	**f [mm/rev]**	**v_c [m/min]**	**Coolant pressure [bar]**
UCC 2	0.3	0.10	150	10 and 90

3.3.2 Force acquisition

The cutting forces was measured during the machining with a Kistler piezo-electric 3-components measuring system of type 9129A.

The tool holder was installed on the Kistler measuring device. The force acquisition started when the workpiece was turning and the high-pressure coolant had reached the correct pressure, right before the cutting process was started. This, because there was a minor force increase caused by the rotating workpiece (not during machining) and the applied cutting fluid. The forces acquired was then entirely cutting process based.

The installation of the tool holder and the attached hose for the cutting fluid was installed as not to directly touch the Kistler measuring device before or under the cutting process, in order to minimize disturbances in the force acquisition.

As can be seen in the diagrams in *11 Appendix C – Cutting forces*, the mean cutting force is calculated, using a Matlab script, from the point where the cutting force is stabilized and to the point before the exit phase of the cutting tool from the workpiece.

3.3.3 Rig

Figure 3-1 presents a rig when machining with the round cutting tools, that are not used in this study. The same rig method was used for machining with the pointed cutting tools; the workpiece can be seen in Figure 3-2.

Figure 3-1. Example of rig for machining with round cutting tools, not used in this study. Instead the workpiece seen in Figure 3-2 was rigged in the same way.

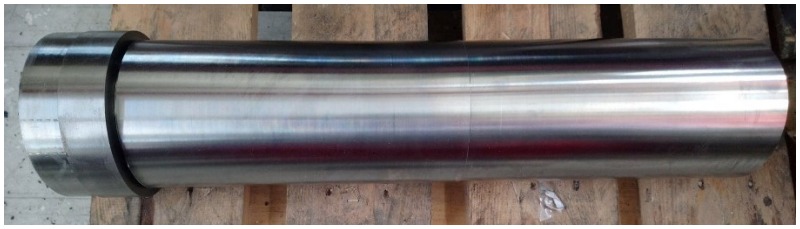

Figure 3-2. Workpiece for machining with the pointed cutting tools.

3.3.4 Cutting data

The cutting data for the pointed cutting tools are selected for finishing operations. For all tests performed, the cutting depth has been a_p = 0.30 mm.

Table 3-7 presents the chosen cutting data for the cutting speed for the pointed cutting tools. The feed for the pointed cutting tools has been selected to f = 0.10 mm/rev.

Table 3-7. Chosen cutting speeds for pointed cutting tools, f = 0.10 mm/rev.

Cutting tool	v_c [m/min]
UCC 2	250
	200
	150
CCC 1	200
	150
PCD 8	350
	300
cBN 2	350
	300
cBN 3	100
	50
	30

3.4 Surface roughness measurement

The surface roughness R_a-value was measured with a MarSurf PS1 on the machined surface. Three measurements was made, distributed evenly on the machined surface, to calculate a mean value. Before starting the measurement, the surface to be measured was cleaned with 95 % ethanol to remove the cutting fluid.

When machining with the pointed cutting tools, the surface roughness was measured for all passes, i.e. the surface roughness was collected with the same interval as the flank wear was measured.

3.5 Microscopy

3.5.1 Flank wear measurement

For measuring the flank wear, the optical stereo microscope Olympus Stream Basic SZX7 was used.

The wear criterion for the pointed cutting tools are presented in Table 3-8. Between each pass, the wear was measured on the flank side of the tool in zone C, see Figure 2-15, in order to follow the tool wear progression. Zone C is selected for the measurement of the flank wear because of the low cutting depth. The maximum flank wear, VB_{max}, of the cutting tool is selected for representing the flank wear, instead of the average flank wear. Considering the time required for testing and gathering data for the flank wear progression, measuring the average flank wear would be too time consuming. See Figure 3-3 for an example of the selection of the maximum flank wear for the pointed cutting tools.

The flank wear can be plotted as a function of both engagement time and engagement distance. When comparing two or more flank wear curves, the flank wear is plotted as a function of the engagement distance if different cutting speeds are used; the flank wear is plotted as a function of the engagement time if different feeds are used. The photocopy of the wear on both flank and rake side were documented.

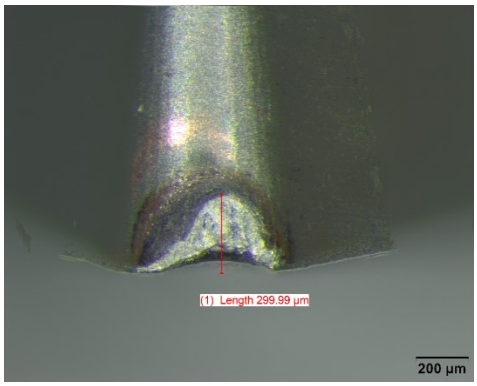

Figure 3-3. Example of measurement of the flank wear for pointed cutting tools.

Table 3-8. Cutting tool shape and the respective wear criterion.

Cutting tool shape	Wear criterion, VB_{max} [mm]
Pointed	0.30

3.5.2 Rake wear measurement

To copy the topography of the worn edge in order to measure and study the rake wear, the program LaboratoryMeasurementModule 5.1 in the Alicona Infinite Focus microscope was used. The rake wear was studied for the listed cutting tools and cutting speeds in Table 3-9. The cutting tools was mounted in a tool holder to have the same fixture for each measurement. The cutting tools were studied as the wear criterion was reached.

Table 3-9. Cutting tools and the cutting speeds on which the rake wear was studied.

Cutting tool	Cutting speed [m/min]
UCC 2	250
	200
	150
CCC 1	200
	150
PCD 8	350
	300
cBN 2	350
	300

3.5.3 FIB-SEM

The SEM analysis was performed as to scan the views of the worn cutting tools. The tools and the respective cutting speed examined with SEM is presented in Table 3-10. The views selected is the flank side, the rake side and on the nose of the edge at approximately 45 ° from the rake side. The magnification used was 200x. The cutting tools were cleaned with isopropanol and dried with N_2 before installation in the SEM.

For SEM analysis and preparation for TEM by using FIB, a FEI Nova NanoLab 600 was used. It has a combined focused ion beam and scanning electron microscope with ultra-high resolution with gas injection sources (Pt, W, Au, SiO_x) available. An omniprobe nanomanipulator is available and used for the FIB-operations.

The SEM analysis and FIB preparation was performed at Lund Nano Lab, part of the division of Solid State Physics at Lund University and the NanoLund Consortium, in a cleanroom environment class ISO 5.

Table 3-10. Cutting tools and the respective cutting speeds on which SEM was performed.

Cutting tool	Cutting speed [m/min]
UCC 2	250
	200
	150
PCD 8	350
	300
cBN 2	350
	300

The pointed cutting tools used in the SEM analysis represent a range of ultra-hard cutting tools with different material compositions. The cutting tool CCC 1 was not used in the SEM analysis due to inferior performance compared to the cutting tool UCC 2. cBN 3 was not used in the SEM analysis due to poor performance.

The tools and the respective cutting speed prepared for TEM using FIB are presented in Table 3-11.

Table 3-11. Cutting tools and the respective cutting speeds on which sample preparation with FIB for later TEM analysis was performed.

Cutting tool	Cutting speed [m/min]
PCD 8	350
cBN 2	300

To prepare for TEM analysis, the cutting tools from Table 3-11 were cleaned with the same procedure as for the SEM analysis.

The milling with FIB was performed as to pick a location of where to remove a small part of the cutting tool, in the shape of a lamella. A deposition of Pt was placed on

the surface and the cutting tool material was removed on each side of the deposition by etching. The material was removed around the material that would become a lamella, except for two small pieces on the side of the Pt deposition. The probe was placed on the Pt deposition and further Pt was deposed on both the lamella and the tip of the probe to bind the lamella to the probe. The remaining material holding the lamella to the cutting tool was removed by etching and the lamella was moved to a Cu-grid and fastened on it with Pt-deposition. The Pt binding the lamella with the probe was removed by etching. The lamella was etched on both sides to achieve smooth and parallel surfaces and to get the desired thickness.

3.5.4 TEM

The TEM analysis was performed at The National Center for High Resolution Electron Microscopy (nCHREM) at the Chemical Center at Lund University. The equipment used was a JEOL 3000F Field Emission Electron Microscope.

Table 3-11 presents the cutting tools and the respective cutting speeds used for TEM analysis. These cutting tools were selected for which the interest in machining in titanium alloys are increasing. The cutting speeds used are not the same – the selection criteria was for a similar engagement time.

3.6 Cost efficiency

To connect the machining performance (tool life and volume of removed material) to the cutting tool cost and the number of available cutting edges per cutting tool, Equation 2-13 was used. The selected values of the factors in the integrated part cost equation are presented in Table 3-13. Simplifications have been made; all factors except those connected to the cutting tool have been set to zero. The integrated cost model can model a variety of cases – this is not of interest for this study, since no given production scenario is given. Therefore, no sensitivity analysis is performed. The values of the factors, beside those presented in Table 3-13 are the tool life, the volume of the removed material, the number of available cutting edges and the tool cost. The latter is not presented and similar values to the cutting tool cost is used in the calculations of the cost efficiency. The cost efficiency is performed on the cutting tools where the prices has been shared with the author.

Table 3-12 presents the cutting tools and the respective cutting data on which cost efficiency is performed.

Table 3-12. Cutting tools, cutting data, acquired tool life and the volume of removed material – the tool life and the volume of removed material are used in the integrated part cost model.

Cutting tool	Feed [mm/rev]	Cutting speed [m/min]
UCC 2	0.10	250 200 150
CCC 1	0.10	200 150
PCD 8	0.10	350 300

Table 3-13. The factors in the integrated part cost equation and the used values.

Factor	Description	Given value
k_A	Tool cost	Cutting tool dependent
z	Cutting edges	Cutting tool dependent
t_e	Engagement time	60 min
T	Tool life	Cutting tool dependent
k_B	Workpiece material cost	0 SEK/part
q_B	Material waste rate	0
q_Q	Rejection rate	0
q_S	Downtime rate	0
q_{rem}	Time loss factor within cycle time	0
q_{tct}	Time loss factor related to tool change	0
k_{CP}	Hourly machines cost during production	0 SEK/h
k_{CS}	Hourly cost of machines during downtime and setup times	0 SEK/h
N_0	Nominal batch size	1
T_{su}	Setup time for a batch	0 min
k_D	Payroll expenses	0 SEK/h
n_{op}	Number of operators	1
V	Volume of removed material	Cutting tool dependent

4 Results

This chapter presents the results acquired or calculated in the study. Included in the chapter is the equivalent chip thickness, the achieved tool life, surface roughness, volume of removed material and calculated material removal rate as well as flank wear development and the final rake wear. Photocopies of the worn cutting tools are presented to visualize the type of wear, and photos of selected cutting tools analyzed with SEM are presented as well as the results from the TEM analysis. The cutting forces acquired can be found in 11 Appendix C – Cutting forces*. The graphs for the cost efficiency for selected cutting tools are presented.*

If there is interest of the reader, all acquired results not suitable in the main report can be found in appendix A to C. Considering the amount of material in the appendixes, not all figures will be referred to in the report.

4.1 Tool life, surface roughness and material removal rate

This section presents acquired tool life, surface roughness and the calculated material removal rate (using Equation 2-4) for the respective cutting data. See *9 Appendix A – Tool life, surface roughness and material removal rate* for the data in graphs.

Table 4-1 presents the tool life and the maximum value of the surface roughness acquired for the respective cutting data and cutting tool of the pointed cutting tools.

Table 4-1. Tool life, surface roughness (maximum) and material removal rate for the respective cutting data (a_p = 0.30 mm, f = 0.10 mm/rev) for the pointed cutting tools.

Cutting tool	**v_c [m/min]**	**T [min]**	**$R_{a,max}$ [µm]**	**MRR [cm^3/min]**
UCC 2	250	1.9	1.25	7.5
	200	4.0	1.37	6.0
	150	23.7	1.15	4.5
CCC 1	200	1.6	0.91	6.0
	150	8.3	1.14	4.5
PCD 8	350	7.8	1.22	10.5
	300	30.0	1.40	9.0
cBN 2	350	3.3	1.57	10.5
	300	5.7	1.11	9.0
cBN 3	100	0.8	1.37	3.0
	50	1.7	1.04	1.5
	30	2.5	3.56	0.9

4.1.1 Coolant pressure test

This section presents the acquired tool life and maximum value of the surface roughness for the two tested coolant pressures using the pointed cutting tool UCC 2, which can be seen in Figure 4-1.

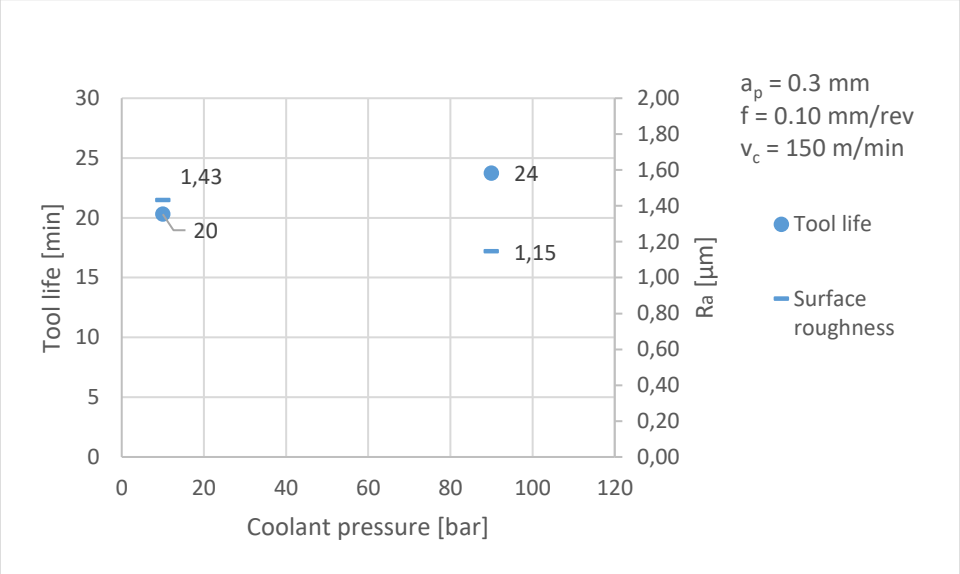

Figure 4-1. Tool life and surface roughness (maximum value acquired) as a function of the coolant pressure when machining with the pointed cutting tool UCC 2.

4.2 Tool wear

This section presents the flank wear as a function of engagement time and engagement distance and includes images of the worn cutting tools viewing both flank wear and rake wear when the wear criterion was reached or passed. The section also presents the height difference in the rake wear. See *10 Appendix B – Flank wear curves* for all tool flank wear curves including the tool wear criterion. Note that the surface roughness is measured with the same interval as the flank wear for the pointed cutting tools, which can be found in the previously referred appendix.

The feed direction for the below cutting tools is to the right.

4.2.1 UCC 2

Figure 4-2 presents the flank wear development for the cutting tool UCC 2 and Figure 4-12 presents the flank wear development for the lower coolant pressure. The flank wear and rake wear as the wear criterion is reached or passed are presented in Figure 4-3, Figure 4-6 and Figure 4-9 for the respective cutting data. Figure 4-13 presents the flank wear and rake wear for the lower coolant pressure.

Figure 4-4, Figure 4-7 and Figure 4-10 presents the scanned views in the Alicona of the worn cutting tools for the respective cutting data. Figure 4-14 presents the scanned views in the Alicona of the worn cutting tools for the lower coolant pressure.

Figure 4-5, Figure 4-8 and Figure 4-11 presents the rake wear height difference. Figure 4-15 presents the rake wear height difference for the lower coolant pressure.

Flank wear and rake wear is present in all tested sets of cutting data for this cutting tool.

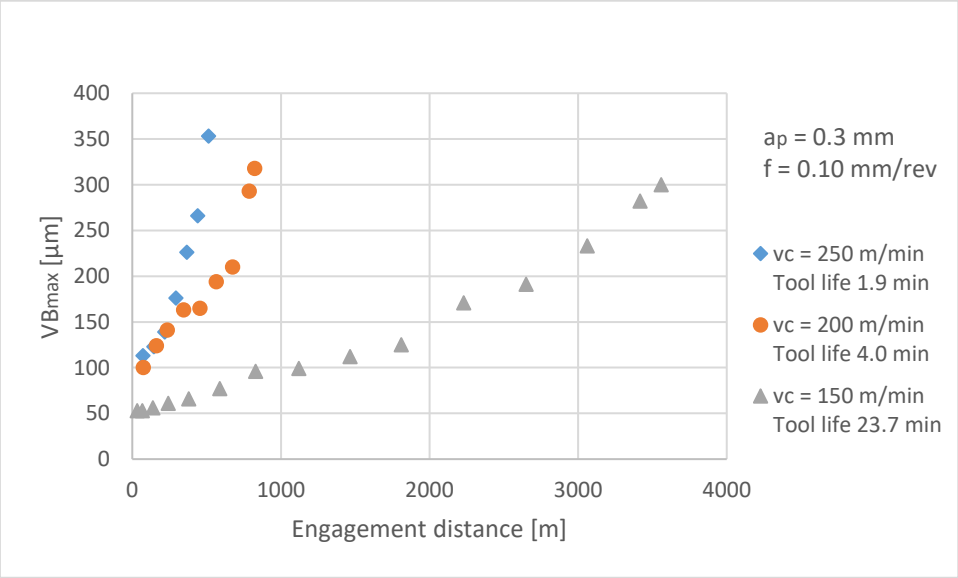

Figure 4-2. UCC 2: The flank wear development as a function of the engagement distance for the cutting data and tool life: a_p = 0.3 mm, f = 0.10 mm/rev, v_c = 250//200//150 m/min, T = 1.9//4.0//23.7 min.

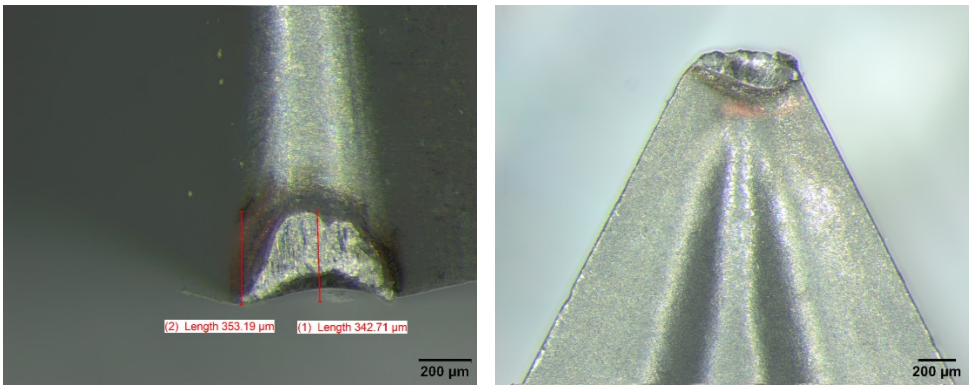

Figure 4-3. UCC 2: Flank wear (left) and rake wear (right). a_p = 0.3 mm, f = 0.10 mm/rev, v_c = 250 m/min, T = 1.9 min.

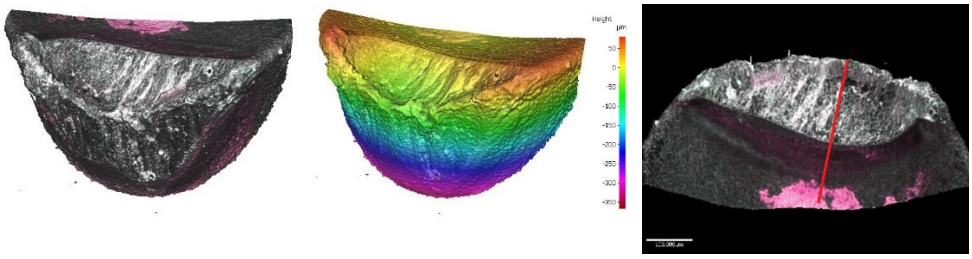

Figure 4-4. UCC 2: Alicona scanned views (left and middle) and the rake wear with the line on which the height difference is measured (right). a_p = 0.3 mm, f = 0.10 mm/rev, v_c = 250 m/min, T = 1.9 min.

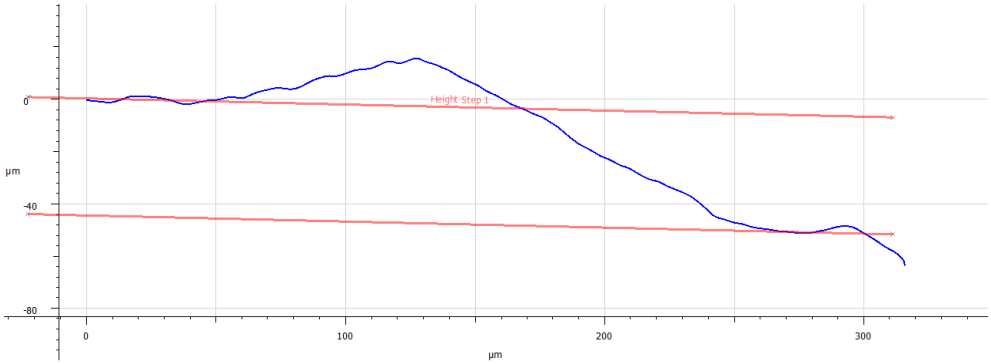

Figure 4-5. UCC 2: Rake wear – height difference = 45 µm.

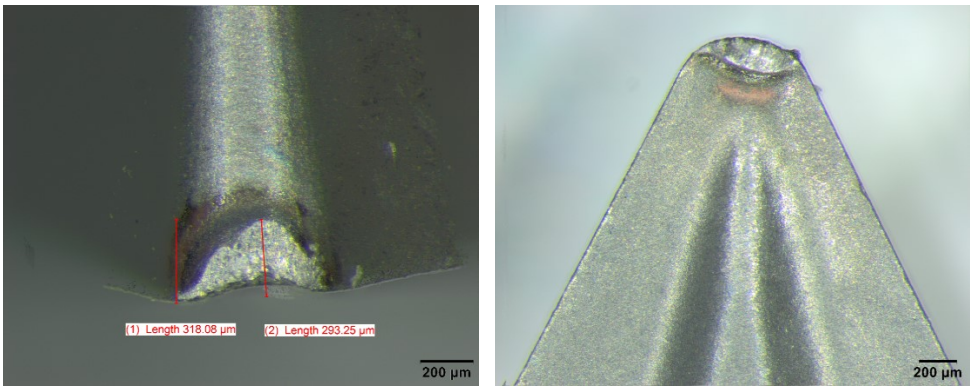

Figure 4-6. UCC 2: Flank wear (left) and rake wear (right).
a_p = 0.3 mm, f = 0.10 mm/rev, v_c = 200 m/min, T = 4.0 min.

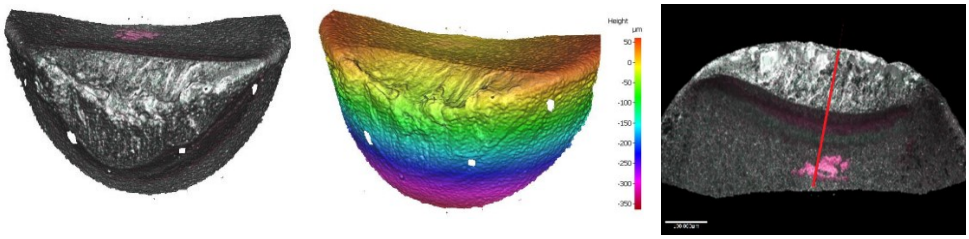

Figure 4-7. UCC 2: Alicona scanned views (left and middle) and the rake wear with the line on which the height difference is measured (right). a_p = 0.3 mm, f = 0.10 mm/rev, v_c = 200 m/min, T = 4.0 min.

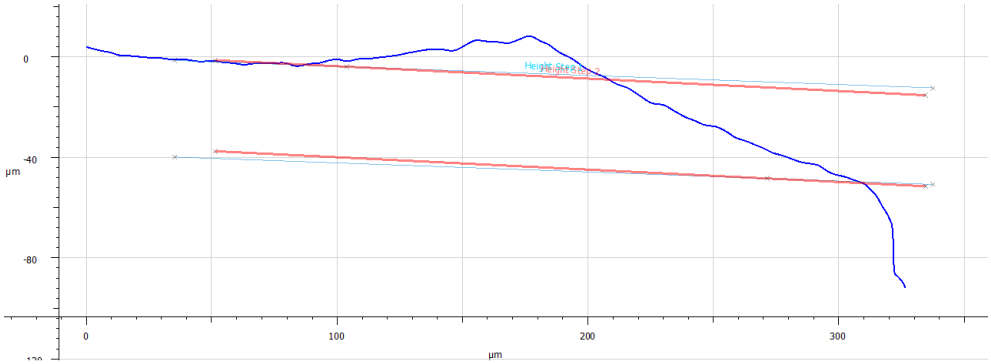

Figure 4-8. UCC 2: Rake wear – height difference = 38 µm.

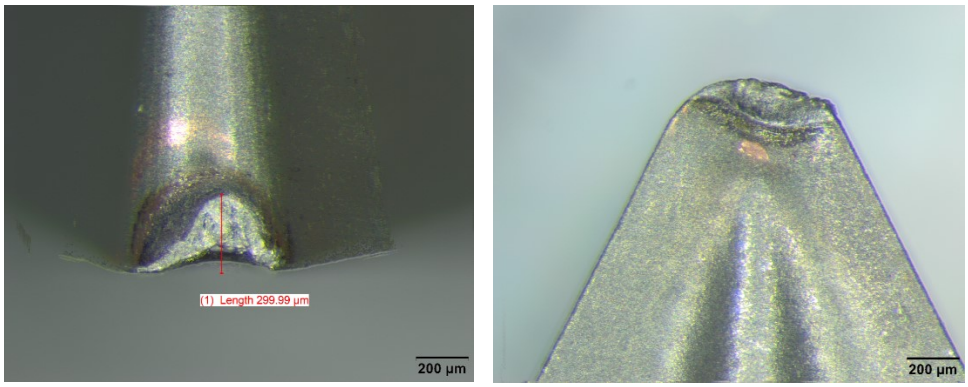

Figure 4-9. UCC 2: Flank wear (left) and rake wear (right).
a_p = 0.3 mm, f = 0.10 mm/rev, v_c = 150 m/min, T = 23.7 min. Coolant pressure = 90 bar.

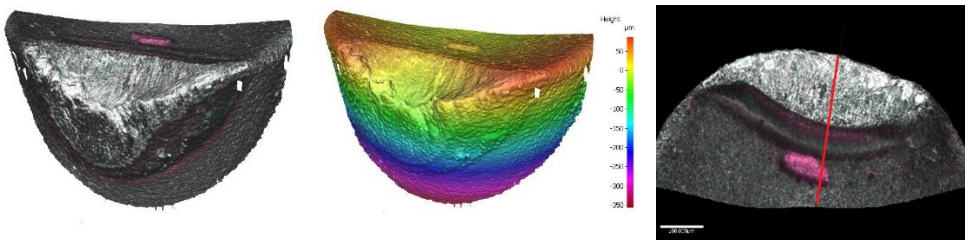

Figure 4-10. UCC 2: Alicona scanned views (left and middle) and the rake wear with the line on which the height difference is measured (right). a_p = 0.3 mm, f = 0.10 mm/rev, v_c = 150 m/min, T = 23.7 min. Coolant pressure = 90 bar.

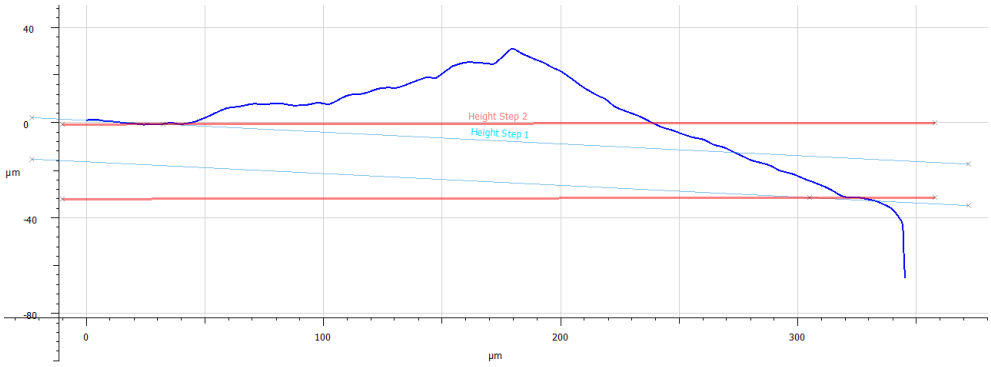

Figure 4-11. UCC 2: Rake wear – height difference = 32 µm.

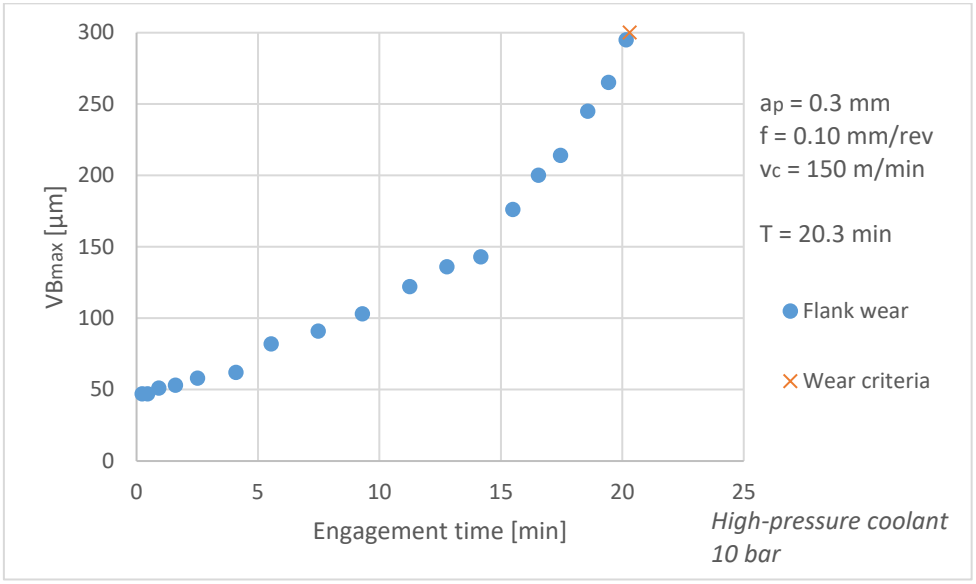

Figure 4-12. UCC 2: The flank wear development as a function of the engagement time for the cutting data and tool life: a_p = 0.3 mm, f = 0.10 mm/rev, v_c = 150 m/min, T = 20.3 min. Coolant pressure = 10 bar.

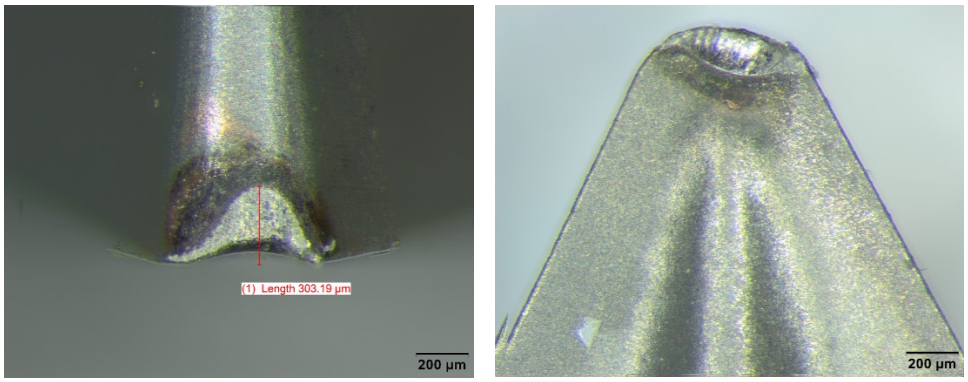

Figure 4-13. UCC 2: Flank wear (left) and rake wear (right). a_p = 0.3 mm, f = 0.10 mm/rev, v_c = 150 m/min, T = 20.3 min. Coolant pressure = 10 bar.

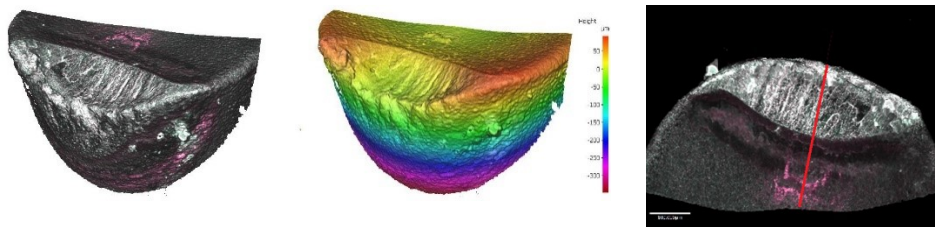

Figure 4-14. UCC 2: Alicona scanned views (left and middle) and the rake wear with the line on which the height difference is measured (right). a_p = 0.3 mm, f = 0.10 mm/rev, v_c = 150 m/min, T = 20.3 min. Coolant pressure = 10 bar.

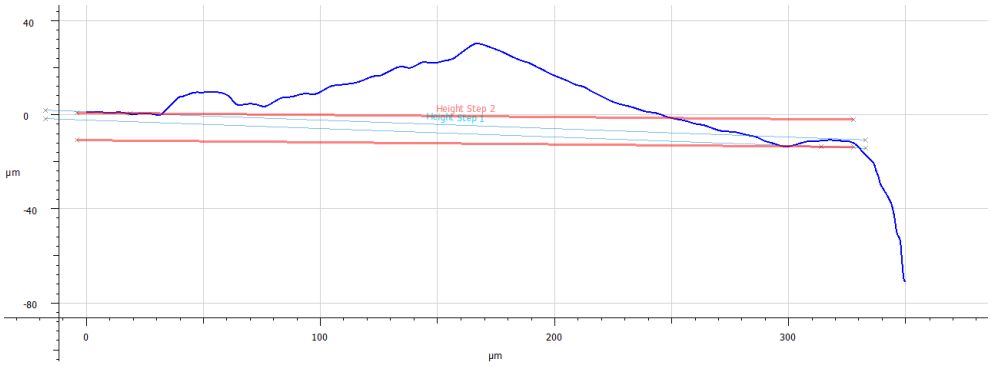

Figure 4-15. UCC 2: Rake wear – height difference = 12 µm.

4.2.2 CCC 1

Figure 4-16 presents the flank wear development for the cutting tool CCC 1. The flank wear and rake wear as the wear criterion is reached or passed are presented in Figure 4-17 and Figure 4-20 for the respective cutting data.

Figure 4-18 and Figure 4-21 presents the scanned views in the Alicona of the worn cutting tools for the respective cutting data.

Figure 4-19 and Figure 4-22 presents the rake wear height difference.

Breakage of the cutting tool on the flank side is present for v_c = 200 m/min, which is indicated by the rapid increase of VB_{max} in Figure 4-16. Otherwise, rake wear is present for both tested cutting data sets. For the cutting speed v_c = 150 m/min flank wear is present.

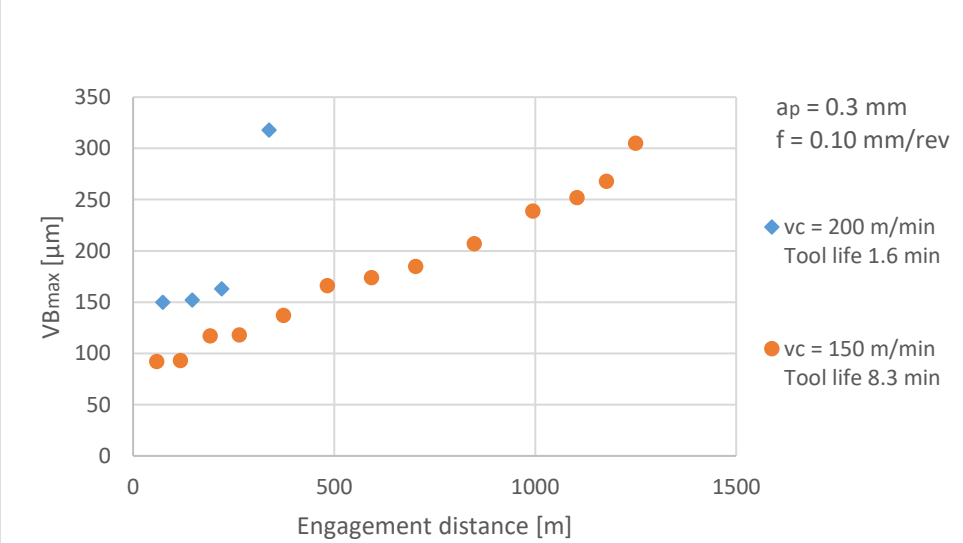

Figure 4-16. CCC 1: The flank wear development as a function of the engagement distance for the cutting data and tool life: a_p = 0.3 mm, f = 0.10 mm/rev, v_c = 200//150 m/min, T = 1.6//8.3 min.

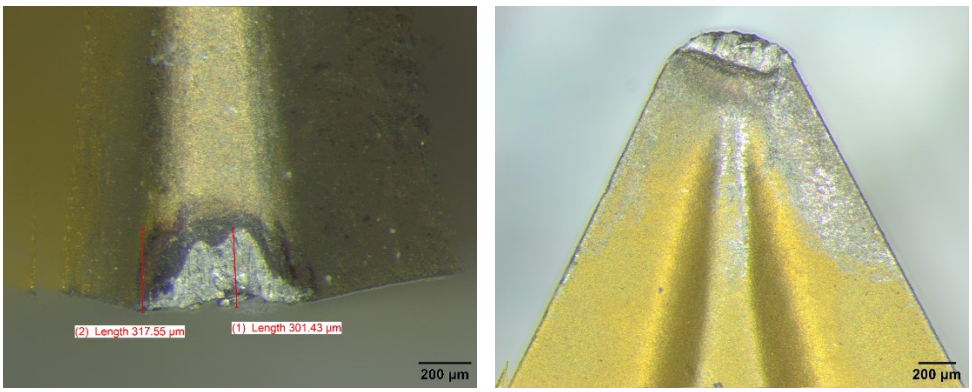

Figure 4-17. CCC 1: Flank wear (left) and rake wear (right).
a_p = 0.3 mm, f = 0.10 mm/rev, v_c = 200 m/min, T = 1.6 min.

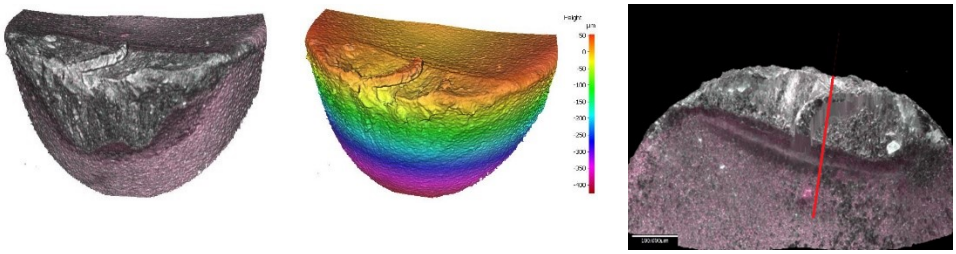

Figure 4-18. CCC 1: Alicona scanned views (left and middle) and the rake wear with the line on which the height difference is measured (right). a_p = 0.3 mm, f = 0.10 mm/rev, v_c = 200 m/min, T = 1.6 min.

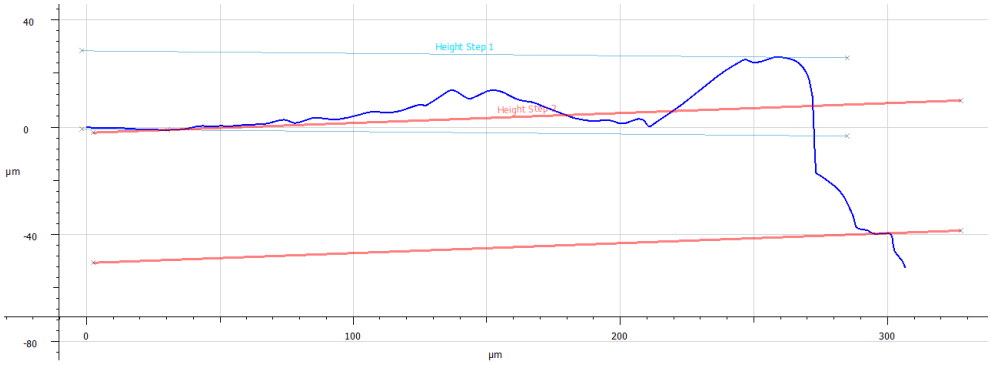

Figure 4-19. CCC 1: Rake wear – height difference step 1 = 29 µm, step 2 = 49 µm.

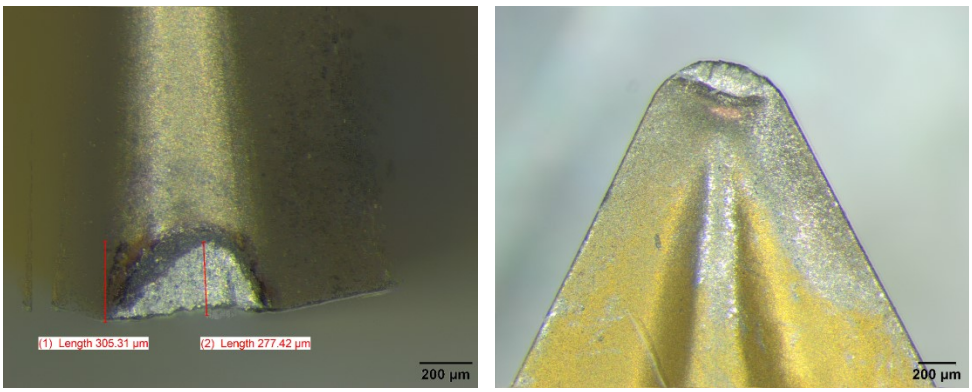

Figure 4-20. CCC 1: Flank wear (left) and rake wear (right).
a_p = 0.3 mm, f = 0.10 mm/rev, v_c = 150 m/min, T = 8.3 min.

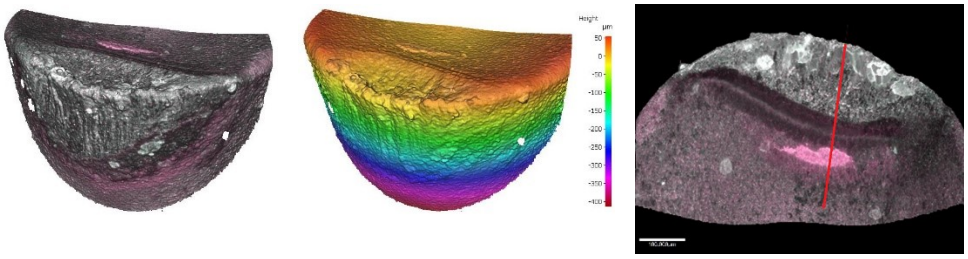

Figure 4-21. CCC 1: Alicona scanned views (left and middle) and the rake wear with the line on which the height difference is measured (right). a_p = 0.3 mm, f = 0.10 mm/rev, v_c = 150 m/min, T = 8.3 min.

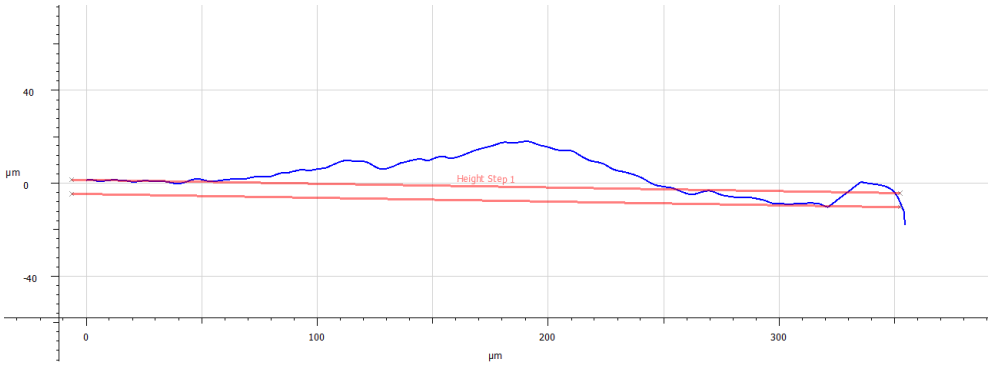

Figure 4-22. CCC 1: Rake wear – height difference = 6 µm.

4.2.3 PCD 8

Figure 4-23 presents the flank wear development for the cutting tool PCD 8. The flank wear and rake wear as the wear criterion is reached or passed are presented in Figure 4-24 and Figure 4-27 for the respective cutting data.

Figure 4-25 and Figure 4-28 presents the scanned views in the Alicona of the worn cutting tools for the respective cutting data.

Figure 4-26 and Figure 4-29 presents the rake wear height difference.

Flank wear and rake wear is present in all tested sets of cutting data for this cutting tool.

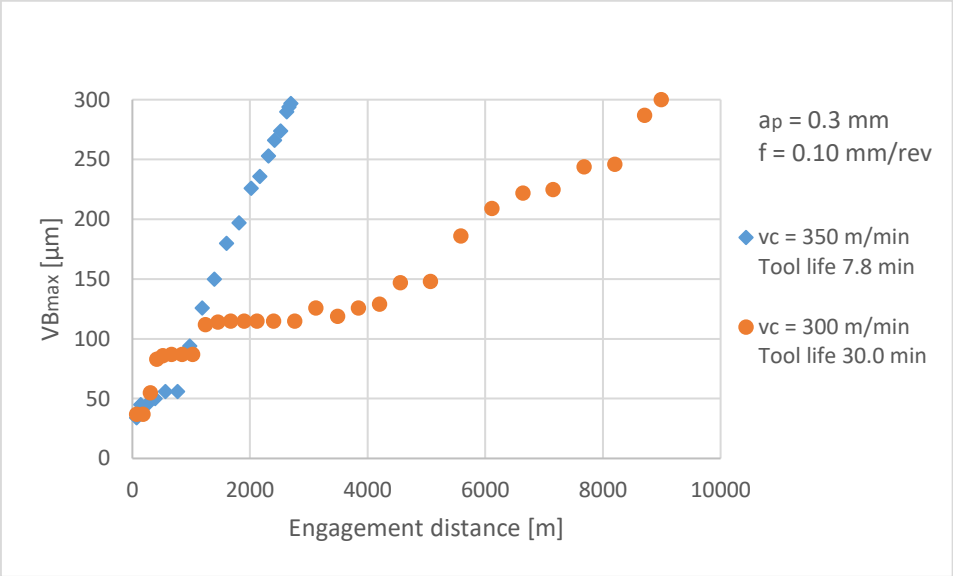

Figure 4-23. PCD 8: The flank wear development as a function of the engagement distance for the cutting data and tool life: a_p = 0.3 mm, f = 0.10 mm/rev, v_c = 350//300 m/min, T = 7.8//30.0 min.

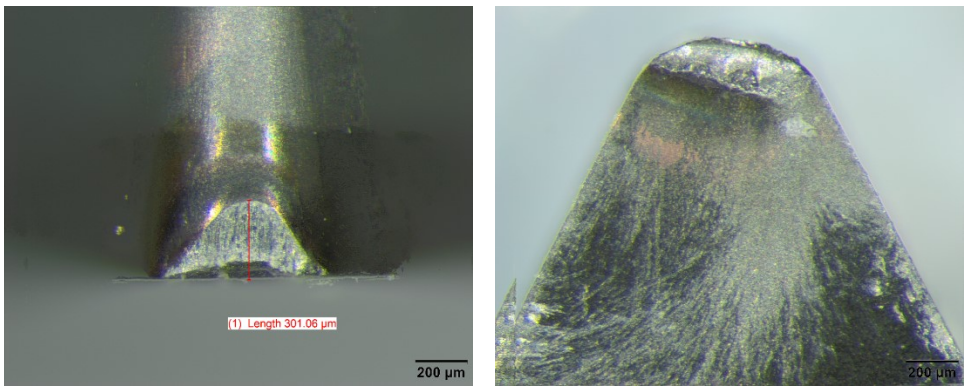

Figure 4-24. PCD 8: Flank wear (left) and rake wear (right). a_p = 0.3 mm, f = 0.10 mm/rev, v_c = 350 m/min, T = 7.8 min.

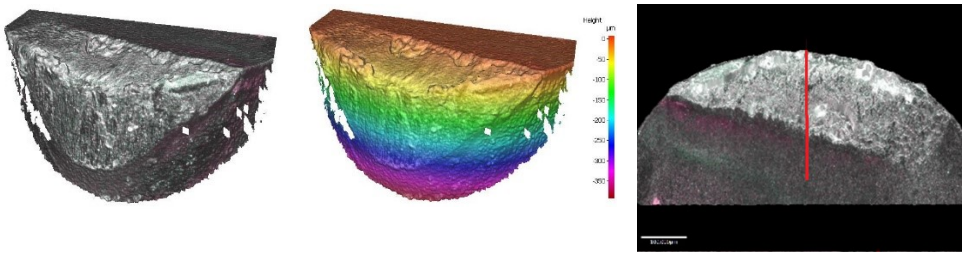

Figure 4-25. PCD 8: Alicona scanned views (left and middle) and the rake wear with the line on which the height difference is measured (right). a_p = 0.3 mm, f = 0.10 mm/rev, v_c = 350 m/min, T = 7.8 min.

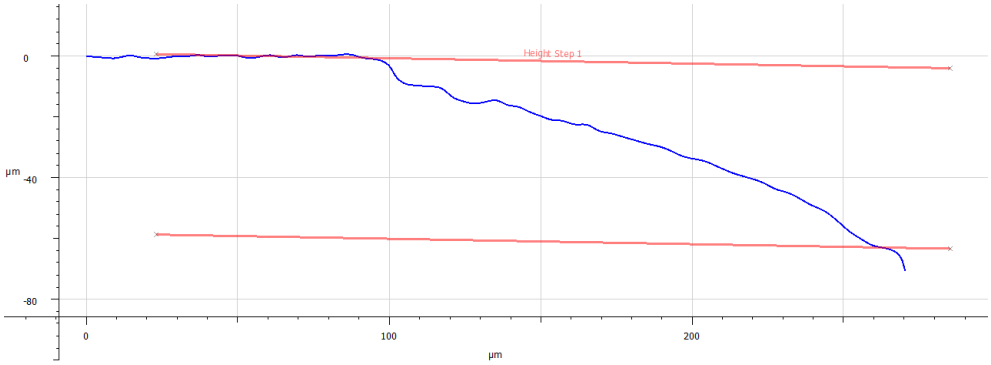

Figure 4-26. PCD 8: Rake wear – height difference = 60 µm.

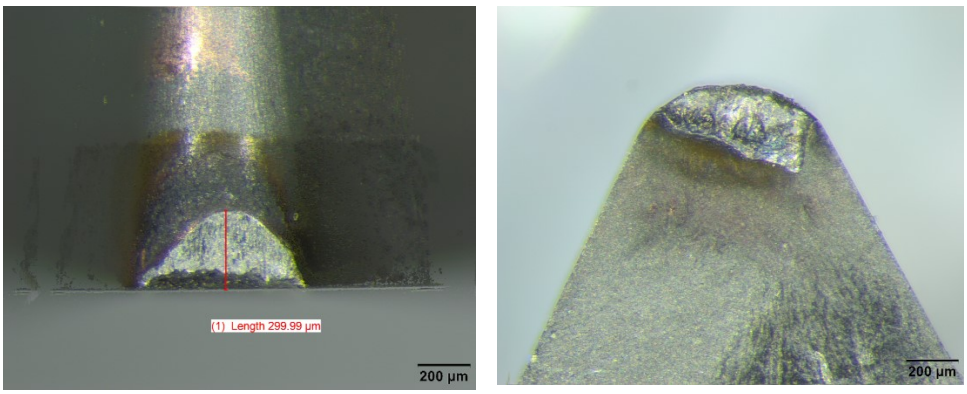

Figure 4-27. PCD 8: Flank wear (left) and rake wear (right). a_p = 0.3 mm, f = 0.10 mm/rev, v_c = 300 m/min, T = 30.0 min.

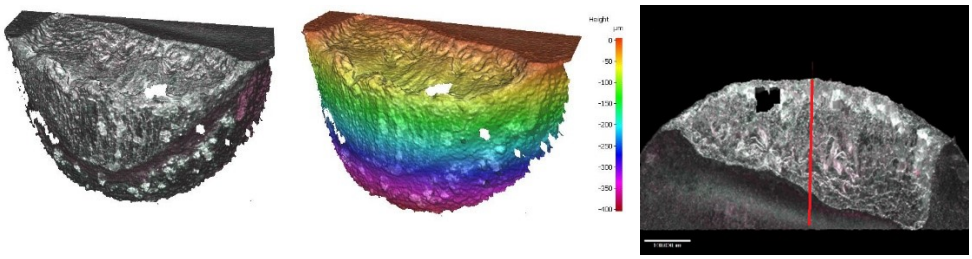

Figure 4-28. PCD 8: Alicona scanned views (left and middle) and the rake wear with the line on which the height difference is measured (right). a_p = 0.3 mm, f = 0.10 mm/rev, v_c = 300 m/min, T = 30.0 min.

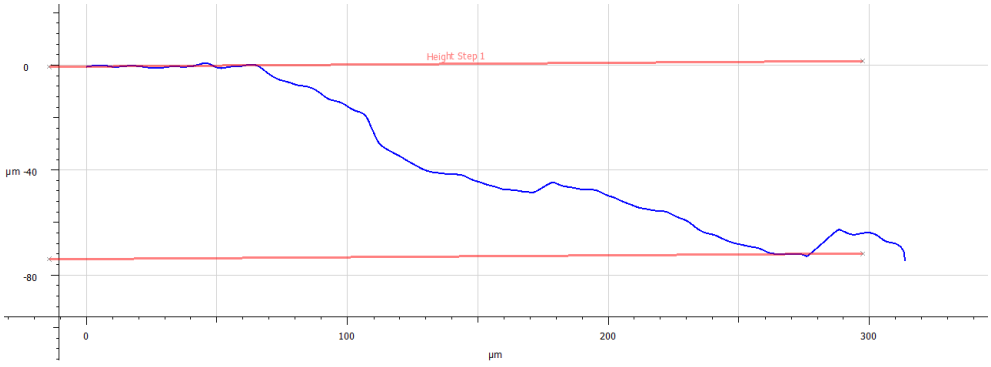

Figure 4-29. PCD 8: Rake wear – height difference = 74 µm.

4.2.4 cBN 2

Figure 4-30 presents the flank wear development for the cutting tool cBN 2. The flank wear and rake wear as the wear criterion is reached or passed are presented in Figure 4-31 and Figure 4-34 for the respective cutting data.

Figure 4-32 and Figure 4-35 presents the scanned views in the Alicona of the worn cutting tools for the respective cutting data.

Figure 4-33 and Figure 4-36 presents the rake wear height difference.

Breakage of the cutting tool on the flank side is present for v_c = 350 m/min, which is indicated by the rapid increase of VB_{max} in Figure 4-30. Otherwise, rake wear is present for both tested cutting data sets. For the cutting speed v_c = 300 m/min flank wear is present.

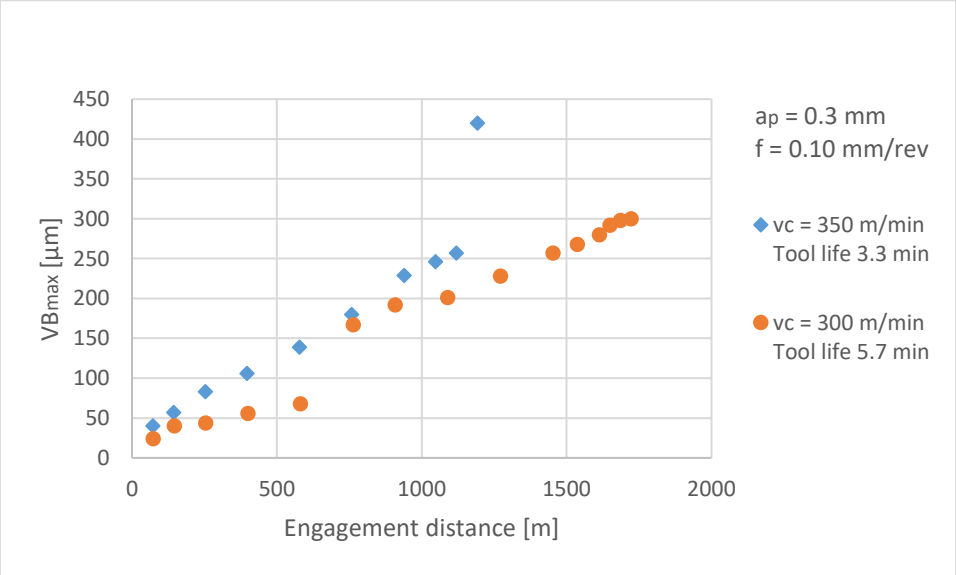

Figure 4-30. cBN 2: The flank wear development as a function of the engagement distance for the cutting data and tool life: a_p = 0.3 mm, f = 0.10 mm/rev, v_c = 350//300 m/min, T = 3.3//5.7 min.

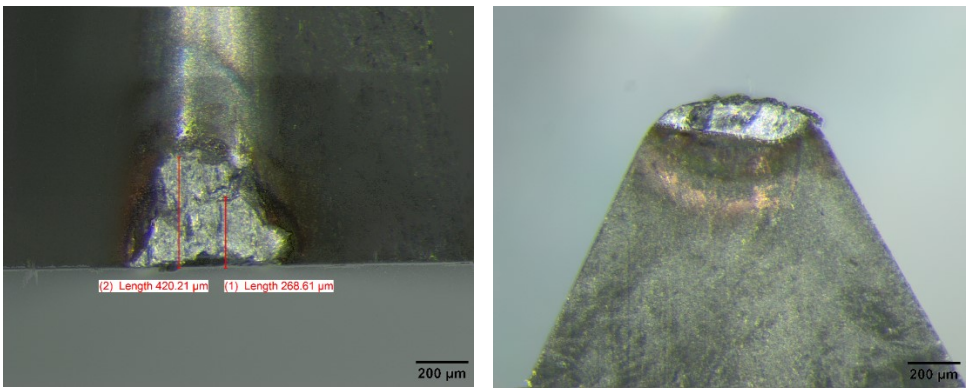

Figure 4-31. cBN 2: Flank wear (left) and rake wear (right). a_p = 0.3 mm, f = 0.10 mm/rev, v_c = 350 m/min, T = 3.3 min.

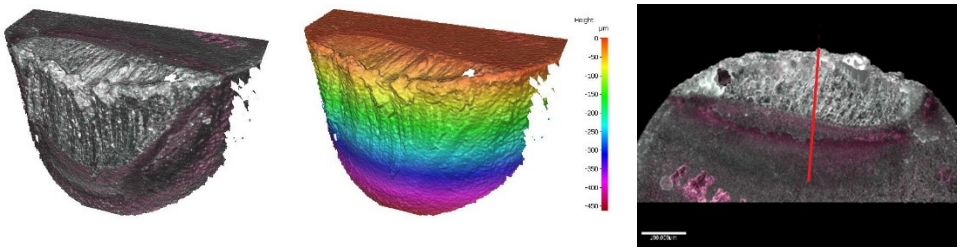

Figure 4-32. cBN 2: Alicona scanned views (left and middle) and the rake wear with the line on which the height difference is measured (right). a_p = 0.3 mm, f = 0.10 mm/rev, v_c = 350 m/min, T = 3.3 min.

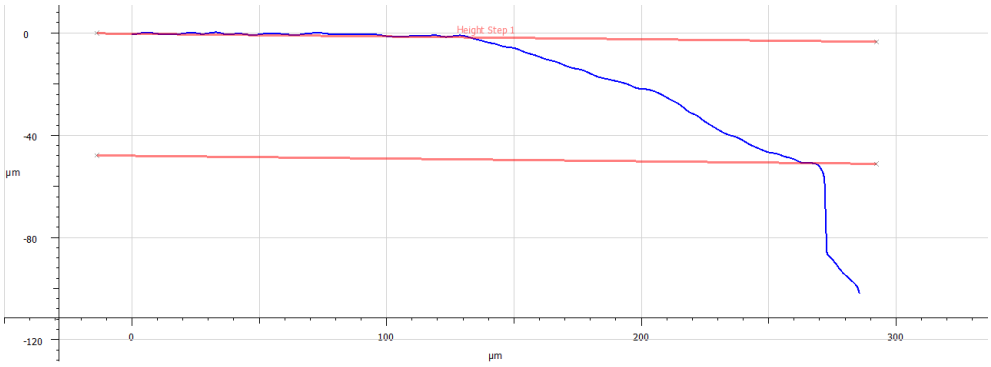

Figure 4-33. cBN 2: Rake wear – height difference = 48 µm.

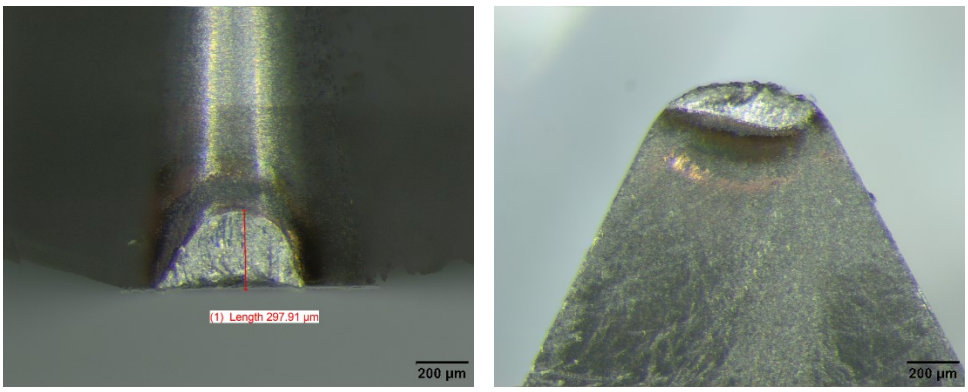

Figure 4-34. cBN 2: Flank wear (left) and rake wear (right). a_p = 0.3 mm, f = 0.10 mm/rev, v_c = 300 m/min, T = 5.7 min.

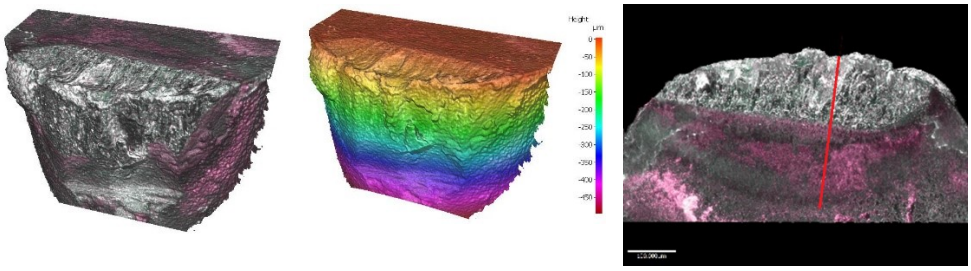

Figure 4-35. cBN 2: Alicona scanned views (left and middle) and the rake wear with the line on which the height difference is measured (right). a_p = 0.3 mm, f = 0.10 mm/rev, v_c = 300 m/min, T = 5.7 min.

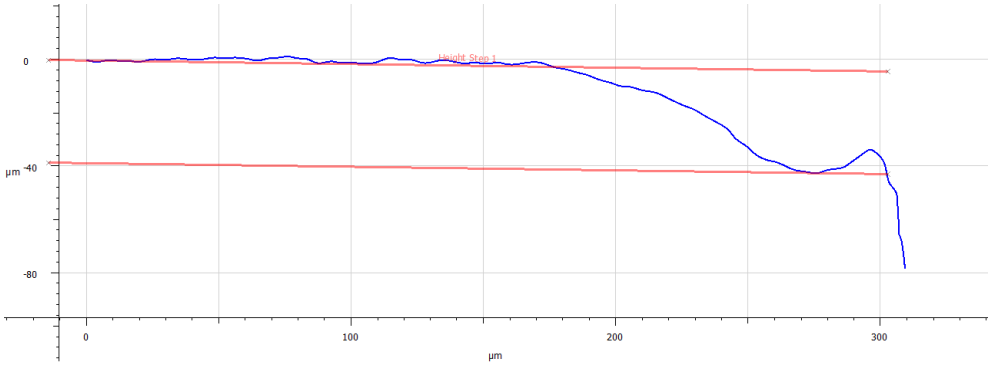

Figure 4-36. cBN 2: Rake wear – height difference = 39 µm.

4.2.5 cBN 3

Figure 4-37 presents the wear development on the flank side for the cutting tool cBN 3. The flank wear and rake wear as the wear criterion is reached or passed are presented in Figure 4-38, Figure 4-39 and Figure 4-40 for the respective cutting data.

For v_c = 100 m/min, fracture of the cutting tool is present. For v_c = 50 m/min and v_c = 30 m/min, notch wear is present.

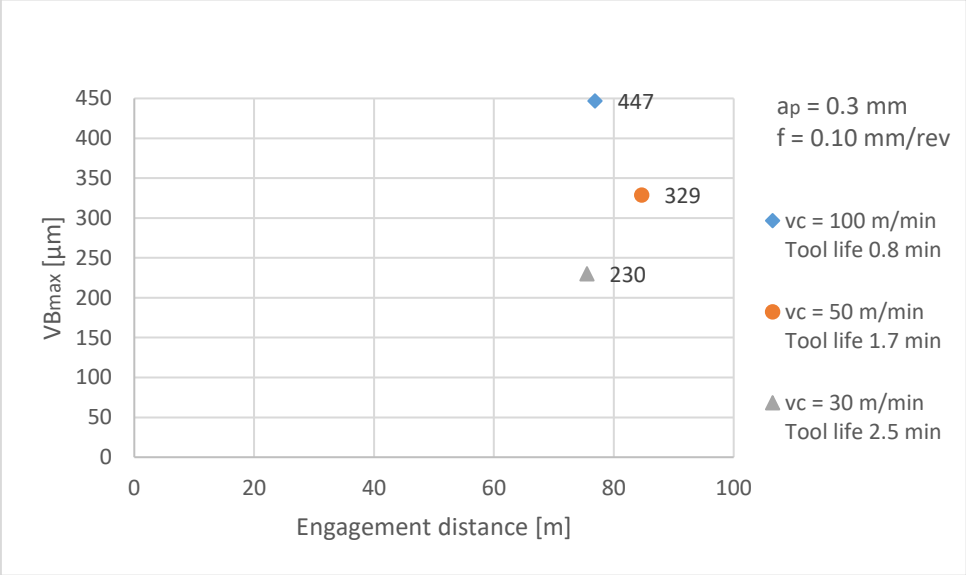

Figure 4-37. cBN 3: The flank wear development as a function of the engagement distance for the cutting data and tool life: a_p = 0.3 mm, f = 0.10 mm/rev, v_c = 100//50//30 m/min, T = 0.8//1.7//2.5 min.

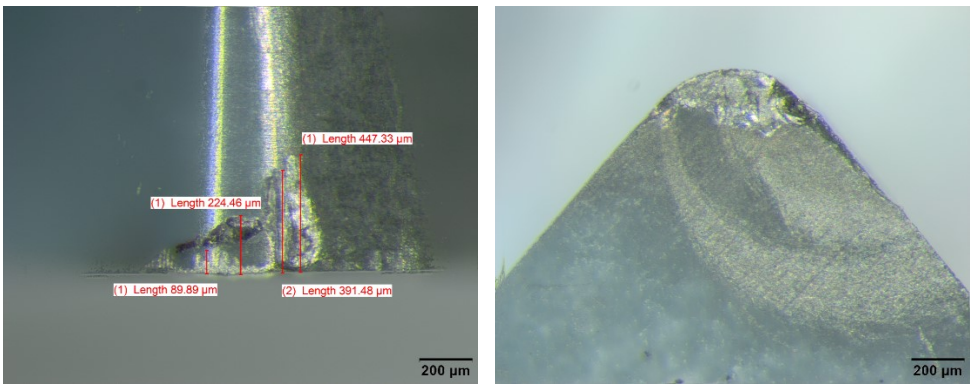

Figure 4-38. cBN 3: Flank wear (left) and rake wear (right). a_p = 0.3 mm, f = 0.10 mm/rev, v_c = 100 m/min, T = 0.8 min.

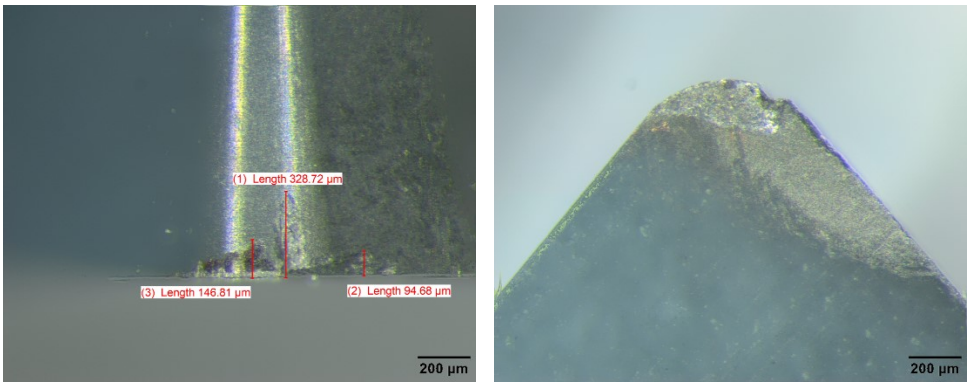

Figure 4-39. cBN 3: Flank wear (left) and rake wear (right). a_p = 0.3 mm, f = 0.10 mm/rev, v_c = 50 m/min, T = 1.7 min.

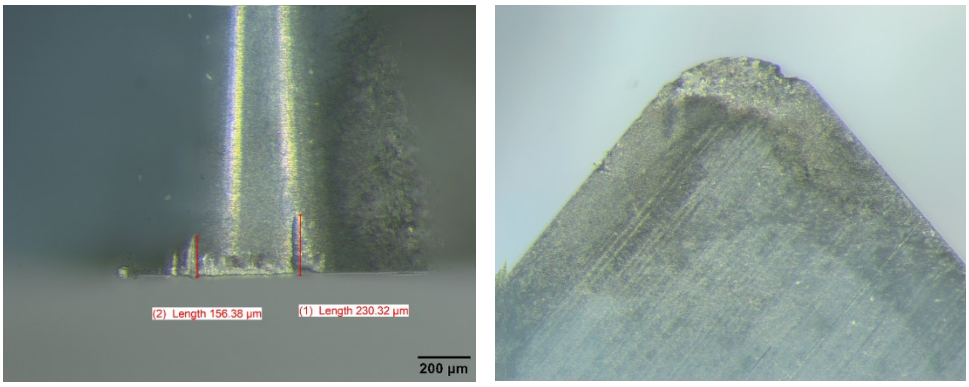

Figure 4-40. cBN 3: Flank wear (left) and rake wear (right). a_p = 0.3 mm, f = 0.10 mm/rev, v_c = 30 m/min, T = 2.5 min.

4.3 SEM

This section to presents the worn cutting tools in more in-depth views of the surfaces by the use of a SEM. The views presented are both flank wear and rake wear (left), flank wear (middle) and rake wear (right).

4.3.1 UCC 2

Figure 4-41 to Figure 4-44 presents the SEM views for the cutting tool UCC 2.

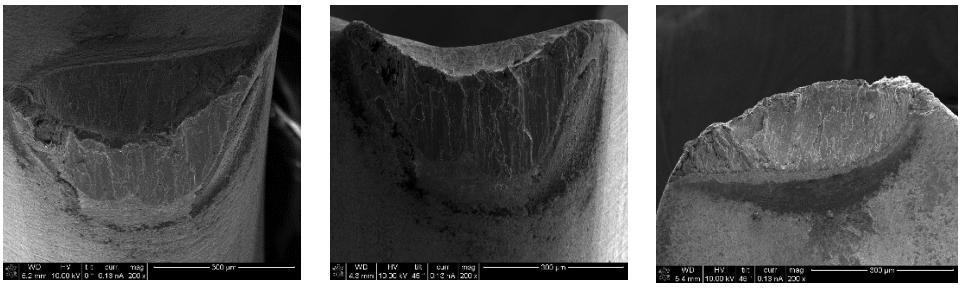

Figure 4-41. UCC 2: SEM views for cutting tool machined with v_c = 250 m/min.

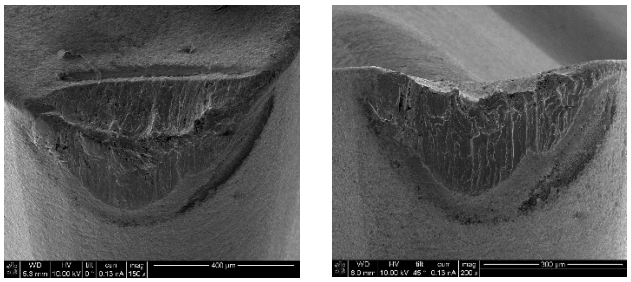

Figure 4-42. UCC 2: SEM views for cutting tool machined with v_c = 200 m/min.

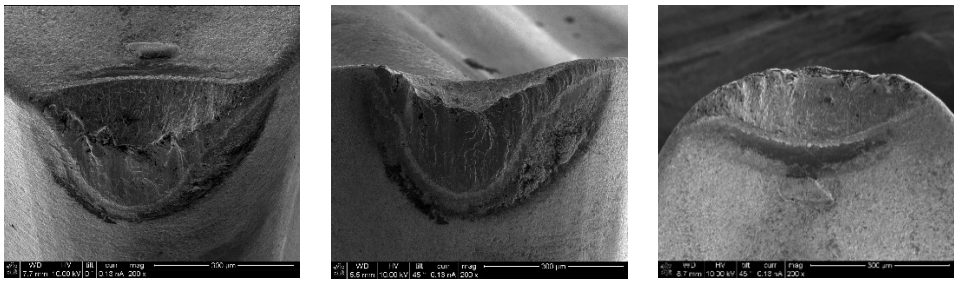

Figure 4-43. UCC 2: SEM views for cutting tool machined with v_c = 150 m/min. Coolant pressure = 90 bar.

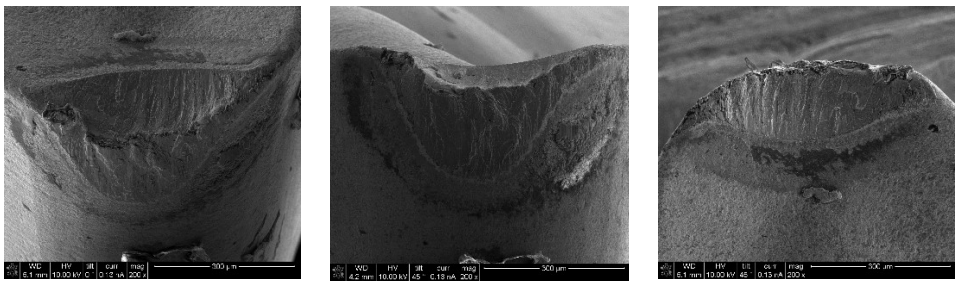

Figure 4-44. UCC 2: SEM views for cutting tool machined with v_c = 150 m/min. Coolant pressure = 10 bar.

4.3.2 PCD 8

Figure 4-45 and Figure 4-46 presents the SEM views for the cutting tool PCD 8.

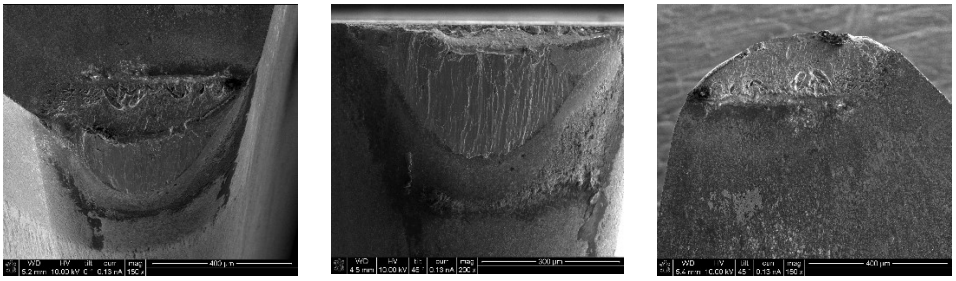

Figure 4-45. PCD 8: SEM views for cutting tool machined with v_c = 350 m/min.

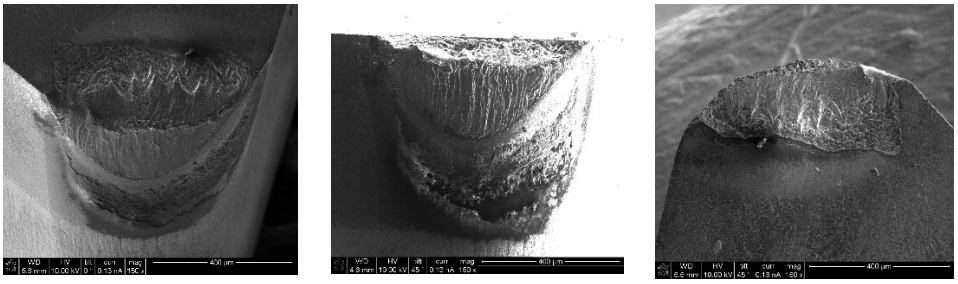

Figure 4-46. PCD 8: SEM views for cutting tool machined with v_c = 300 m/min.

4.3.3 cBN 2

Figure 4-47 and Figure 4-48 presents the SEM views for the cutting tool cBN 2.

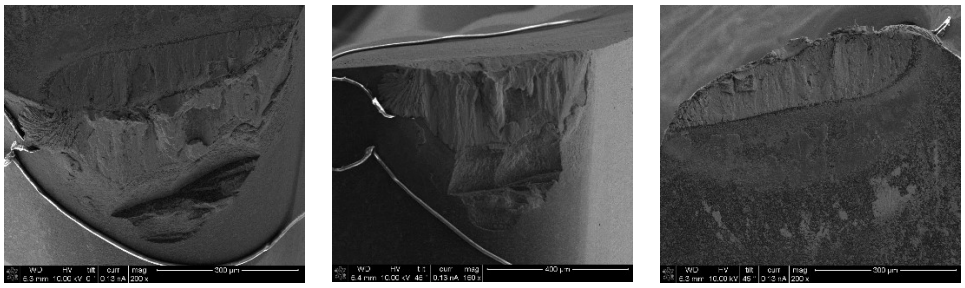

Figure 4-47. cBN 2: SEM views for cutting tool machined with v_c = 350 m/min. A fiber from the cleaning tissue can be observed.

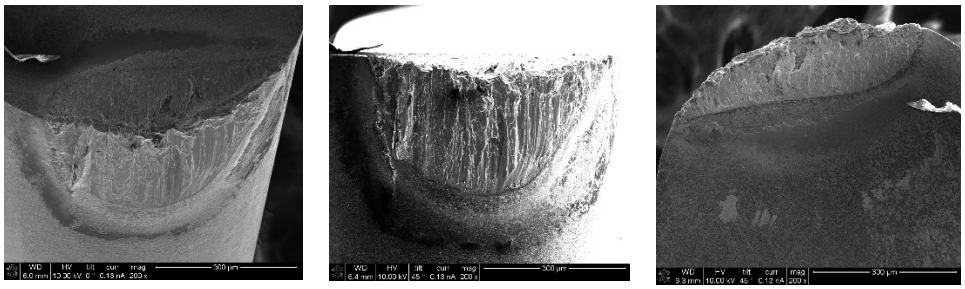

Figure 4-48. cBN 2: SEM views for cutting tool machined with v_c = 300 m/min. A fiber from the cleaning tissue can be observed.

4.4 TEM

The following section presents the results from the TEM analysis.

4.4.1 PCD 8

Figure 4-49 presents the cutting tool rake side and where the cutting tool material was removed in the lamella shape using FIB. Figure 4-50 presents the lamella seen from both sides. Figure 4-51 presents the thickness of the analyzed lamella. Figure 4-52 presents a HAADF image of the lamella seen from one side.

Figure 4-53 presents the lamella and the location on which a line-scan was performed. Figure 4-54 presents line-scan diagrams and Figure 4-55 presents the line-scan graphs. Figure 4-56 and Figure 4-57 presents element mapping for two different locations on the lamella in the boundary area.

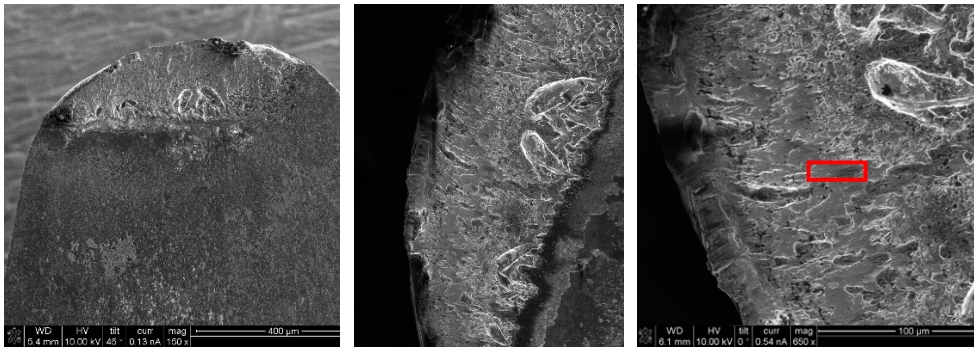

Figure 4-49. Cutting tool rake side and where the material was removed with FIB for TEM analysis.

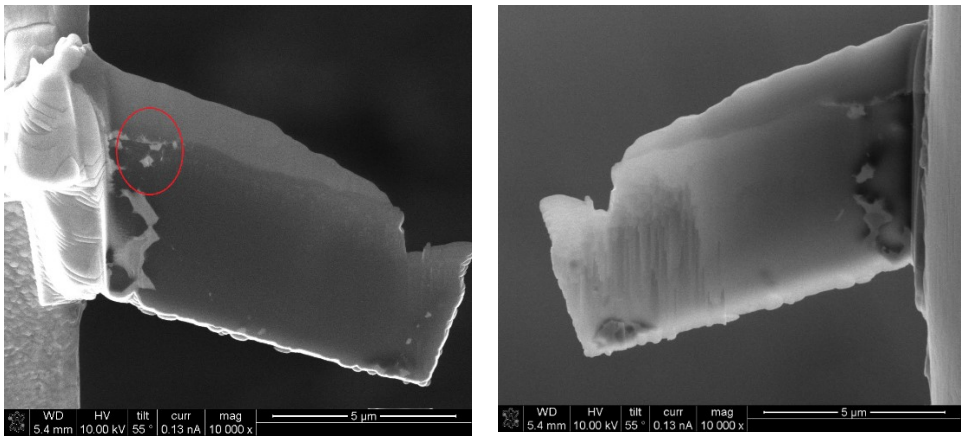

Figure 4-50. Cutting tool material in the lamella shape seen from both sides. Adhered titanium can be seen on the top of the lamella. The red circle in the left figure presents an interesting area to be analyzed.

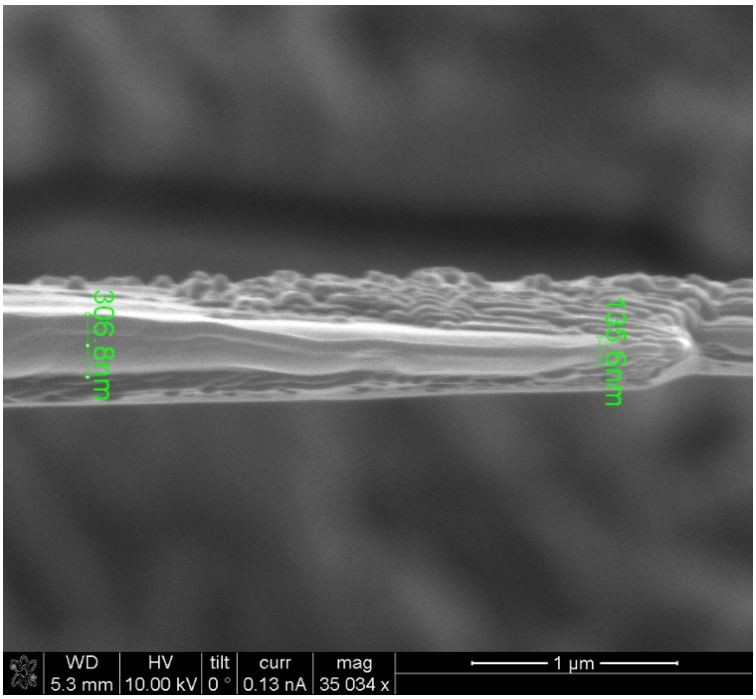

Figure 4-51. Thickness of the lamella. Left: 307 nm, right: 136 nm.

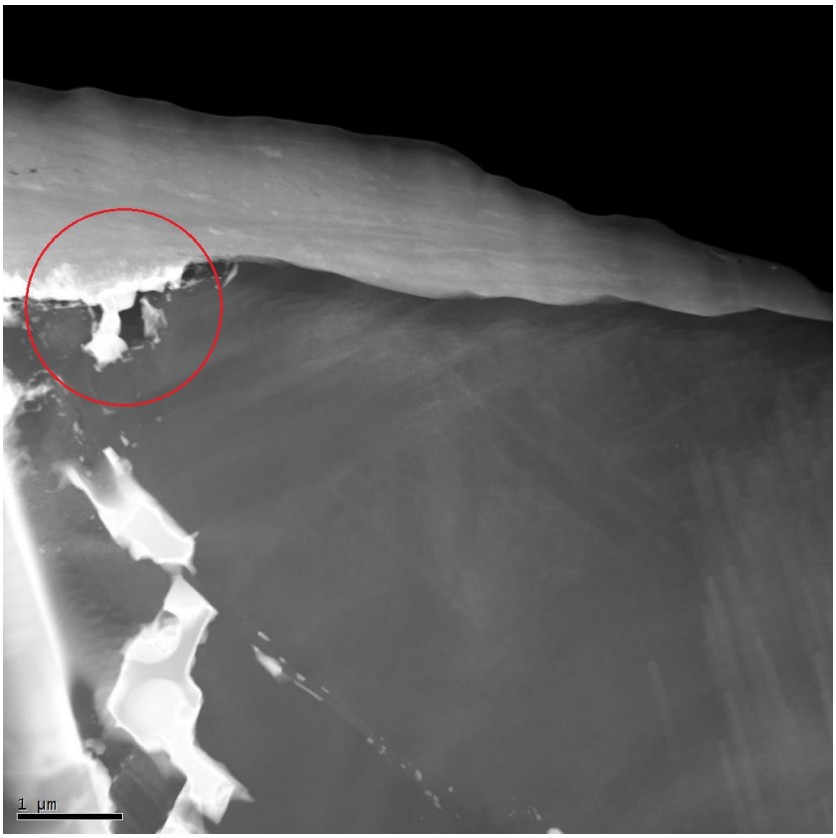

Figure 4-52.HAADF picture of the lamella in the thicker area. The top is the adhered titanium and the bottom is the cutting tool material. The red circle shows an interesting area that is analyzed with element mapping.

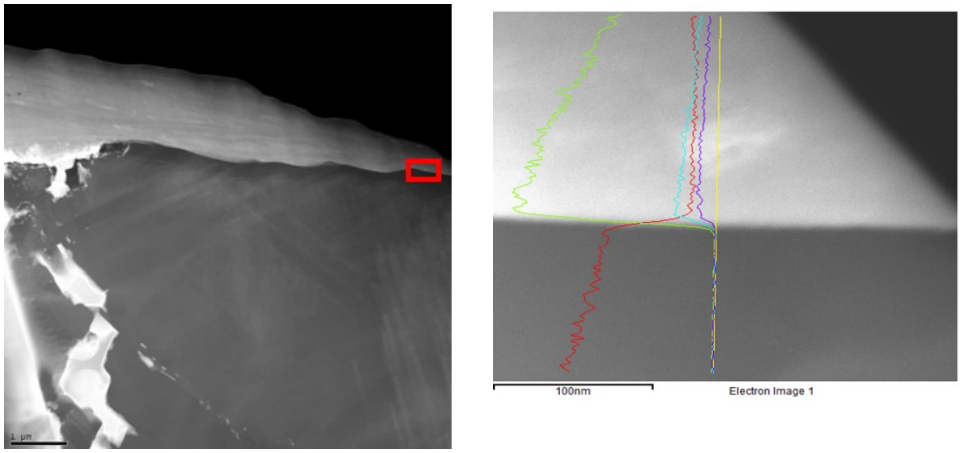

Figure 4-53. Left: Location on where the line-scan was performed. Right: Line-scan of boundary area.

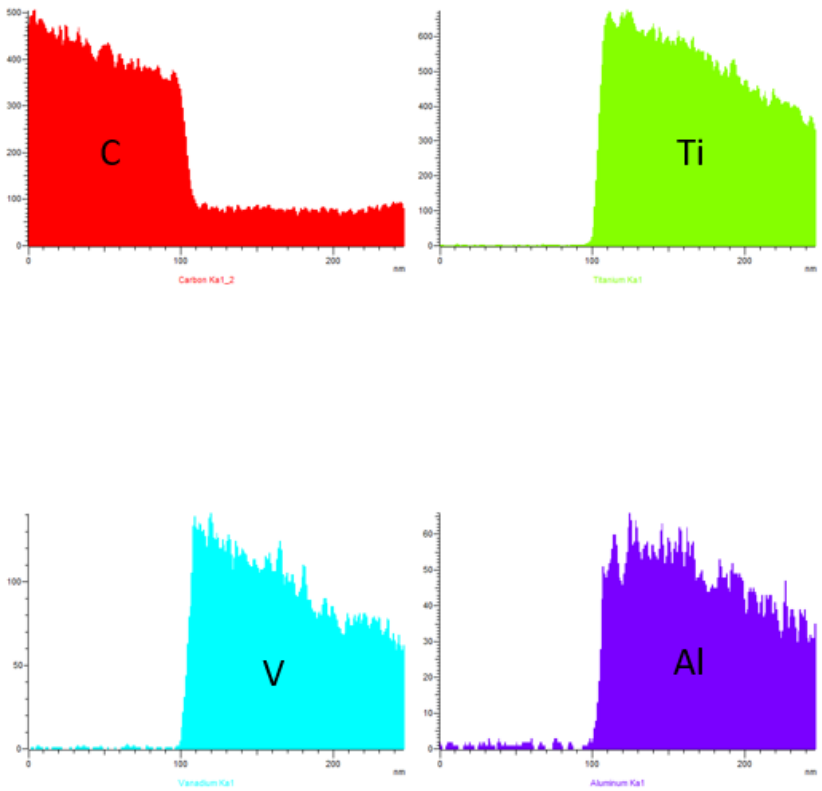

Figure 4-54. Line-scan diagrams for C, Ti, V and Al.

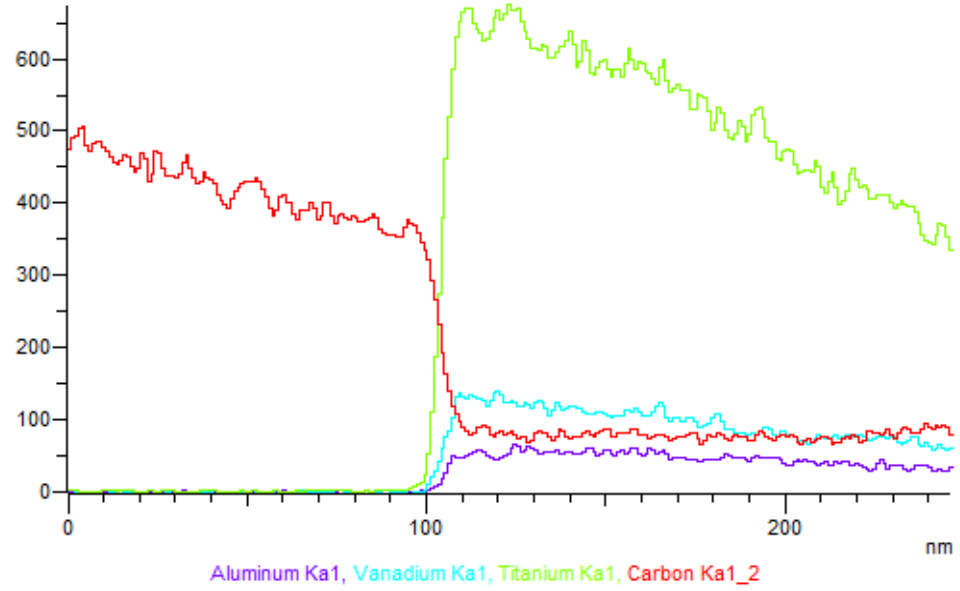

Figure 4-55. Line-scan graphs plotting Al, V, Ti and C.

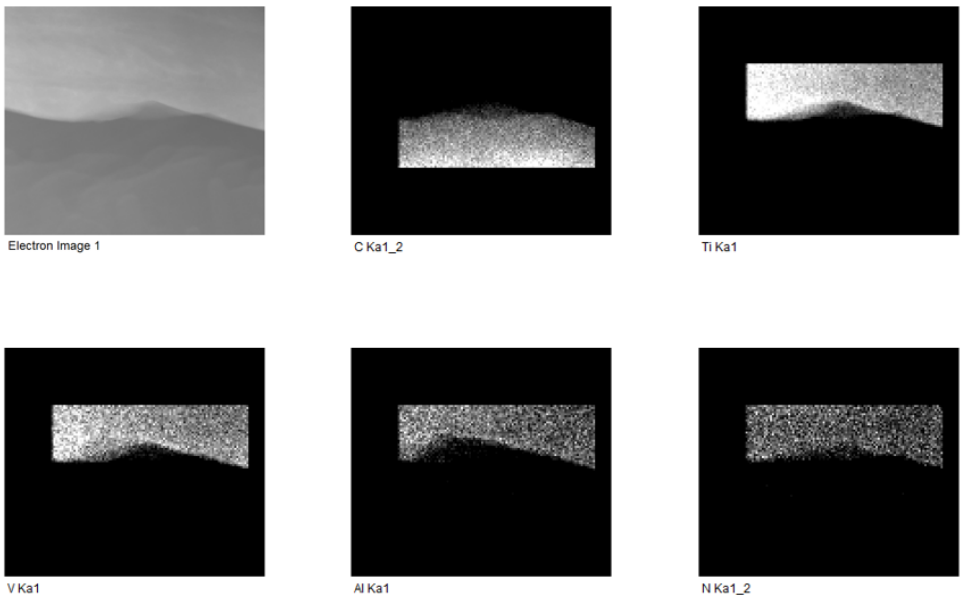

Figure 4-56. Element mapping for one boundary area results for C, Ti, V, Al and N.

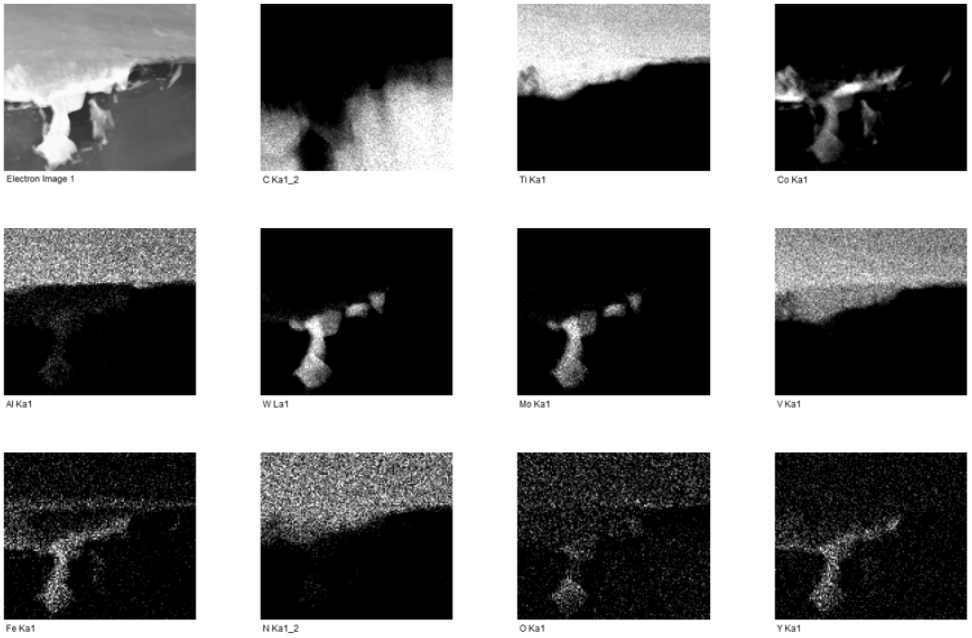

Figure 4-57. Element mapping for one boundary area results for C, Ti, Co, Al, W, Mo, V, Fe, N, O and Y.

4.4.2 cBN 2

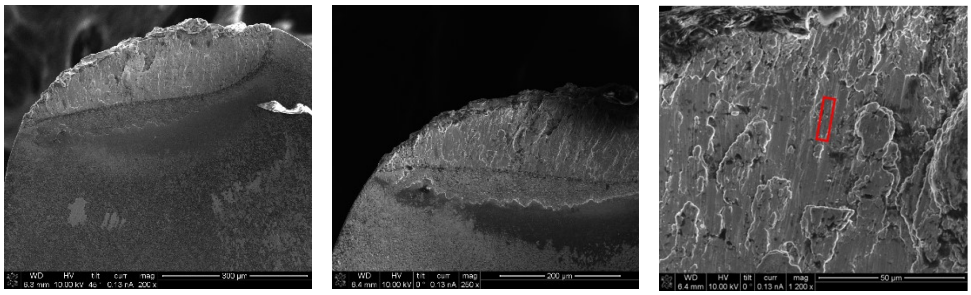

Figure 4-58. Cutting tool rake side and where the material was removed with FIB for TEM analysis.

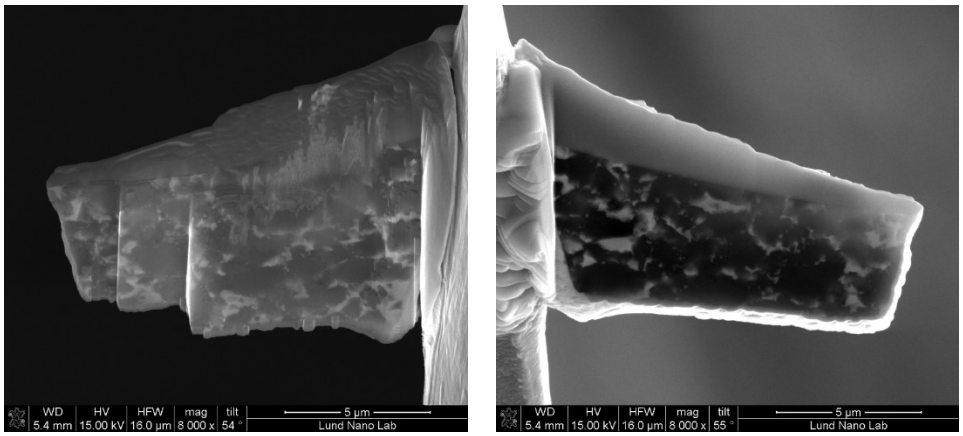

Figure 4-59. Cutting tool material in the lamella shape seen from both sides. Adhered titanium can be seen on the top of the lamella.

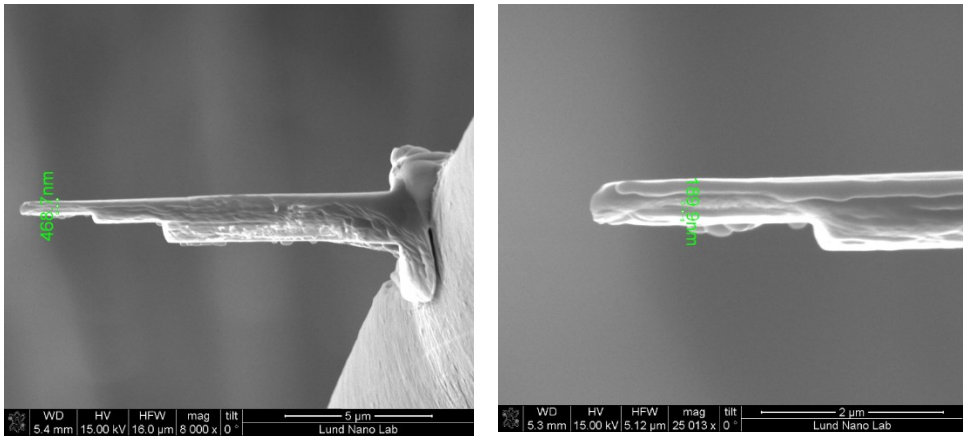

Figure 4-60. Thickness of the lamella. Left: 469 nm, right: 190 nm.

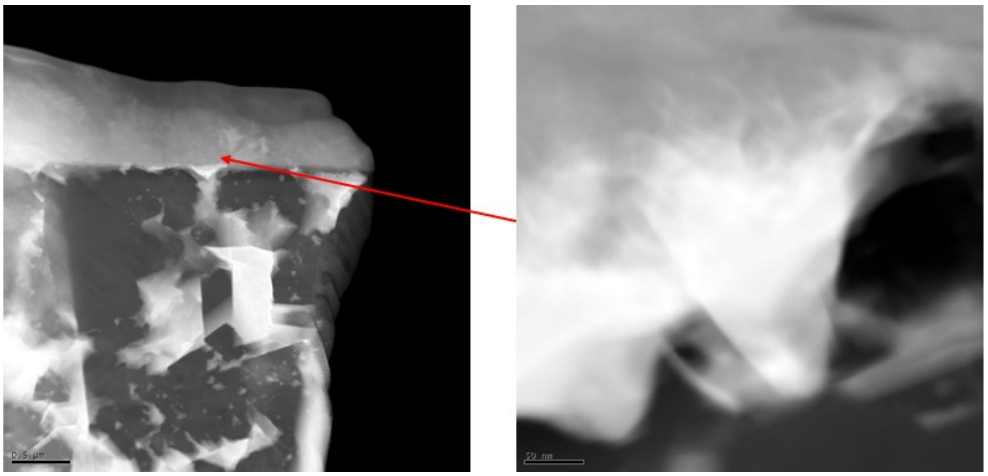

Figure 4-61. Location in the boundary area where veins can be seen.

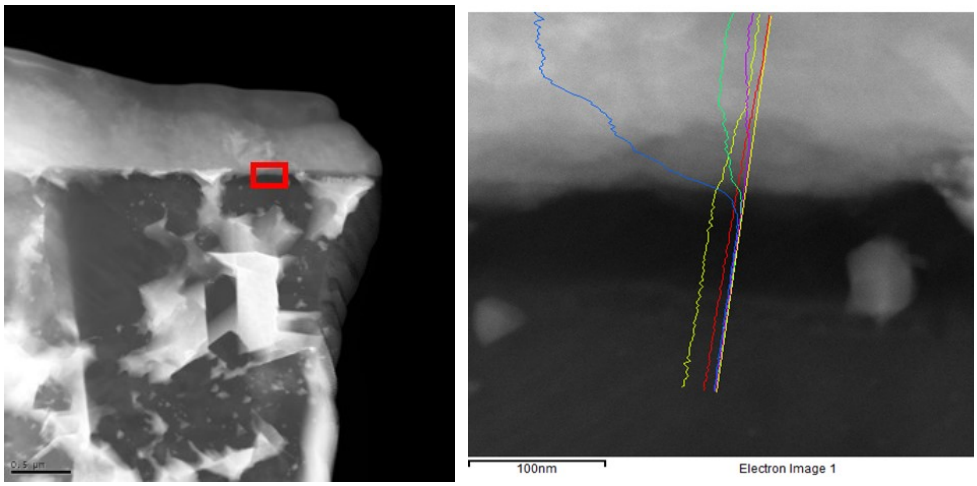

Figure 4-62. Left: Location on where the line-scan was performed. Right: Line-scan of boundary area.

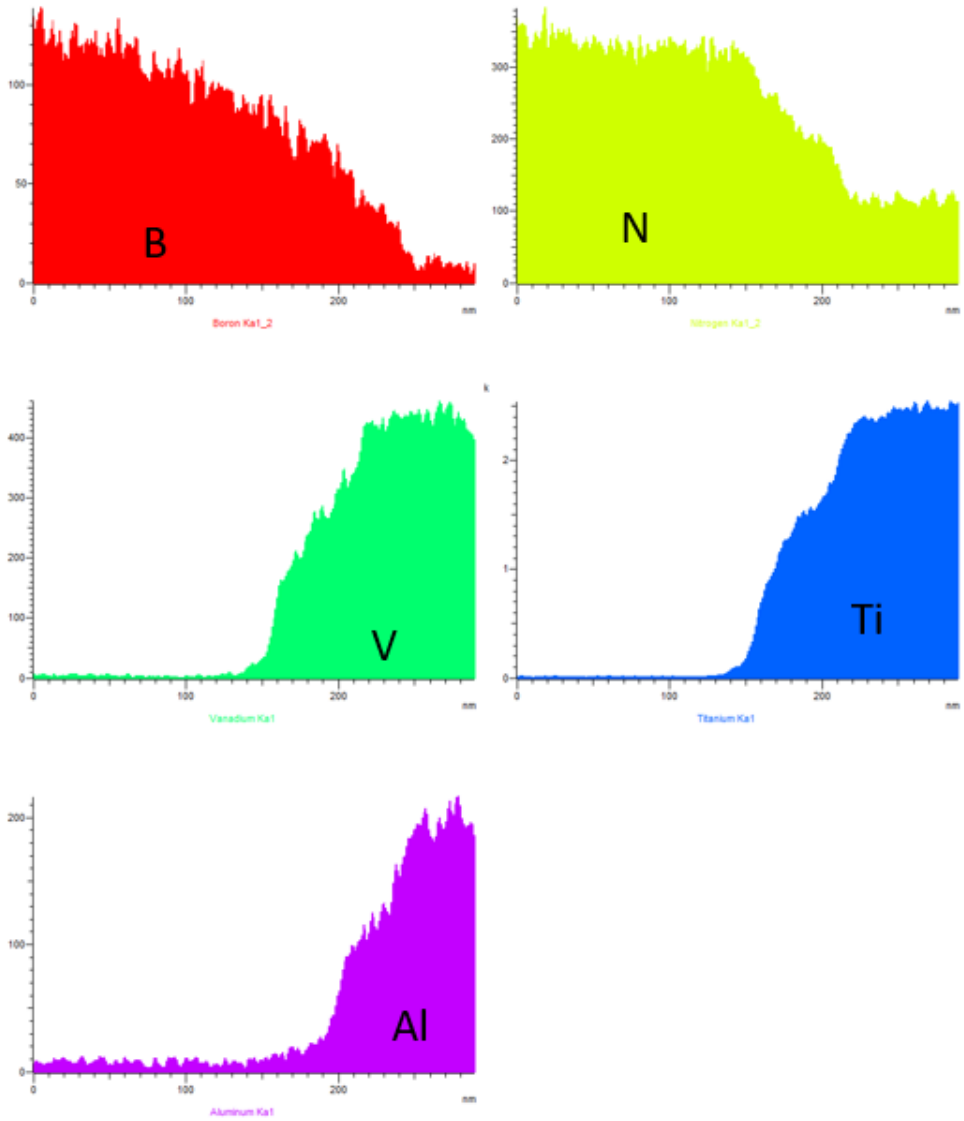

Figure 4-63. Line-scan diagrams for B, N, V, Ti and Al.

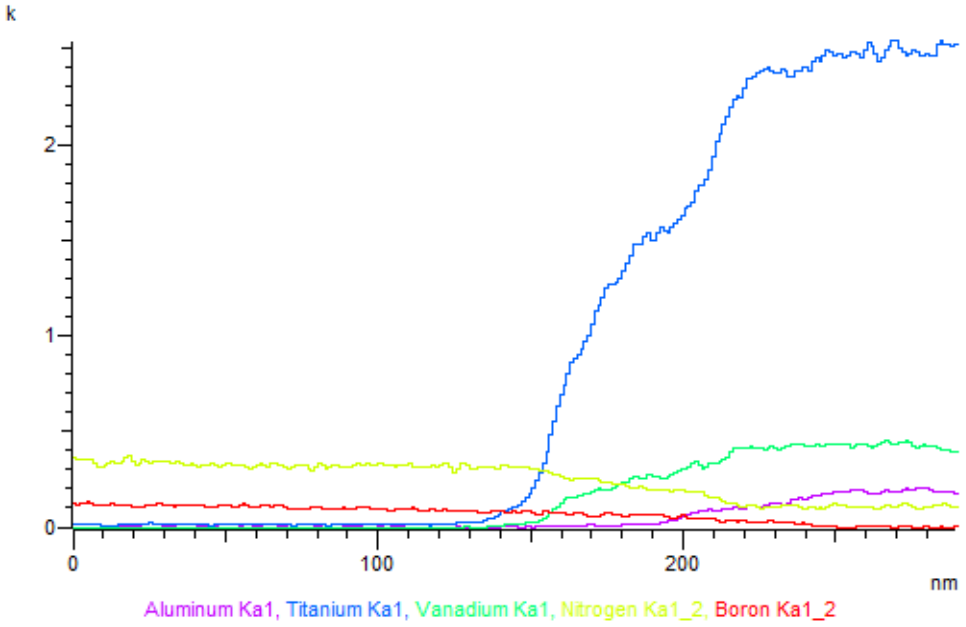

Figure 4-64. Line-scan graphs plotting Al, Ti, V, N and B.

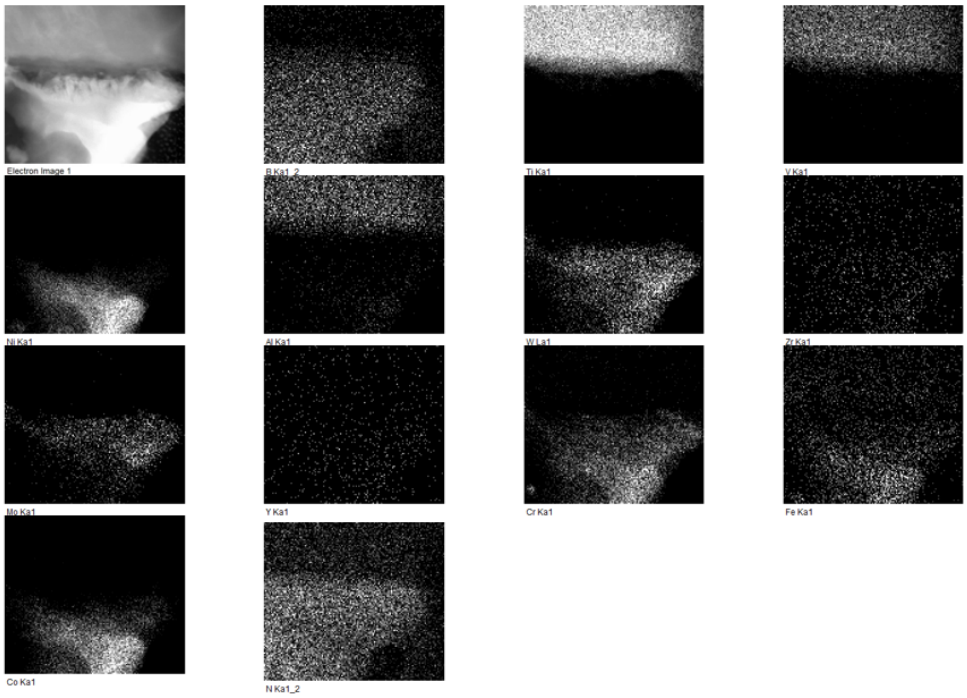

Figure 4-65. Element mapping for one boundary area results for B, Ti, V, Ni, Al, W, Zr, Mo, Y, Cr, Fe, Co and N.

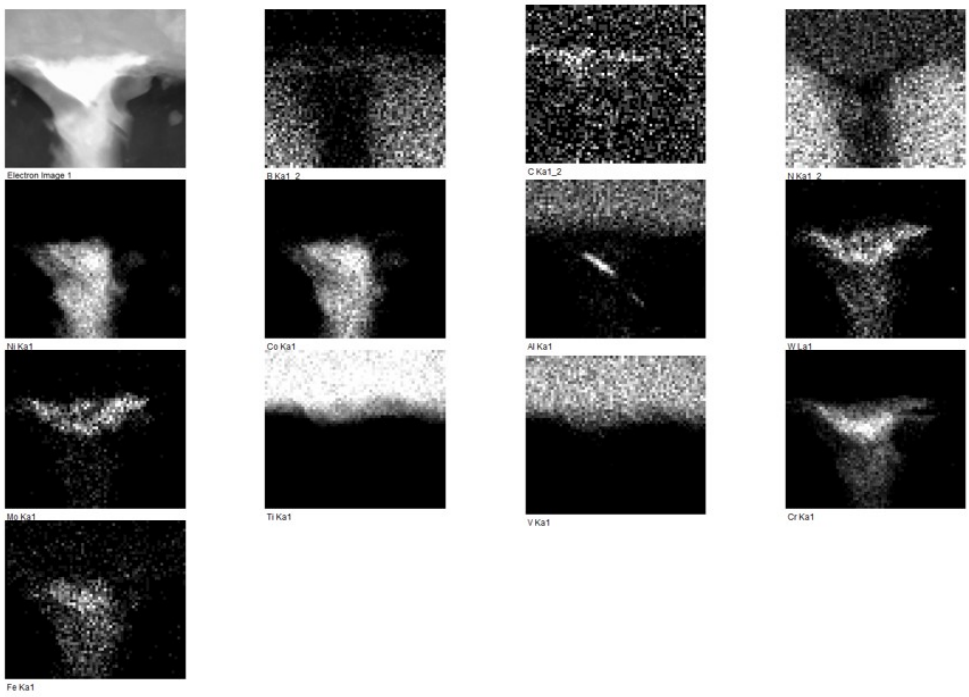

Figure 4-66. Element mapping for one boundary area results for B, C, N, Ni, Co, Al, W, Mo, Ti, V, Cr and Fe.

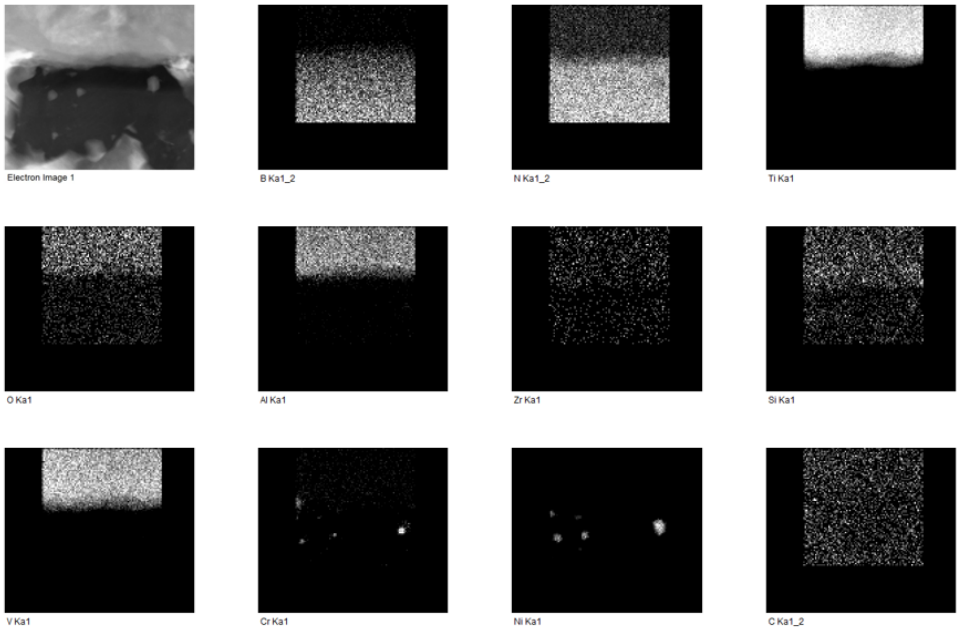

Figure 4-67. Element mapping for one boundary area results for B, N, Ti, O, Al, Zr, Si, V, Cr, Ni and C.

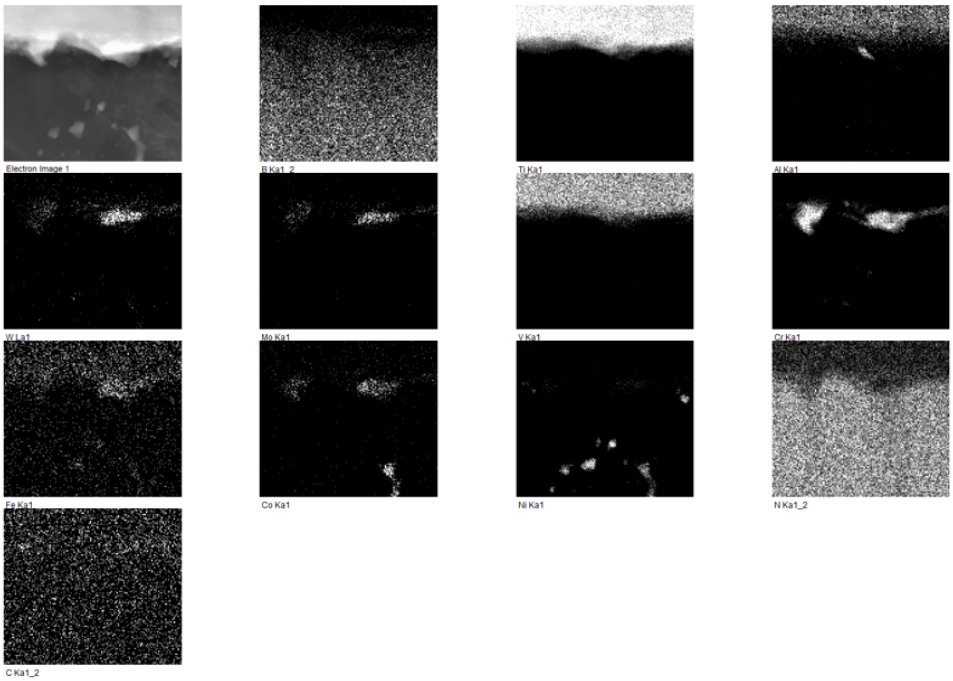

Figure 4-68. Element mapping for one boundary area results for B, Ti, Al, W, Mo, V, Cr, Fe, Co, Ni, N and C.

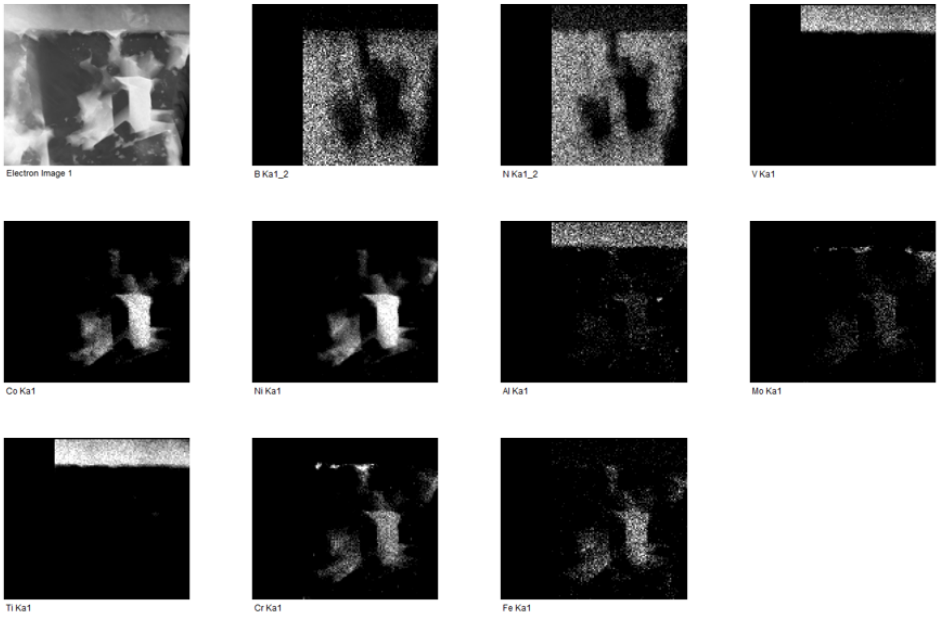

Figure 4-69. Element mapping for one boundary area results for B, N, V, Co, Ni, Al, Mo, Ti, Cr and Fe.

4.5 Cutting forces

The cutting forces acquired during the cutting process are found in *11 Appendix C – Cutting forces.*

4.6 Cost efficiency

The manufacturing cost per volume unit as a function of the tool life for the cutting tools UCC 2, CCC 1 and PCD 8 are presented in Figure 4-70, Figure 4-71 and Figure 4-72 below. Table 4-2 also presents the results for the costs per volume unit.

Table 4-2. Cutting tools, cutting data, acquired tool life, volume of removed material and the acquired production cost per volume of removed material calculated with the integrated part cost model.

Cutting tool	Feed [mm/rev]	Cutting speed [m/min]	Tool life [min]	Volume of removed material [cm^3]	Cost per volume unit [SEK/cm^3]
UCC 2	0.10	250	1.9	15	94.7
		200	4.0	25	27.0
		150	23.7	104	1.1
CCC 1	0.10	200	1.6	8	281.3
		150	8.3	37	11.7
PCD 8	0.10	350	7.8	82	70.4
		300	30.0	263	5.7

4.6.1 UCC 2

The manufacturing cost per volume unit as a function of the tool life for the cutting tool UCC 2 is presented in Figure 4-70.

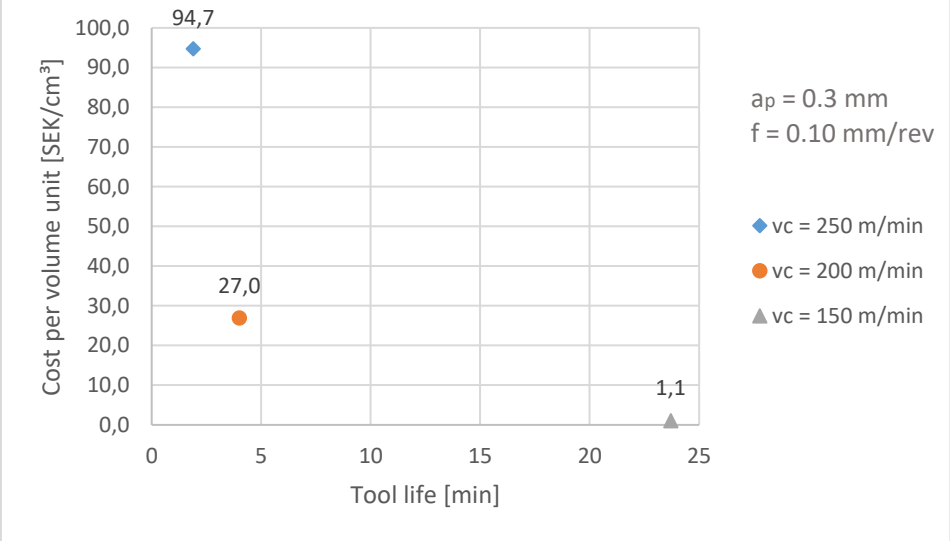

Figure 4-70. UCC 2: The manufacturing cost per volume unit plotted for the corresponding tool life.

4.6.2 CCC 1

The manufacturing cost per volume unit as a function of the tool life for the cutting tool UCC 1 is presented in Figure 4-71.

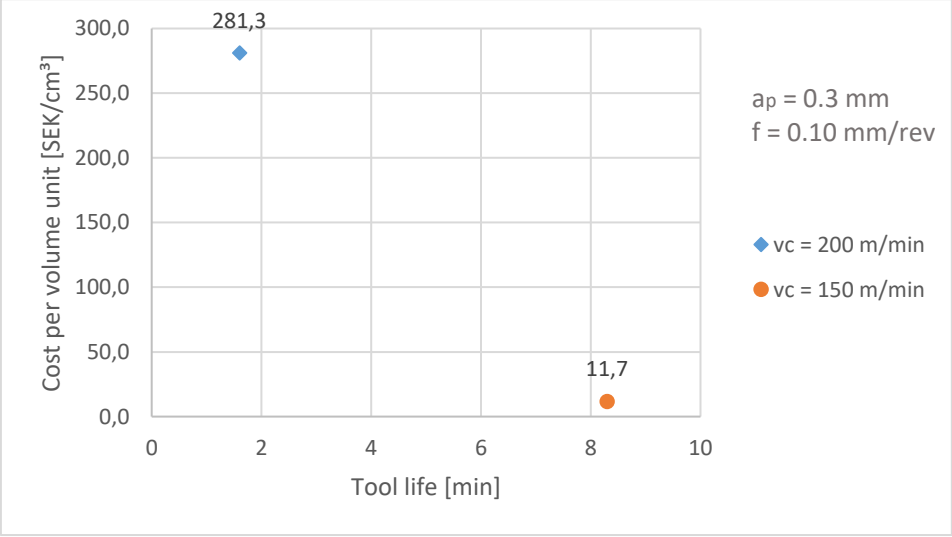

Figure 4-71. CCC 1: The manufacturing cost per volume unit plotted for the corresponding tool life.

4.6.3 PCD 8

The manufacturing cost per volume unit as a function of the tool life for the cutting tool UCC 1 is presented in Figure 4-72.

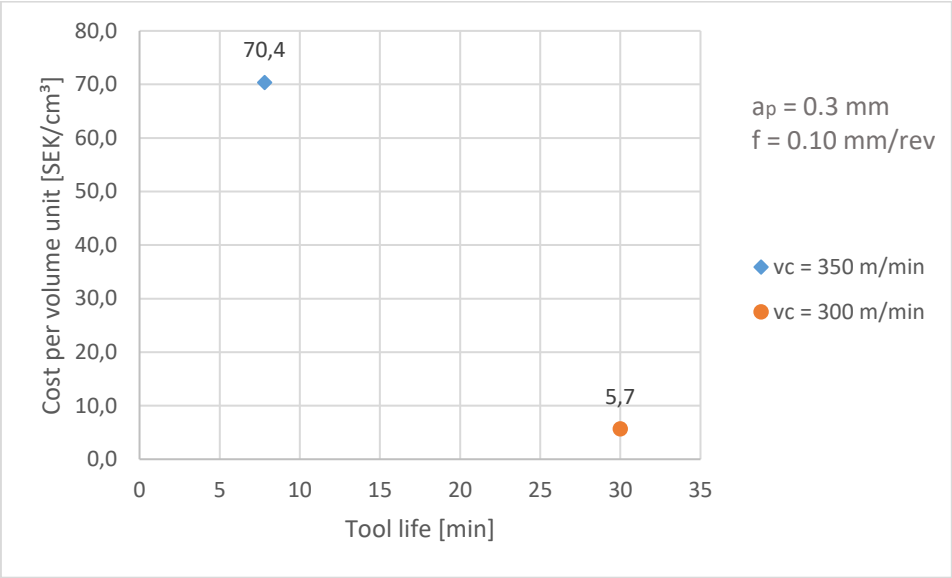

Figure 4-72. PCD 8: The manufacturing cost per volume unit plotted for the corresponding tool life.

5 Discussion

This chapter discusses the machining performance of the cutting tools used in the study, the wear mechanisms, the acquired surface quality as well the cost efficiency. The summation of the findings are found above the individually analyzed cutting tools.

The cutting data variance for the pointed cutting tools are the cutting speed. The cutting tool being able to manage the highest cutting speeds of 300 m/min and 350 m/min are PCD 8. cBN 2 was also tested for these cutting speeds, although with shorter tool lives acquired. UCC 2 was found to manage the higher cutting speed 250 m/min and had longer tool life values of the cutting speeds of 200 m/min and 150 m/min compared to CCC 1. cBN 3 had short tool life values and with much lower cutting speeds (100 m/min, 50 m/min and 30 m/min, which are not in the classification for high speed machining). The wear mechanisms of breakage and notch wear is not comparable to the other wear mechanisms found in the study (flank wear and crater wear).

Regarding the maximum value of the surface roughness acquired, the lowest value was 0.91 μm machined with the higher cutting speed with the CCC grade.

The wear patterns observed has been flank wear and crater wear for the cutting tools PCD 8 (cutting speed 300 m/min) and cBN 2 (cutting speed 300 m/min). Smaller crater wear is found in CCC 1, compared to UCC 2, the coating probably functions as a protection from crater wear.

The chemical analysis with TEM on PCD 8 and cBN 2 is somewhat difficult to read. There are small boundary areas between the cutting tool material and the adhered workpiece material. Probably, there are formations of titanium carbides or diffusion of carbon into the workpiece material in the cutting tool PCD 8. Between the diamond grains, there seems to have been titanium working its way down into the cutting tool material. Regarding cBN 2, the boundary area between the cutting tool material and the adhered workpiece material are somewhat sharp. There might be formations of titanium nitrides in this boundary area or possibly diffusion of boron or nitrogen into the workpiece material. Other elements from the cutting tool manufacturing process are noted.

5.1 UCC 2

The maximum surface roughness acquired is the lowest for the lowest cutting speed used and the lowest material removal rate.

The flank wear development in Figure 4-2 shows a steady increase for the two higher cutting speeds, looking like the end of the typical wear curve seen in Figure 2-11. Compared to the typical flank wear development, the lowest cutting speed shows a flank wear development approaching the wear criterion at a slower rate which is beneficial since the risk for a rapid tool wear is smaller. The cutting forces show a

more extreme tool wear deterioration for the higher cutting speed, to become more constant for the lower cutting speed, see Figure 11-2, Figure 11-4 and Figure 11-6.

Rake wear can be observed for all cutting speeds used, but to a lesser degree for the cutting speed 200 m/min, see Figure 4-4, Figure 4-7 and Figure 4-10. It can be noted that the rake wear decreases with the cutting speed, see Figure 4-5, Figure 4-8 and Figure 4-11, showing the speed dependency of the cutting tool.

The surface roughness developed during the machining process looks somewhat constant for the cutting speeds 150 m/min. An increasing surface roughness for the cutting speed 200 m/min is observed, and slight drop in the surface roughness before reaching the wear criterion for the cutting speed 250 m/min is observed, see Figure 10-2, Figure 10-4 and Figure 10-6.

When using the lower coolant pressure, the flank wear has the same shape as for the higher coolant pressure; the rake wear however, is smaller – one reason can be that the cutting tool with the longer engagement time. The tool life when comparing the coolant pressures, see Figure 4-1, are 16 % longer for the higher coolant pressure, and the surface roughness is smaller for the higher pressure, indicating that an increase in coolant pressure improves the surface quality and tool life. However, an increased coolant pressure might damage the cut surface with the chips following the stream, something to keep in mind when selecting coolant pressure. When comparing the surface roughness development for the two coolant pressures, the surface quality increase with a slightly faster rate for the lower coolant pressure. The flank wear development shows similar development formations, see Figure 10-6 and Figure 10-9.

5.2 CCC 1

Compared to the UCC 2, the coated cutting tool has smaller values of the tool life for the same used cutting data. This is interesting, because usually coated cutting tools has longer tool lives due to the protective layer. Since this is not the case, one can speculate if there is a chemical reaction between the titanium workpiece material and the coating in this cutting tool. Since this is not validated with TEM, the answer is unknown. Another reason for the shorter tool life could be that the substrate material below the coating is different compared to the uncoated version, possibly leading to a faster degradation. The possible tool protection layer in the cutting tool UCC 2 created in the cutting process can be caused by not having the coating reacting with the workpiece material.

The flank wear development are somewhat similar in shape compared to the UCC 2, as well as the flank wear shape. There does not seem to have become too great crater wear on this cutting tool, possibly a cause by the coating. The maximum values of the acquired surface roughness are lower compared to the ones acquired by UCC 2. The rake wear in the uncoated cutting tool must affect the cut surface to the extent that the crater wear created caused the cut surface more damage. For the coated cutting tool, the surface quality improves as the flank wear develops. This might be

an effect of that the rake wear causes the edge radius to decrease, since the edge radius of a new cutting tool looks larger compared to the worn cutting tool.

Comparing the cutting forces for this cutting tool, the last passing shows a somewhat more stable force curve for the lower cutting speed, see Figure 11-10 and Figure 11-12, implying that the flank wear is more predictable closer to the wear criterion when using the lower cutting speed. The main cutting force has the most controlled increase, implying that the rake wear build up is controlled.

5.3 PCD 8

This cutting tool is applicable for higher cutting speeds of 300 m/min and 350 m/min. The flank wear development are steady, not showing the same formation as the common tool wear curve. For the lower cutting speed, the flank wear shows an interesting development because of the stair formation. Probably there has been a tool protection layer present, and when the temperature becomes too high it dissolves and the cutting tool is open for flank wear. The 30.0 min in tool life for the cutting speed 300 m/min shows great potential in the machining of titanium with this cutting tool material. The flank wear shape is more round compared to the cemented carbide cutting tools. The rake wear has taken the form as a chamfer and not a crater.

The surface roughness for both cutting speeds shows similarities since they start to increase, followed by a decrease to the point where the flank wear gets closer to the wear criterion so that it ends with increasing, see Figure 10-16 and Figure 10-18.

Looking at the cutting forces in Figure 11-13 and Figure 11-15, it is noted that the main cutting forces are rather stable compared to the passive force, implying that the flank wear increase is more rapid compared to the rake wear rate. Looking at Figure 11-14 and Figure 11-16, the cutting forces are rather stable implying that the tool wear is rather continuous close to the wear criterion.

The location of the analyzed material with TEM on the rake side is chosen as to represent a suitable area where possible chemical reactions or diffusion has taken place, see Figure 4-49. The removed cutting tool material in the lamella shape seen in Figure 4-50 shows an adhered layer of titanium on the cutting tool material. The thickness might be somewhat thick, see Figure 4-51; the results from the analysis might have been more clear if the thickness would have been approximately 100 nm. Figure 4-52 shows some structure of the adhered titanium and the PCD. The boundary area is observed. The location on where the line-scan is performed, see Figure 4-53, is in the thinner section of the lamella, which is positive. The line-scan results regarding the elements C, Ti, V and Al, seen in Figure 4-54 and Figure 4-55, shows a very short boundary area between the adhered workpiece material and the cutting tool. However, there seems to be a short overlap of C and Ti in the boundary area. This might be a formation of titanium carbide. It might also be a cause of a tilted boundary area. Since the carbon content is somewhat continuous in the adhered workpiece material, this might be a cause of carbon diffusion or simply a remaining of the carbon in the workpiece material.

Regarding the element mapping in Figure 4-56 and Figure 4-57, two different location on the boundary area on the lamella has been analyzed. In Figure 4-56, the results obtained are somewhat difficult to analyze. What is noted is that there is a wave shape in the boundary area, where there seems to be a smaller content of C, N and Ti. On the left part of the wave shape, V occurs more compared to for example Ti and Al. In Figure 4-57, some leftover Co is noted from the sintering process. This location is a boundary area between the diamond grains, which is supported by the distribution of C. In between the grains, besides from Co, W, Mo, Fe, O and Y is in the area. Some Al also seems to have worked its way down in between the diamond grains. There seems to be a higher concentration of Ti closer to the Co area, whereas V and N is not as concentrated in this area.

5.4 cBN 2

This cutting tool uses the same cutting speeds as PCD 8, although the tool life and therefore performance is not as good. The flank wear development ends with a rapid increase in the flank wear for the cutting speed 350 m/min, possibly caused by chipping. For the cutting speed 300 m/min, the flank wear development is more stable, especially in the end phase. There are stair formations in the flank wear development, possibly caused by a tool protection layer. The flank wear shape is similar to PCD 8. A crater is formed for the cutting tool using the cutting speed of 300 m/min. The maximum surface roughness value acquired is smaller when using the cutting speed of 300 m/min, see Table 4-1. In Figure 10-21 and Figure 10-23, the surface roughness is presented and it can be observed that there is a decrease in the acquired value, to increase as the flank wear is getting closer to the wear criterion. This is not surprising, since the flank wear increases.

In Figure 11-18 it is observed that the cutting forces shift, probably caused by the rapid flank wear increase. In Figure 11-20 it is observed that the cutting forces are rather stable in the last passing, showing the stability of the flank wear development as the tool wear criterion is about to be reached. In Figure 11-19 it is observed how the passive force increases as the tool wear criterion is about to be reached, indicating a flank wear increase. As the main cutting force has a rather stable increase, it is indicated that the rake wear increase is developing in a controlled manner.

The location of the analyzed material with TEM on the rake side is chosen as to represent a suitable area where possible chemical reactions or diffusion has taken place, see Figure 4-58. The removed cutting tool material in the lamella shape seen in Figure 4-59 shows an adhered layer of titanium on the cutting tool material. The thickness might be somewhat thick, see Figure 4-60; the results from the analysis might have been more clear if the thickness would have been approximately 100 nm. Only the outer part of the lamella is analyzed, which is noted by the smallest thickness. Figure 4-61 shows the boundary area where an interesting area with vein like formation is observed. The figure also shows some structure of the adhered titanium and the cBN. The boundary area is observed. The location on where the line-scan is performed, see Figure 4-62, is in the thinner section of the lamella. The

line-scan results regarding the elements B, N, V, Ti and Al, seen in Figure 4-63 and Figure 4-64, shows a short boundary area between the adhered workpiece material and the cutting tool. However, there seems to be a short overlap of Ti N and B in the boundary area. This might be a formation of titanium nitrides. It might also be a cause of a tilted boundary area. Since the nitrogen and boron content is somewhat continuous in the boundary area, this might be a cause of diffusion.

Regarding the element mapping in Figure 4-65, Figure 4-66, Figure 4-67, Figure 4-68 and Figure 4-69, different locations on the boundary area on the lamella has been analyzed. The results obtained for the element mapping are somewhat difficult to analyze. In Figure 4-65, it is noted that B, Ni, W, Mo, Cr, Fe, Co and N is in the cutting tool material part of the lamella and that Ti, V and Al is in the adhered layer. However, Y and Fe seems to be spread in both the adhered material and cutting tool material.

In Figure 4-66, it is noted that Ni, Co, W, Cr and Fe is in between the cBN grains. Some Mo is in the upper part of the area between the cBN grains. The workpiece material Ti, V and Al seems not have diffused into the cutting tool material. However, a spear of Al is noted in the cutting tool material. The N and B is noted in the cutting tool material as the cBN grains.

In Figure 4-67, it is noted that there seems to be a boundary area between the adhered workpiece material and the cutting tool material. The Ti and N concentration is decreased in this area, implying that there might have been formations of titanium nitrides. Particles of Cr and Ni are present and is probably a result from other elements used in the cutting tool manufacturing process.

In Figure 4-68, it is noted that in the boundary area between the workpiece material and the cutting tool material seems to be formations of W, Mo, Cr, Fe Co and Ni, probably leftovers from the cutting tool manufacturing process. The Cr and Ni are present deeper into the cutting tool as well. In the boundary area between the cutting tool material and the workpiece material, there seems to be a short overlap of B, N, Ni, Ti, Al and V. There might possibly have been a diffusion of N and B into the adhered workpiece material.

In Figure 4-69, it is noted that there are other elements from the cutting tool manufacturing process od Co, Ni, Mo, Cr and Fe, and that some Al is present in the same locations as well. The B and N are present in the rest of the cutting tool material part of the lamella. Ti, Al and V is present in the adhered layer and the boundary area does not appear as thick.

5.5 cBN 3

This cutting tool could not handle the higher cutting speeds, instead rather low values of cutting speeds are used – implying that this cutting tool material should not be used in high speed machining. The tool life values acquired are very short and the tool wear shows signs of flaking and notch effects. As can be seen in Figure 11-22,

Figure 11-24 and Figure 11-26, the cutting forces have a bigger amplitude compared to the other cutting tools examined, indicating the flaking and notch wear effects.

5.6 Cost efficiency

The results acquired regarding cost efficiency is based on the tool life, the cutting tool cost, the number of cutting edges and the volume of removed material, meaning that a higher tool life and volume of removed material combined with a lower cutting tool cost and more available cutting edges per cutting tool results in a better cost efficiency. This method can be discussed, but has functioned as a limitation since this study is not focusing on modeling the manufacturing costs.

When comparing UCC 2 and CCC 1, it can be observed that UCC 2 shows a lower cost per volume unit for all variances in cutting data tested. Regarding PCD 8, with the cutting speed 300 m/min can be equaled to UCC 2 with the cutting speed 150 m/min. For the highest tested cutting speed for both UCC 2 and PCD 8, PCD 8 shows a better cost efficiency compared to UCC 2.

6 Conclusions

Regarding the pointed cutting tools, the highest material removal rate achieved by the highest cutting speeds used, is the cutting tool PCD 8. The same cutting speeds are used for cBN 2, although shorter tool lives are acquired in comparison. One interesting finding is that UCC 2 has better performance compared to CCC 1 – possibly caused by chemical reactions in the coating and tool protection layers occurring on UCC 2. The cutting tool cBN 3 did not respond well to the machining, even for as low cutting speed as 30 m/min, with tool lives of 0.8 min to 2.5 min with flaking and chipping as tool wear.

The highest acquired surface roughness is 1.57 μm with cBN 2, except from the high surface roughness acquired with the bad performing cBN 3. The smallest value of the surface roughness obtained was acquired with CCC 1. The wear mechanisms observed for the analyzed cutting tools are those of flank wear, rake wear and crater wear – no signs of plastic deformation has been observed.

The pointed cutting tools shows that UCC 2 has a better cost efficiency compared to CCC 1. For the higher values of the cutting speed for UCC 2 and PCD 8, PCD 8 is superior regarding cost efficiency compared to UCC 2. For the higher cutting speed for these cutting tools, the maximum surface roughness acquired can be considered equal. PCD 8 has a better cost efficiency compared to cBN 2.

The chemical analysis with TEM on PCD 8 and cBN 2 is somewhat difficult to read. There are small boundary areas between the cutting tool material and the adhered workpiece material. Probably, there are formations of titanium carbides or diffusion of carbon into the workpiece material in the cutting tool PCD 8. Between the diamond grains, there seems to have been titanium working its way down into the cutting tool material. Regarding cBN 2, the boundary area between the cutting tool material and the adhered workpiece material are somewhat sharp. There might be formations of titanium nitrides in this boundary area or possibly diffusion of boron or nitride into the workpiece material. Leftover elements from the cutting tool manufacturing process are noted.

7 Further work

The wide range of titanium alloys being developed besides the common Ti6Al4V requests for similar testing and analysis as the ones performed in this study. Since this study deals with an (α + β)-alloy, the next steps would be to test α- or near α-alloys and β- or near β-alloys. This in order to acquire knowledge about the wear mechanisms achieved by the range of alloys used commercially, which can be compared to the results achieved in this study.

The tests should be repeated for the cutting tools UCC 2, PCD 8 and cBN 2 to achieve some statistics of the tool life and the surface roughness acquired, to analyze the stability of the results acquired in this study. The cutting tools not selected to be further tested are because of the poor machining performance perceived in this study.

For further studies, temperature measurements during the machining process would be interesting to obtain. This, to connect possible phase transformations in the workpiece material to chemical reactions in the cutting tool and other wear mechanisms.

FIB-SEM and TEM should be performed on cutting tool UCC 2 and CCC 1 to figure out if there is chemical reactions between the cutting tool and the workpiece material. This, to get a deeper understanding of the chemical reactions with the bulk material and coating in the cutting tool to be able to reason why a certain cutting tool should be used for different cutting data.

One case was tested where the tool life and the corresponding surface roughness was measured for the same cutting tool and cutting data, see Table 3-6. This test was performed to get a sense of the effect from the high-pressure coolant pressure on the specified cutting tool. Further testing of different cutting fluid pressures needs to be performed and the results in the study can work as a base for this.

8 References

[1] J.-E. Ståhl, Metal Cutting Theories and Models, Lund, Sweden: Seco Tools, 2012.

[2] S. Hägglund, Methods and Models for Cutting Data Optimization, Gothenburg, Sweden: Department of Materials and Manufacturing Technology, Chalmers University of Technology, 2013.

[3] "ISO 3685 - Tool-life testing with single-point turning tools," ISO (the International Organization for Standardization), Second edition 1993-11-15.

[4] J.-E. Ståhl, Industriella tillverkningssystem, Del 2 - Länken mellan teknik och ekonomi, Fjärde upplagan, Lund, Sweden: Lunds Tekniska Högskola, Lunds Universitet, Lund, 2016.

[5] P. de Vos and J.-E. Ståhl, Applied Metal Cutting Physics - Best Practice, Fagersta, Sweden: SECO TOOLS AB, 2016.

[6] Svarvning, Katalog och teknisk guide, Seco Tools AB, 2015.

[7] H. Schultz and T. Moriwaki, "High-speed Machining," *Annals of the CIRP,* vol. 41, no. 2, pp. 637-643, 1992.

[8] P. de Vos and J.-E. Ståhl, Metal Cutting - Theories in Practice, Lund - Fagersta, Sweden: Seco Tools AB, 2014.

[9] J.-E. Ståhl, Writer, *Metal Cutting - Advanced Course (seminar).* [Performance]. Division of Industrial Production, Production and Materials Engineering, Faculty of Engineering, Lund University, 2017.

[10] J.-E. Ståhl, Skäreggars spontanhaverier, Lund: Institutionen för Mekanisk Teknologi och Verktygsmaskiner, Lunds Tekniska Högskola, 1986.

[11] R. Smallman and A. Ngan, Physical Metallurgy and Advanced Materials, 7th Edition, ISBN: 978 0 7506 6906 1: Elsevier Ltd., 2007.

[12] M. J. J. Donachie, Titanium - A Technical Guide - Second Edition, United States of America: ASM International, 2000.

[13] "Computational Thermodynamics - Calculation of Phase Diagrams using the CALPHAD Method," Computational Thermodynamics Inc. , 2011. [Online]. Available: http://www.calphad.com/titanium-aluminum.html. [Accessed 21 May 2018].

[14] D. J. Schrock, D. Kang, T. R. Bieler and P. Kwon, "Phase Dependent Tool Wear in Turning Ti-6Al-4V Using Polycrystalline Diamond and Carbide Inserts," *Journal of Manufacturing Science and Engineering,* vol. 136, p. 6, 2014.

[15] D. Jacobsson, Crystal Structures in GaAs Nanowires - Growth and Characterization, Lund: Lund University - Solid State Physics, 2015.

[16] D. Lindgren, Optical Characterization of III-Nitride and III-V Semiconductor Nanowires, Lund: Lund University, Department of Physics, Division of Solid State Physics, 2014.

[17] J. Gierak, "Focused ion beam technology and ultimate applications," *SEMICONDUCTOR SCIENCE AND TECHNOLOGY,* vol. 24, p. 1, 2009.

[18] "Zeiss, Home/Products/FIB-SEM instruments/Crossbeam/crossbeam-technology," Carl Zeiss, Inc., [Online]. Available: https://www.zeiss.com/microscopy/us/products/fib-sem-instruments/crossbeam/crossbeam-technology.html. [Accessed 13 06 2018].

[19] J.-E. Ståhl, "An integrated cost model for metal cutting operations based on engagement time and a cost breakdown approach," *Int. J. Manufacturing Research,* vol. 12, no. 4, pp. 379-404, 2017.

[20] D. Johansson, F. Schultheiss, V. Bushlya, J. Zhou and J.-E. Ståhl, "Tool life and wear model in metal cutting, part 1 - Influence of varying flank wear criterion on Colding's tool life equation," p. 3, 2014.

9 Appendix A – Tool life, surface roughness and material removal rate

This appendix presents the tool lives, surface roughness and material removal rate acquired for all cutting tools.

9.1 UCC 2

Figure 9-1 presents the used cutting speeds and feeds and the respective tool life acquired. Figure 9-2 presents the acquired surface roughness, for the last machined pass, in addition to the chosen cutting speed and feed. Figure 9-3 presents the material removal rate in addition to the chosen cutting speed and feed.

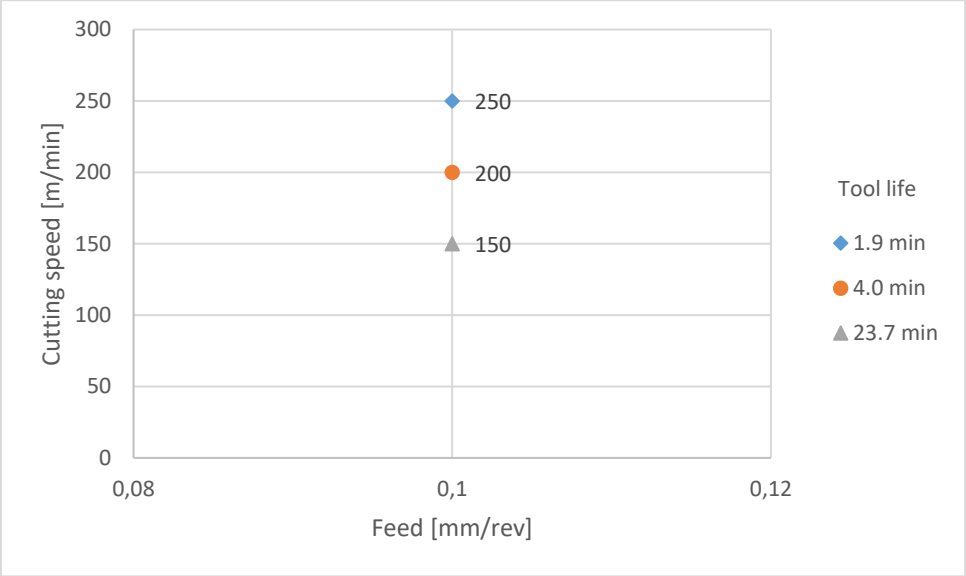

Figure 9-1. The used cutting speeds and feeds for UCC 2 with the respective tool life.

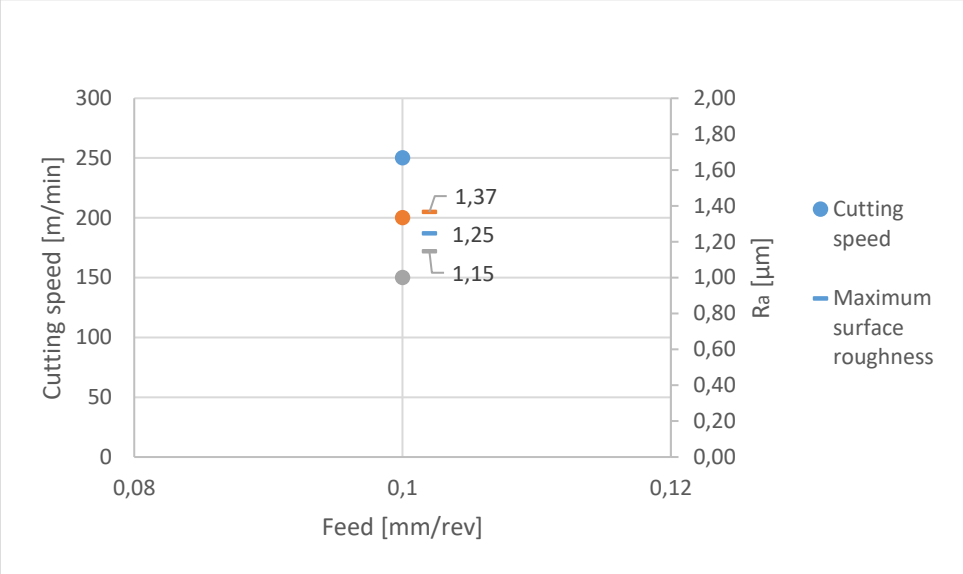

Figure 9-2. The cutting speeds and feeds with the corresponding surface roughness for UCC 2.

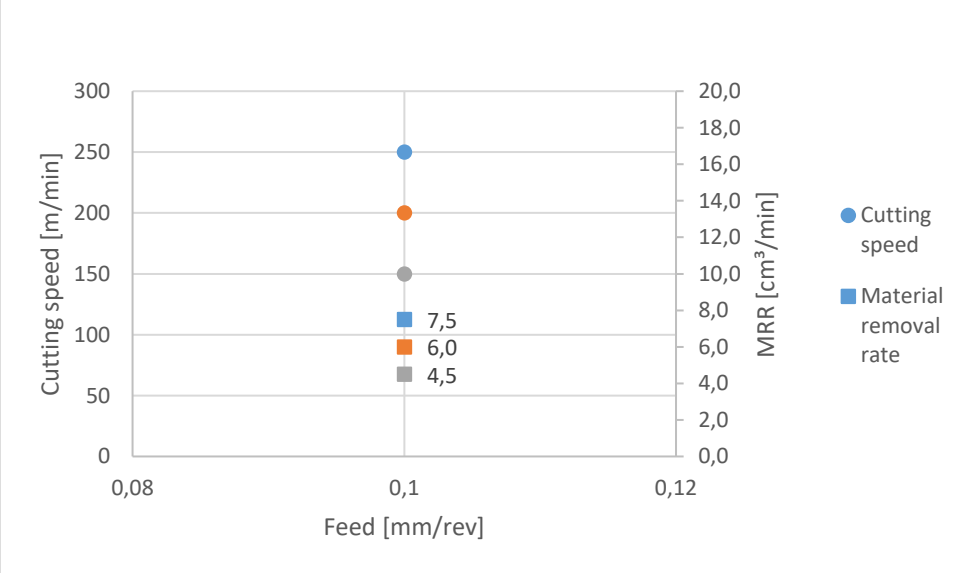

Figure 9-3. The cutting speeds and feeds with the corresponding material removal rate for UCC 2.

9.2 CCC 1

Figure 9-4 presents the used cutting speeds and feeds and the respective tool life acquired. Figure 9-5 presents the acquired surface roughness, for the last machined pass, in addition to the chosen cutting speed and feed. Figure 9-6 presents the material removal rate in addition to the chosen cutting speed and feed.

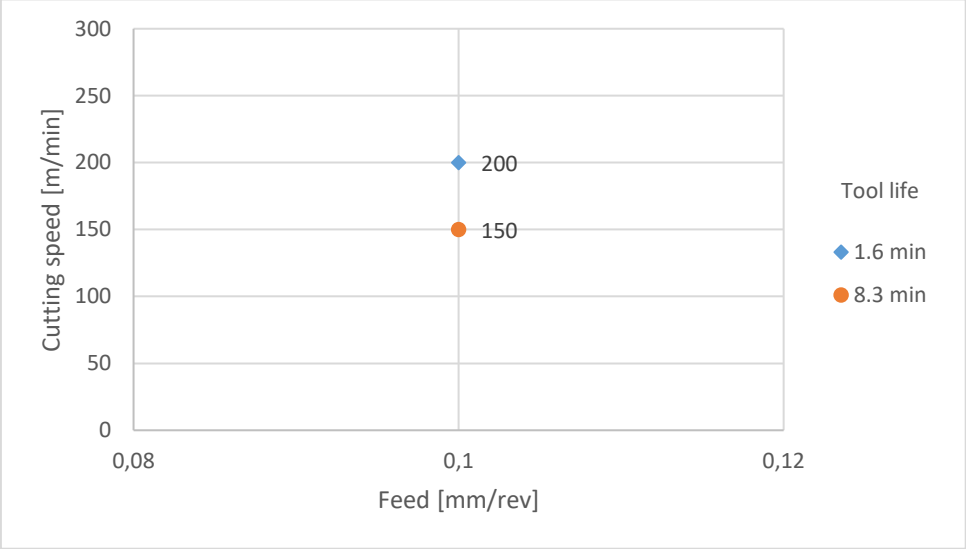

Figure 9-4. The used cutting speeds and feeds for CCC 1 with the respective tool life.

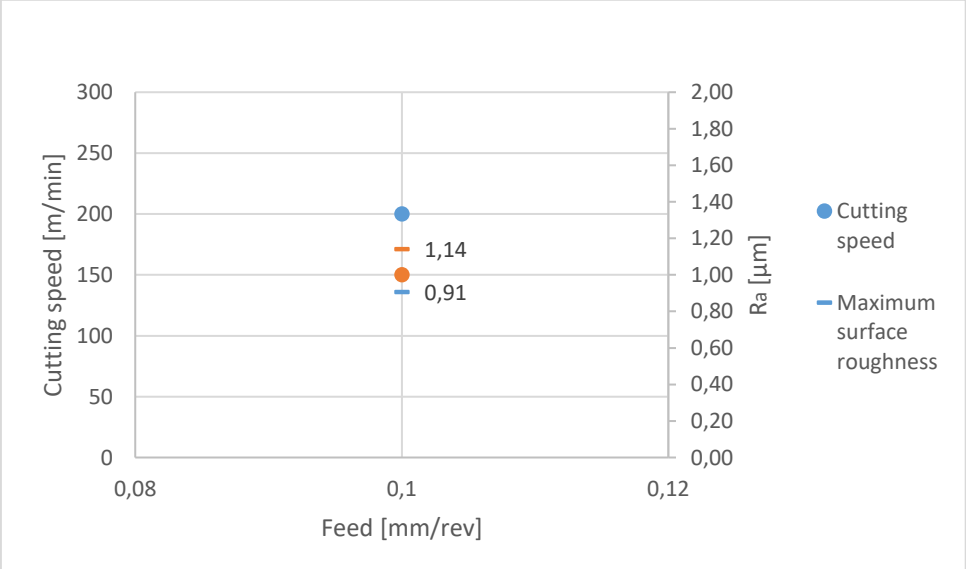

Figure 9-5. The cutting speeds and feeds with the corresponding surface roughness for CCC 1.

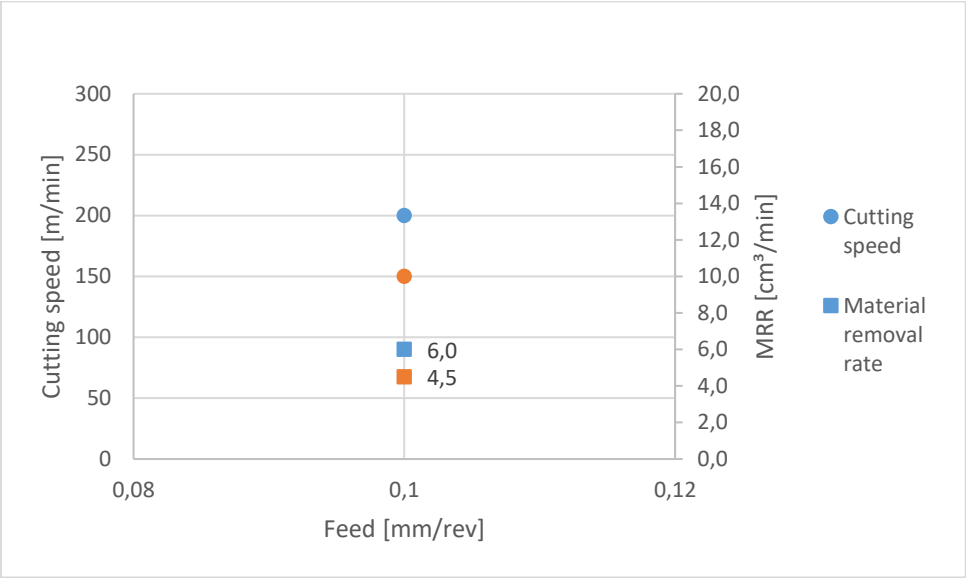

Figure 9-6. The cutting speeds and feeds with the corresponding material removal rate for CCC 1.

9.3 PCD 8

Figure 9-7 presents the used cutting speeds and feeds and the respective tool life acquired. Figure 9-8 presents the acquired surface roughness, for the last machined pass, in addition to the chosen cutting speed and feed. Figure 9-9 presents the material removal rate in addition to the chosen cutting speed and feed.

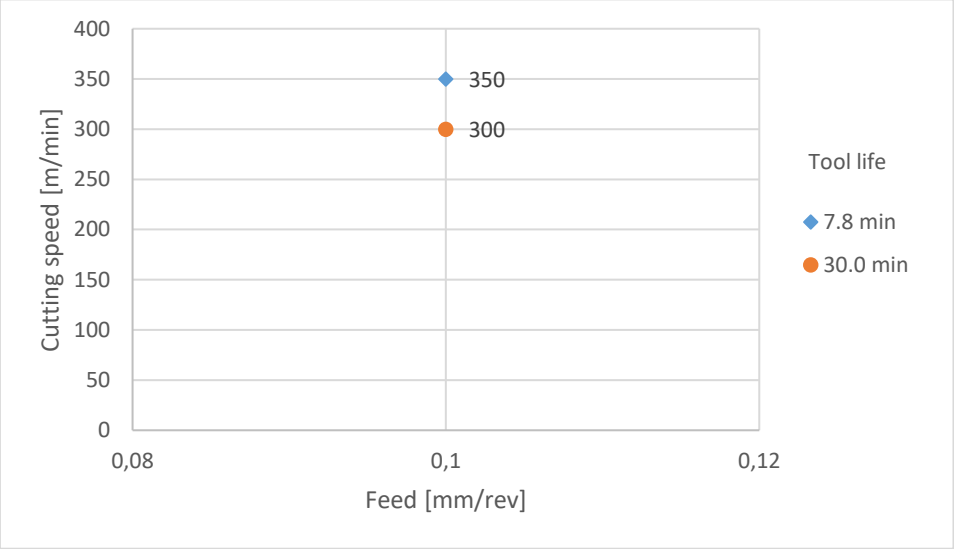

Figure 9-7. The used cutting speeds and feeds for PCD 8 with the respective tool life.

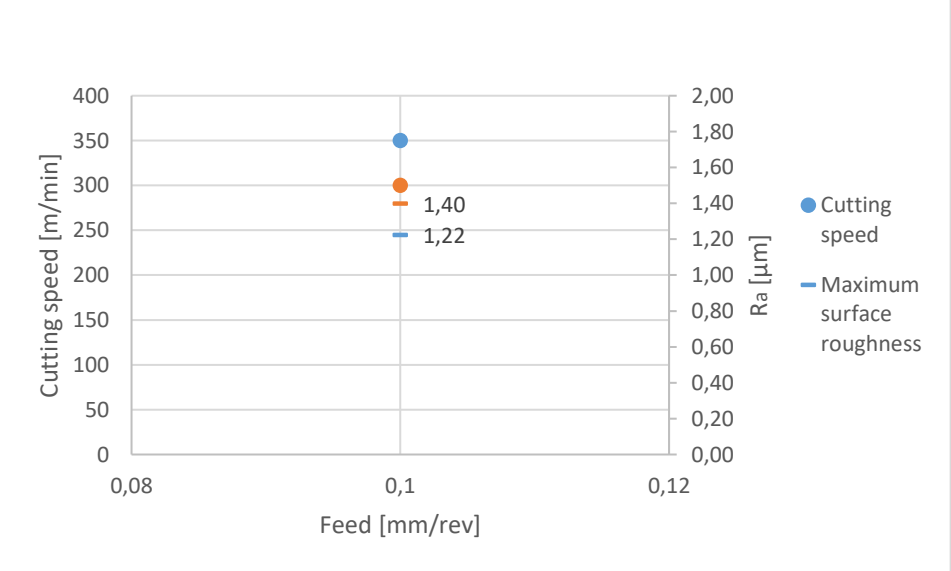

Figure 9-8. The cutting speeds and feeds with the corresponding surface roughness for PCD 8.

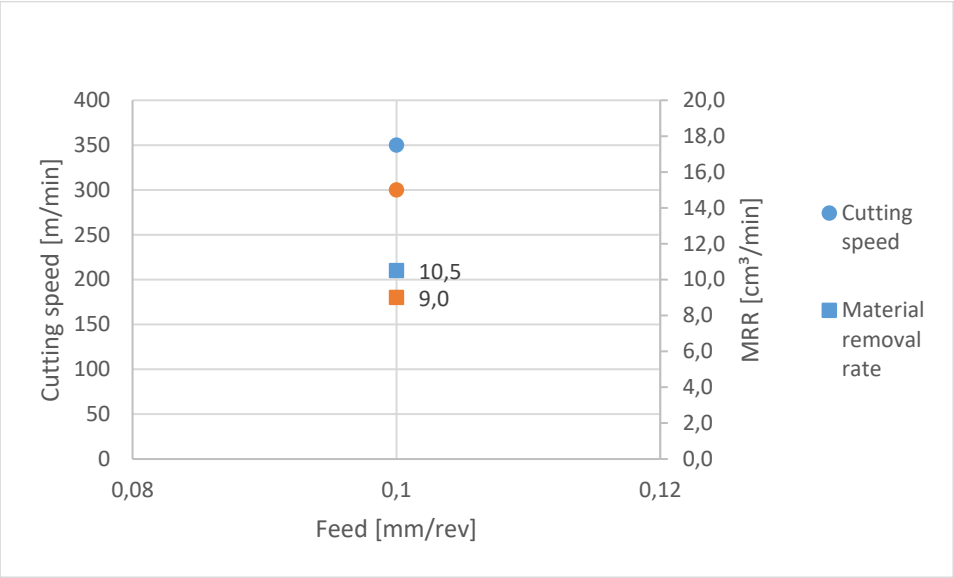

Figure 9-9. The cutting speeds and feeds with the corresponding material removal rate for PCD 8.

9.4 cBN 2

Figure 9-10 presents the used cutting speeds and feeds and the respective tool life acquired. Figure 9-11 presents the acquired surface roughness, for the last machined pass, in addition to the chosen cutting speed and feed. Figure 9-12 presents the material removal rate in addition to the chosen cutting speed and feed.

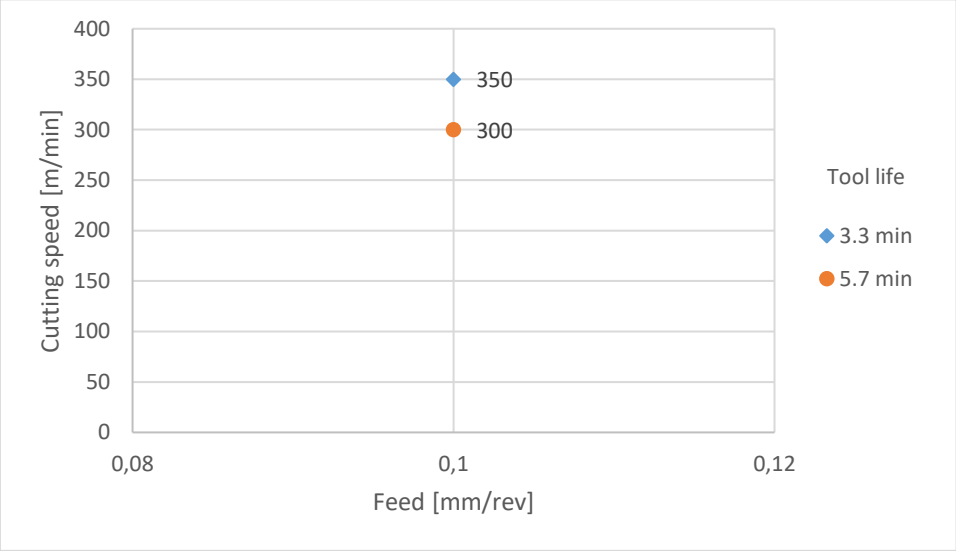

Figure 9-10. The used cutting speeds and feeds for cBN 2 with the respective tool life.

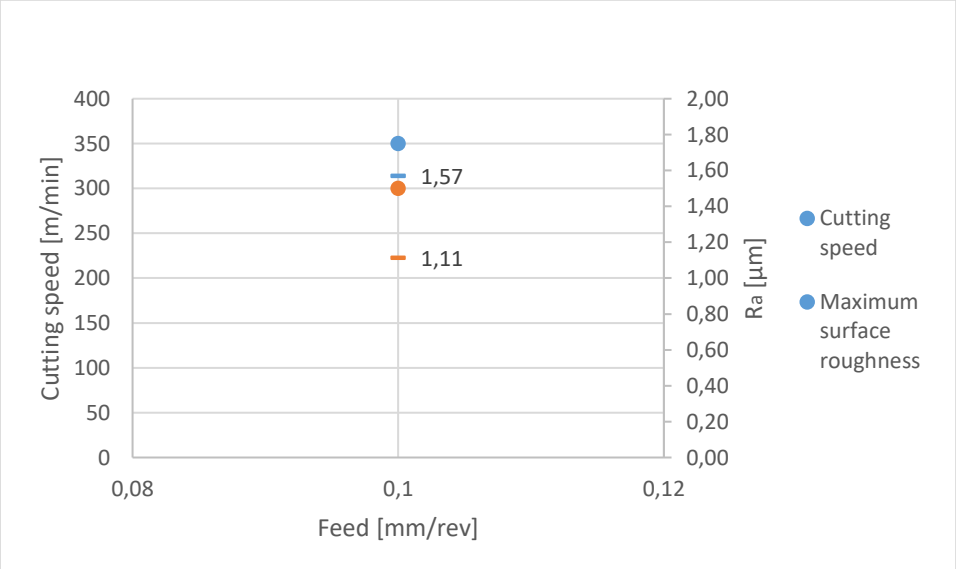

Figure 9-11. The cutting speeds and feeds with the corresponding surface roughness for cBN 2.

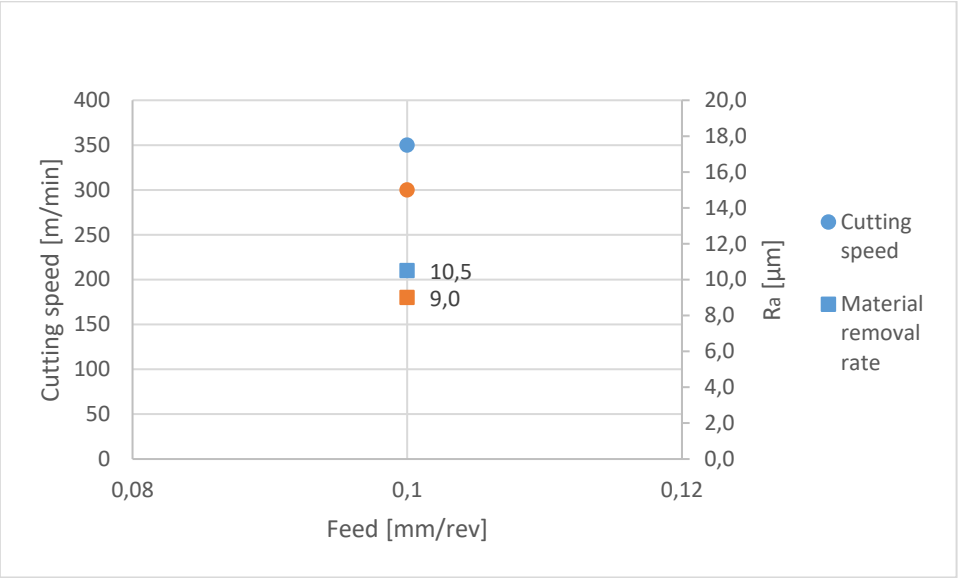

Figure 9-12. The cutting speeds and feeds with the corresponding material removal rate for cBN 2.

9.5 cBN 3

Figure 9-13 presents the used cutting speeds and feeds and the respective tool life acquired. Figure 9-14 presents the acquired surface roughness, for the last machined pass, in addition to the chosen cutting speed and feed. Figure 9-15 presents the material removal rate in addition to the chosen cutting speed and feed.

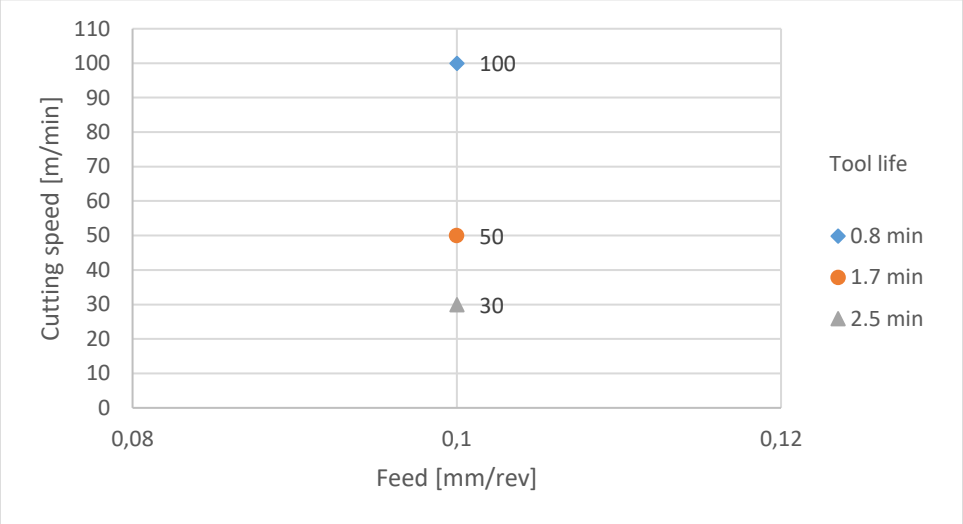

Figure 9-13. The used cutting speeds and feeds for cBN 3 with the respective tool life.

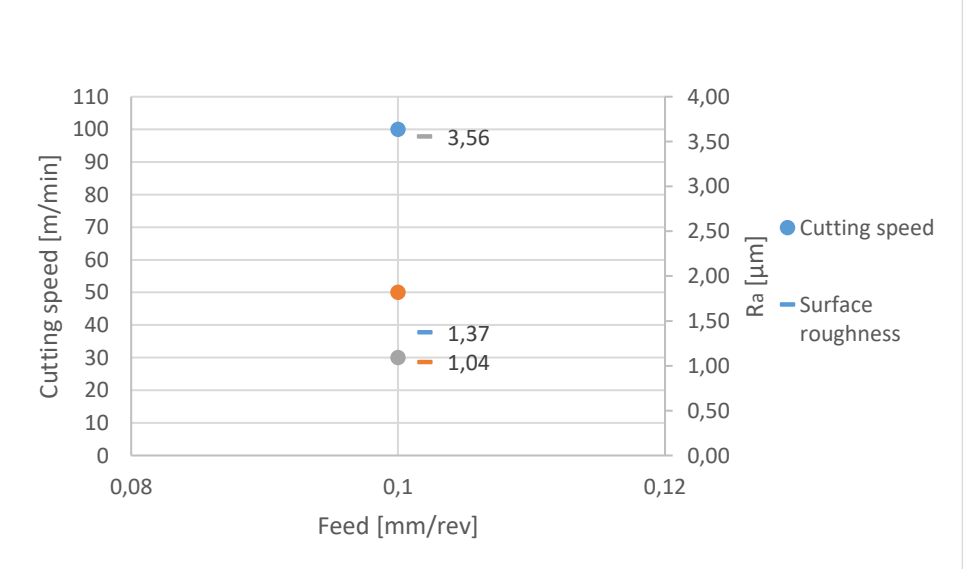

Figure 9-14. The cutting speeds and feeds with the corresponding surface roughness for cBN 3.

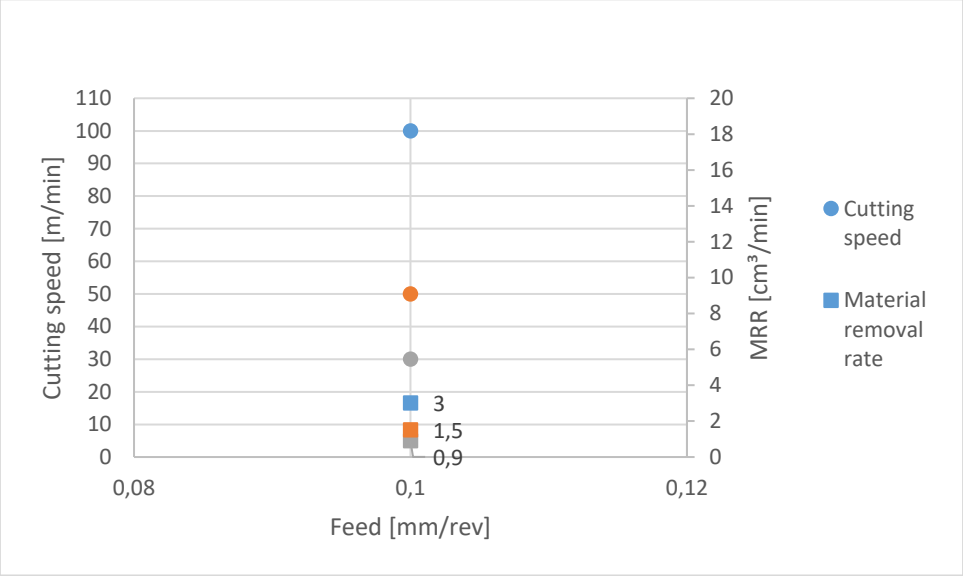

Figure 9-15. The cutting speeds and feeds with the corresponding material removal rate for cBN 3.

10 Appendix B – Flank wear curves

This appendix presents the flank wear development as a function of both the engagement time and engagement distance.

10.1 UCC 2

Figure 10-1 presents the flank wear development as a function of the engagement time.

Figure 10-2, Figure 10-4, Figure 10-6 and Figure 10-8 presents the flank wear and the surface roughness development as a function of the engagement time.

Figure 10-3, Figure 10-5, Figure 10-7 and Figure 10-9 presents the flank wear and the surface roughness development as a function of the engagement distance.

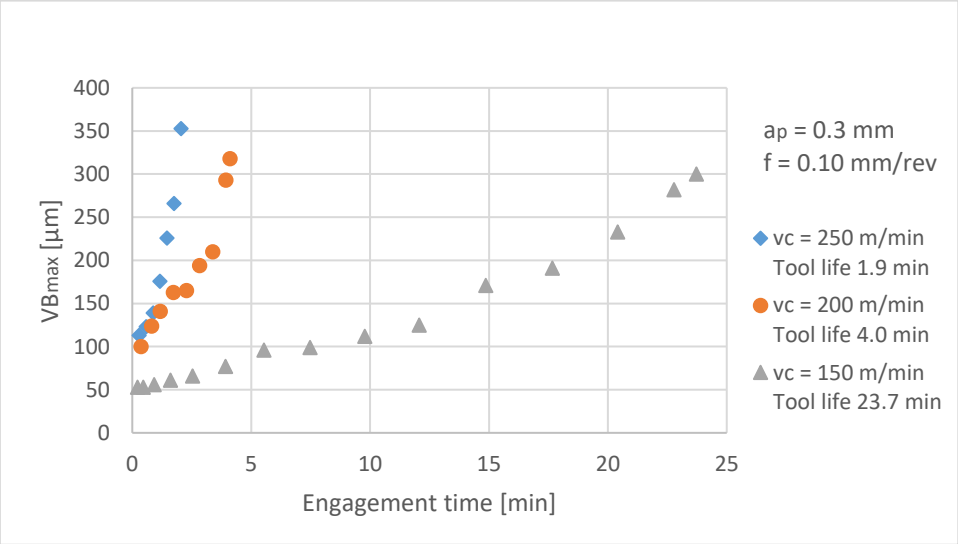

Figure 10-1. UCC 2: The flank wear development as a function of the engagement time for the cutting data and tool life: a_p = 0.3 mm, f = 0.10 mm/rev, v_c = 250//220//150 m/min, T = 1.9//4.0//23.7 min.

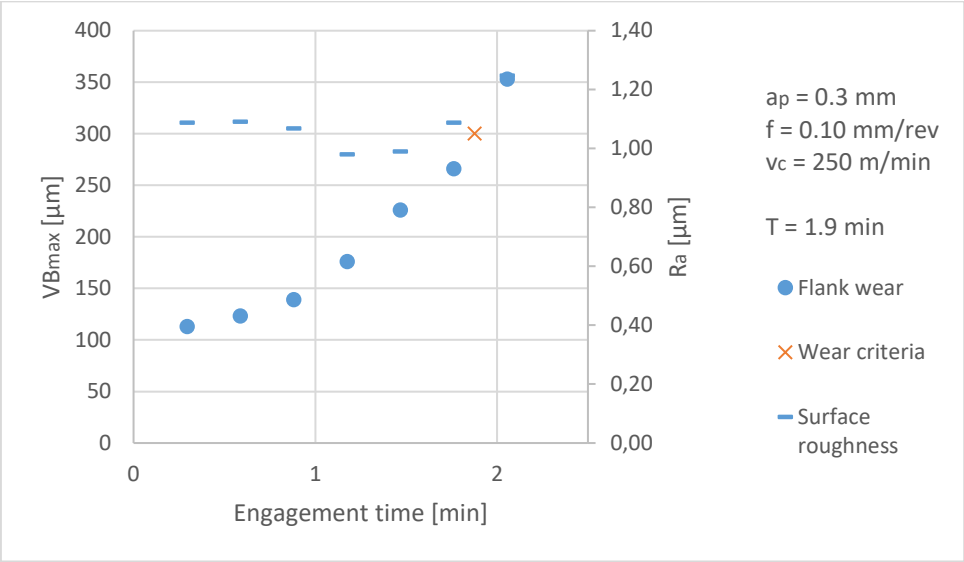

Figure 10-2. UCC 2: The flank wear and the surface roughness development as a function of the engagement time for the cutting data and tool life: a_p = 0.3 mm, f = 0.10 mm/rev, v_c = 250 m/min, T = 1.9 min.

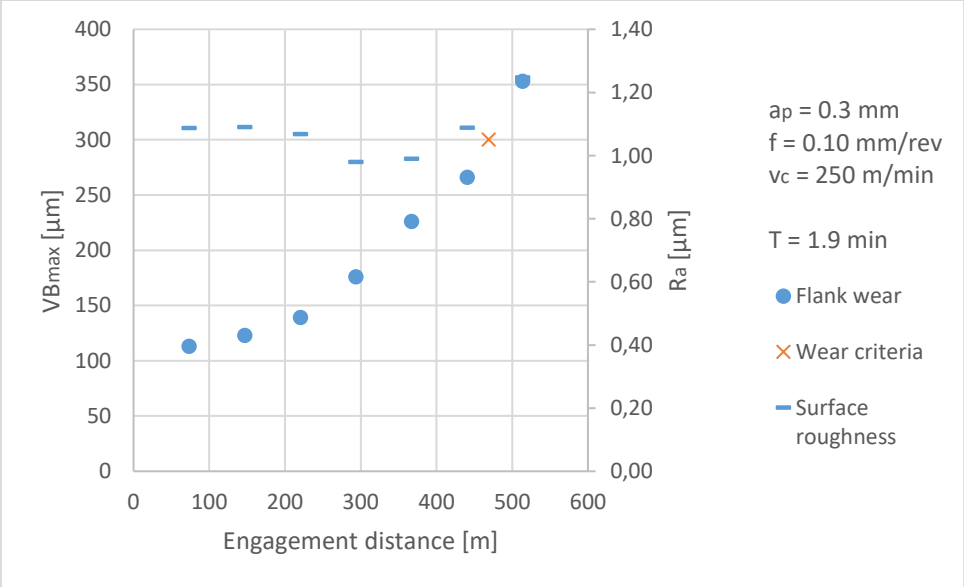

Figure 10-3. UCC 2: The flank wear and the surface roughness development as a function of the engagement distance for the cutting data and tool life: a_p = 0.3 mm, f = 0.10 mm/rev, v_c = 250 m/min, T = 1.9 min.

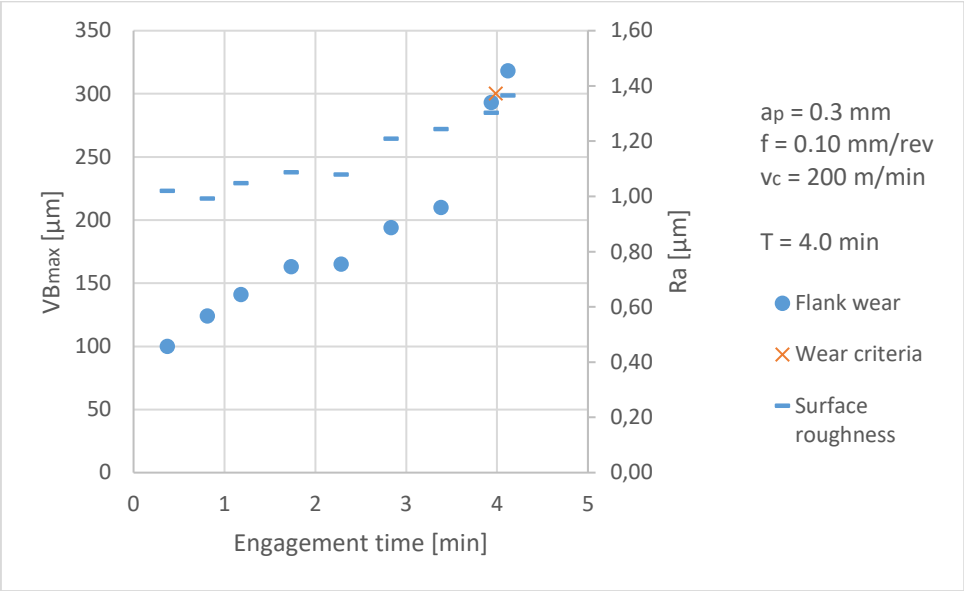

Figure 10-4. UCC 2: The flank wear and the surface roughness development as a function of the engagement time for the cutting data and tool life: a_p = 0.3 mm, f = 0.10 mm/rev, v_c = 200 m/min, T = 4.0 min.

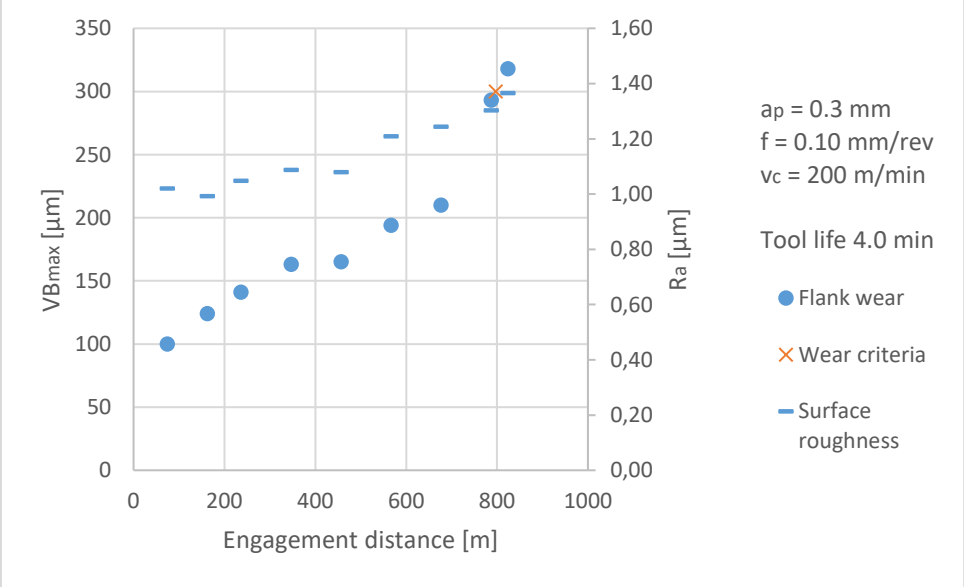

Figure 10-5. UCC 2: The flank wear and the surface roughness development as a function of the engagement distance for the cutting data and tool life: a_p = 0.3 mm, f = 0.10 mm/rev, v_c = 200 m/min, T = 4.0 min.

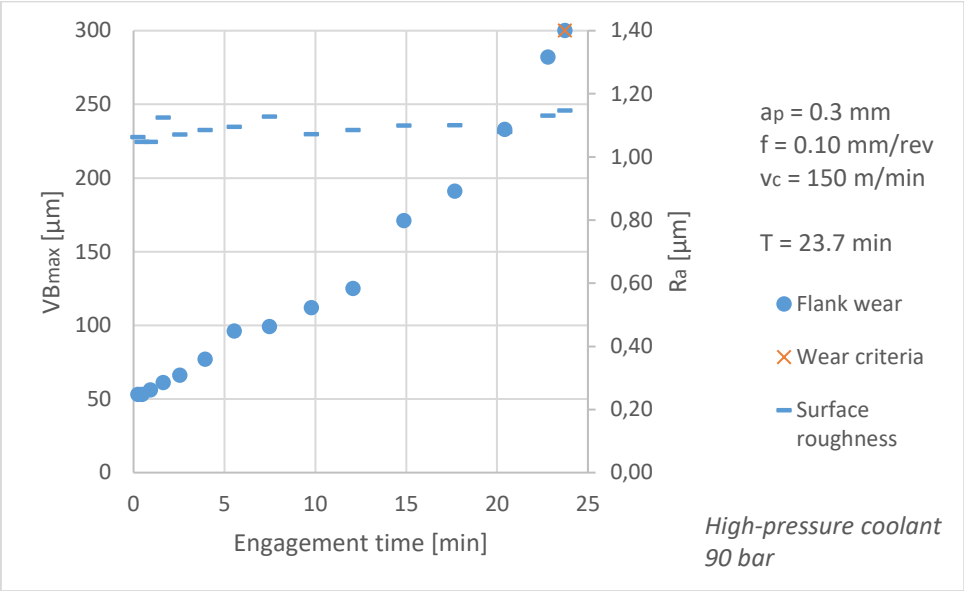

Figure 10-6. UCC 2: The flank wear and the surface roughness development as a function of the engagement time for the cutting data and tool life: a_p = 0.3 mm, f = 0.10 mm/rev, v_c = 150 m/min, T = 23.7 min. Coolant pressure 90 bar.

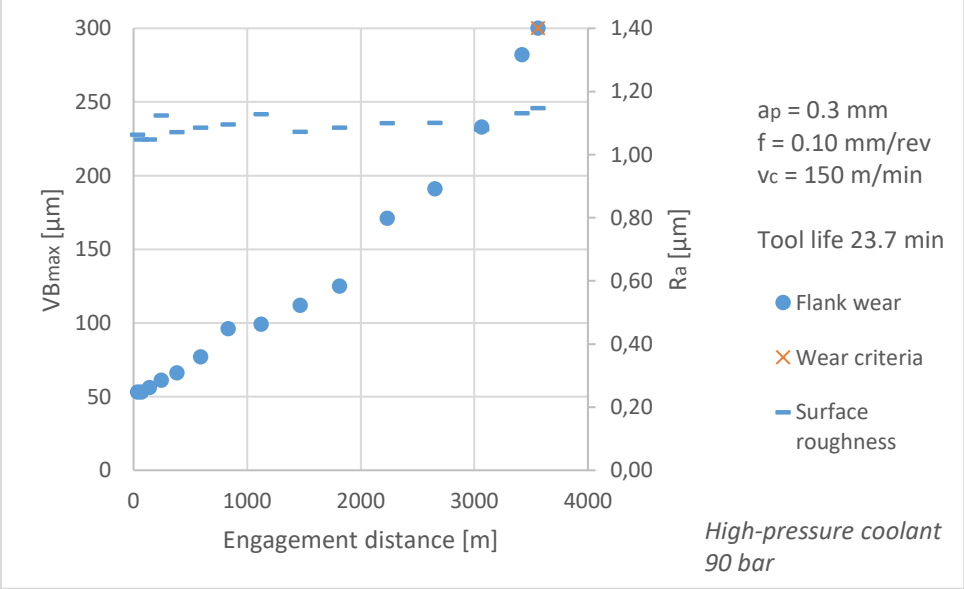

Figure 10-7. UCC 2: The flank wear and the surface roughness development as a function of the engagement distance for the cutting data and tool life: a_p = 0.3 mm, f = 0.10 mm/rev, v_c = 150 m/min, T = 23.7 min. Coolant pressure 90 bar.

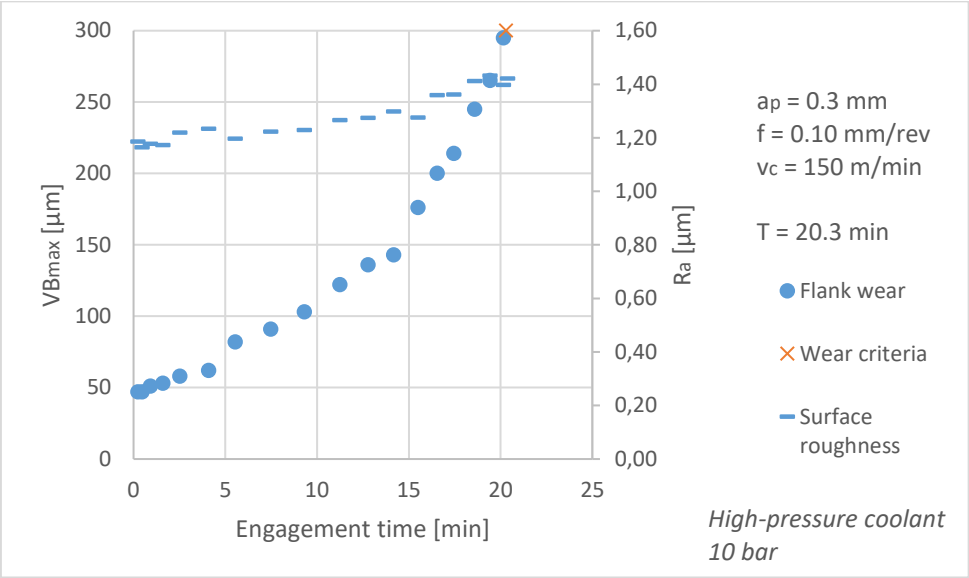

Figure 10-8. UCC 2: The flank wear and the surface roughness development as a function of the engagement time for the cutting data and tool life: a_p = 0.3 mm, f = 0.10 mm/rev, v_c = 150 m/min, T = 20.3 min. Coolant pressure 10 bar.

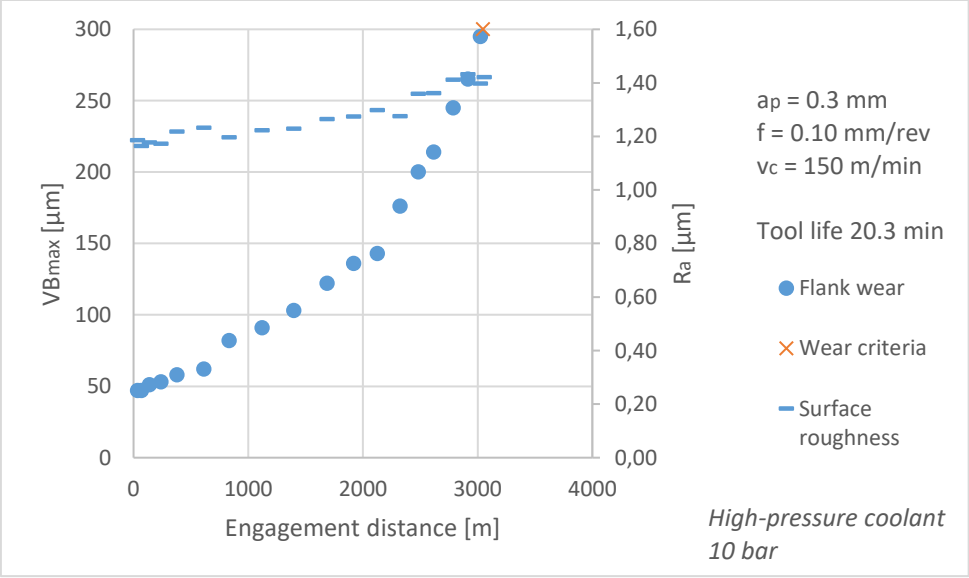

Figure 10-9. UCC 2: The flank wear and the surface roughness development as a function of the engagement distance for the cutting data and tool life: a_p = 0.3 mm, f = 0.10 mm/rev, v_c = 150 m/min, T = 20.3 min. Coolant pressure 10 bar.

10.2 CCC 1

Figure 10-10 presents the flank wear development as a function of the engagement time.

Figure 10-11 and Figure 10-13 presents the flank wear and the surface roughness development as a function of the engagement time.

Figure 10-12 and Figure 10-14presents the flank wear and the surface roughness development as a function of the engagement distance.

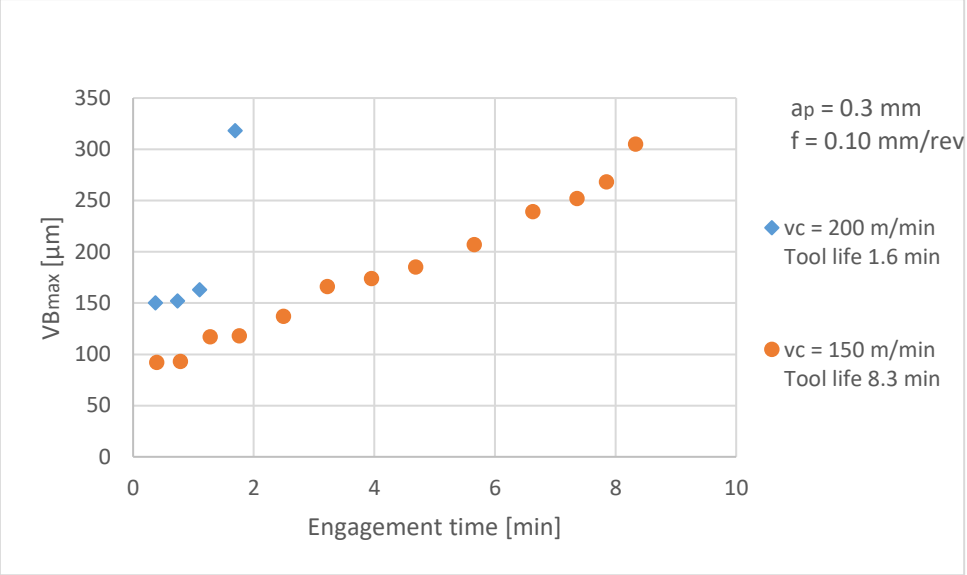

Figure 10-10. CCC 1: The flank wear and the surface roughness development as a function of the engagement time for the cutting data and tool life: a_p = 0.3 mm, f = 0.10 mm/rev, v_c = 200//150 m/min, T = 1.6//8.3 min.

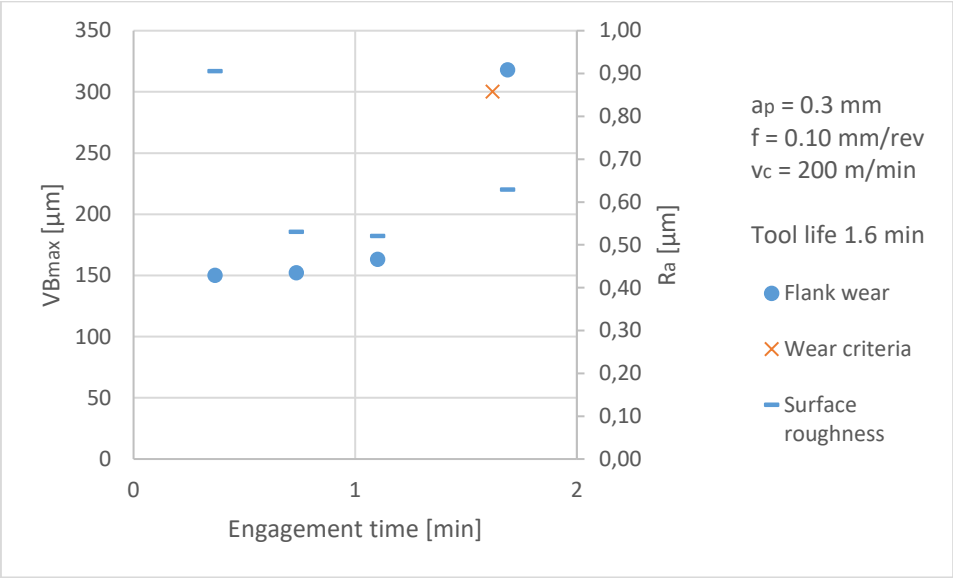

Figure 10-11. CCC 1: The flank wear and the surface roughness development as a function of the engagement time for the cutting data and tool life: a_p = 0.3 mm, f = 0.10 mm/rev, v_c = 200 m/min, T = 1.6 min.

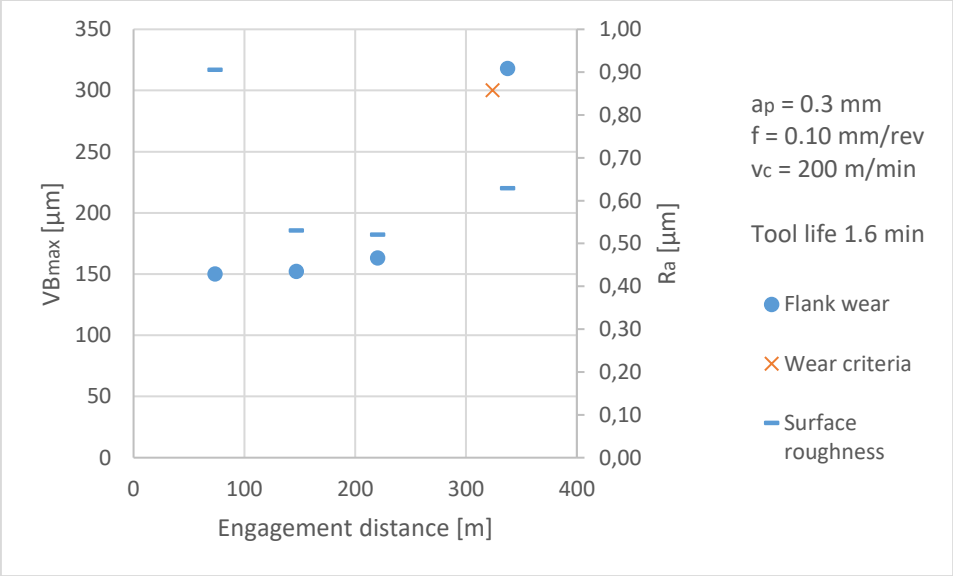

Figure 10-12. CCC 1: The flank wear and the surface roughness development as a function of the engagement distance for the cutting data and tool life: a_p = 0.3 mm, f = 0.10 mm/rev, v_c = 200 m/min, T = 1.6 min.

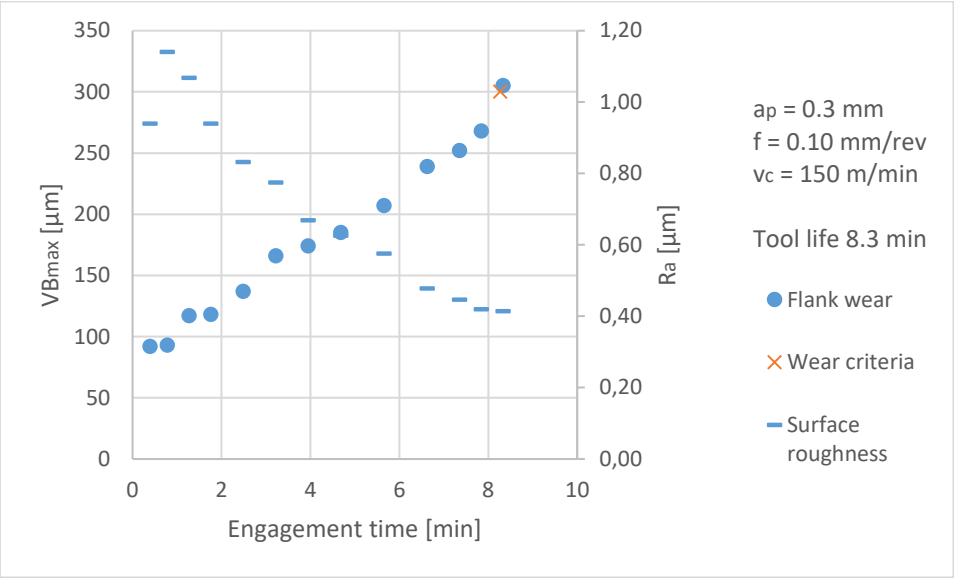

Figure 10-13. CCC 1: The flank wear and the surface roughness development as a function of the engagement time for the cutting data and tool life: a_p = 0.3 mm, f = 0.10 mm/rev, v_c = 150 m/min, T = 8.3 min.

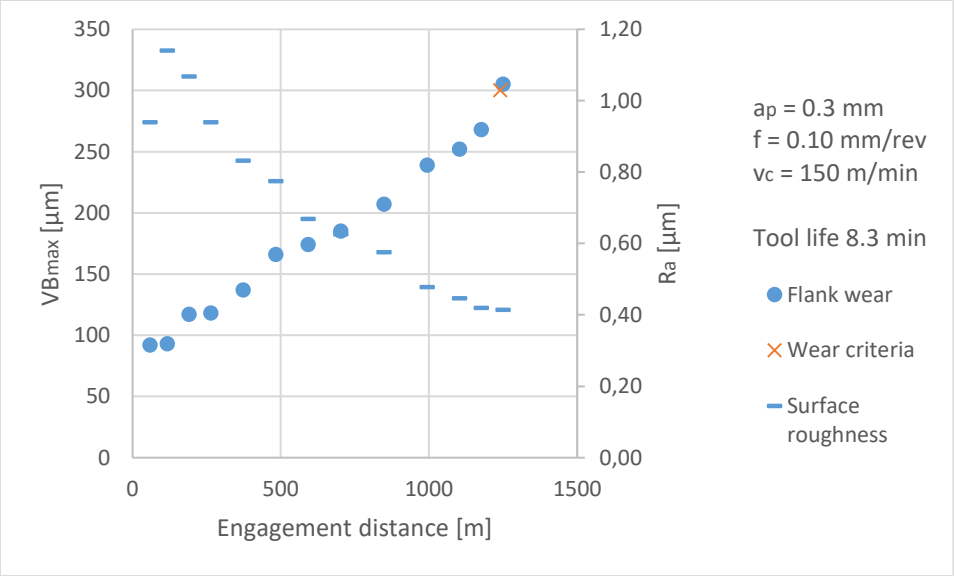

Figure 10-14. CCC 1: The flank wear and the surface roughness development as a function of the engagement distance for the cutting data and tool life: a_p = 0.3 mm, f = 0.10 mm/rev, v_c = 150 m/min, T = 8.3 min.

10.3 PCD 8

Figure 10-15 presents the flank wear development as a function of the engagement time.

Figure 10-16 and Figure 10-18 presents the flank wear and the surface roughness development as a function of the engagement time.

Figure 10-17 and Figure 10-19 presents the flank wear and the surface roughness development as a function of the engagement distance.

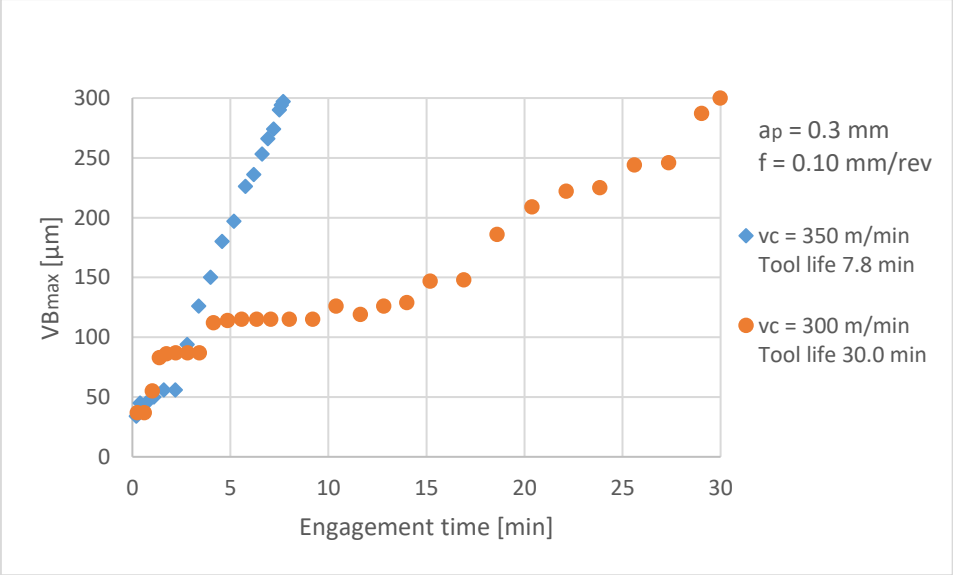

Figure 10-15. PCD 8: The flank wear development as a function of the engagement time for the cutting data and tool life: a_p = 0.3 mm, f = 0.10 mm/rev, v_c = 350//300 m/min, T = 7.8//30.0 min.

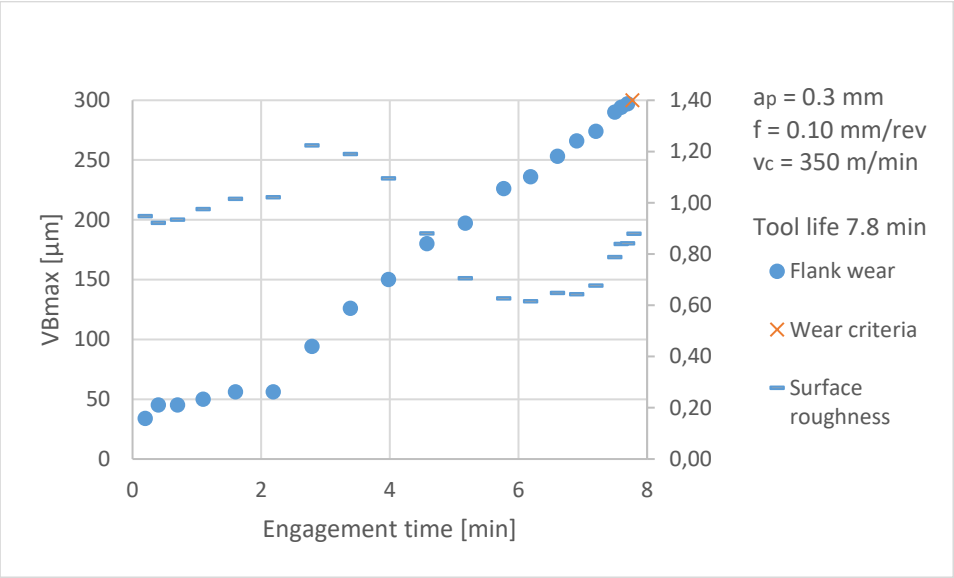

Figure 10-16. PCD 8: The flank wear and the surface roughness development as a function of the engagement time for the cutting data and tool life: a_p = 0.3 mm, f = 0.10 mm/rev, v_c = 350 m/min, T = 7.8 min.

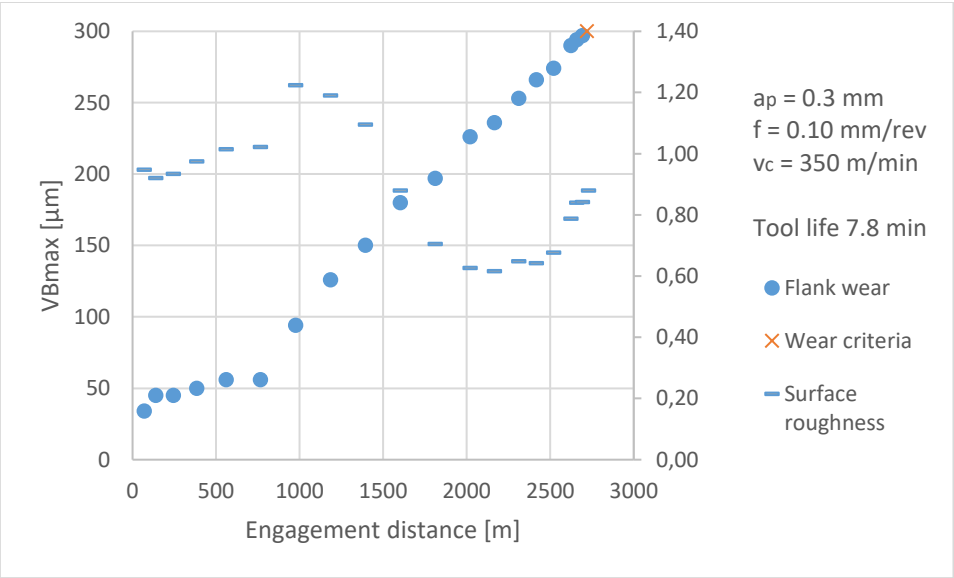

Figure 10-17. PCD 8: The flank wear and the surface roughness development as a function of the engagement distance for the cutting data and tool life: a_p = 0.3 mm, f = 0.10 mm/rev, v_c = 350 m/min, T = 7.8 min.

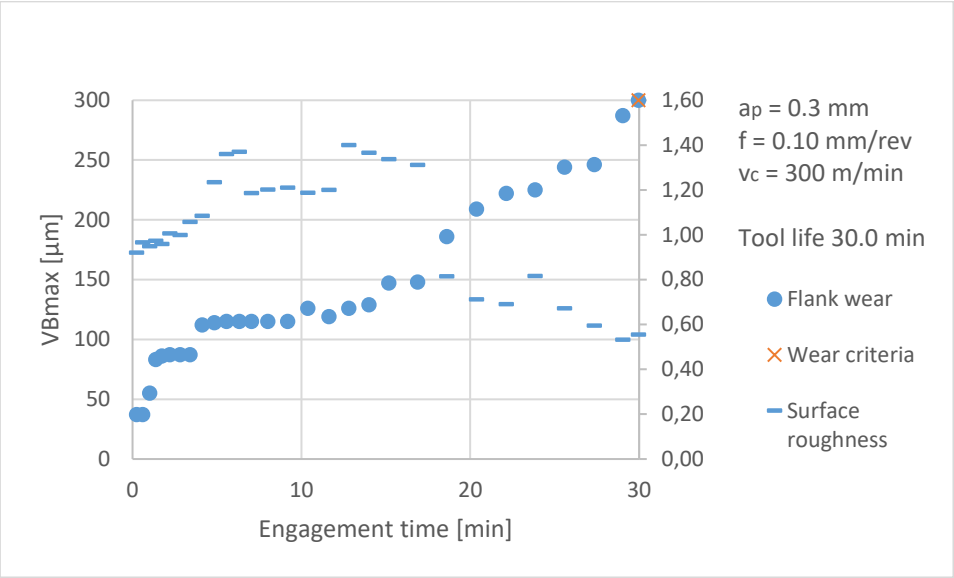

Figure 10-18. PCD 8: The flank wear and the surface roughness development as a function of the engagement time for the cutting data and tool life: a_p = 0.3 mm, f = 0.10 mm/rev, v_c = 300 m/min, T = 30.0 min.

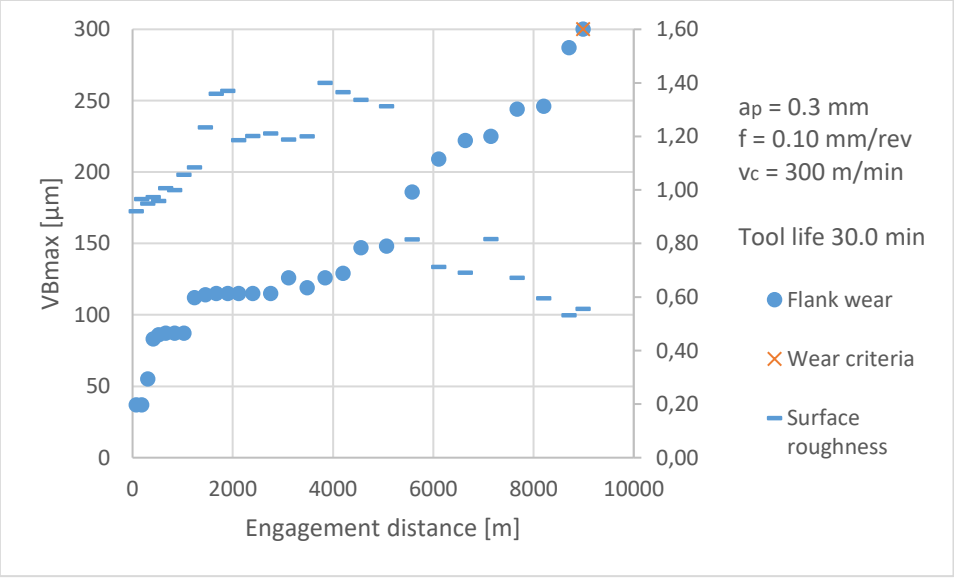

Figure 10-19. PCD 8: The flank wear and the surface roughness development as a function of the engagement distance for the cutting data and tool life: a_p = 0.3 mm, f = 0.10 mm/rev, v_c = 300 m/min, T = 30.0 min.

10.4 cBN 2

Figure 10-20 presents the flank wear development as a function of the engagement time.

Figure 10-21 and Figure 10-23 presents the flank wear and the surface roughness development as a function of the engagement time.

Figure 10-22 and Figure 10-24 presents the flank wear and the surface roughness development as a function of the engagement distance.

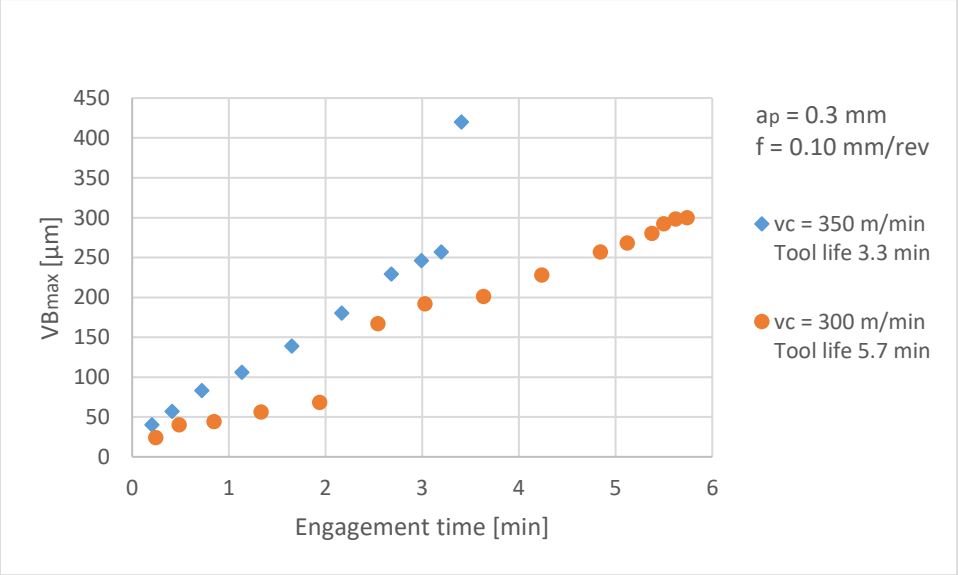

Figure 10-20. cBN 2: The flank wear and the surface roughness development as a function of the engagement time for the cutting data and tool life: a_p = 0.3 mm, f = 0.10 mm/rev, v_c = 350//300 m/min, T = 3.3//5.7 min.

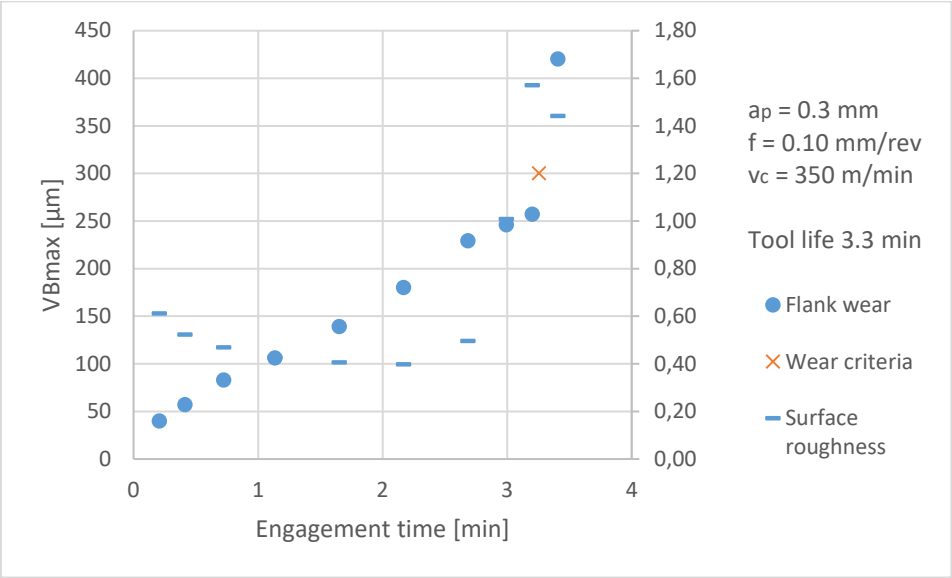

Figure 10-21. cBN 2: The flank wear and the surface roughness development as a function of the engagement time for the cutting data and tool life: a_p = 0.3 mm, f = 0.10 mm/rev, v_c = 350 m/min, T = 3.3 min.

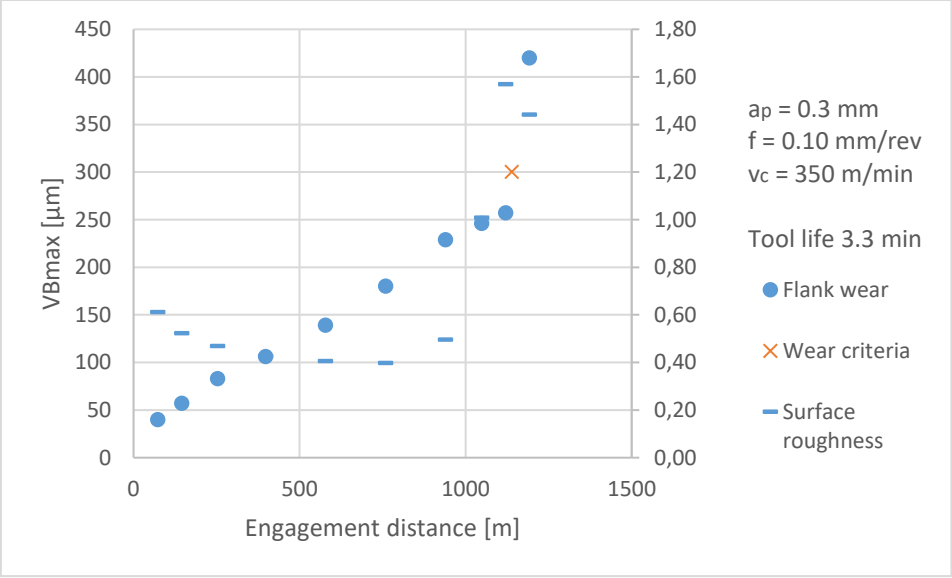

Figure 10-22. cBN 2: The flank wear and the surface roughness development as a function of the engagement distance for the cutting data and tool life: a_p = 0.3 mm, f = 0.10 mm/rev, v_c = 350 m/min, T = 3.3 min.

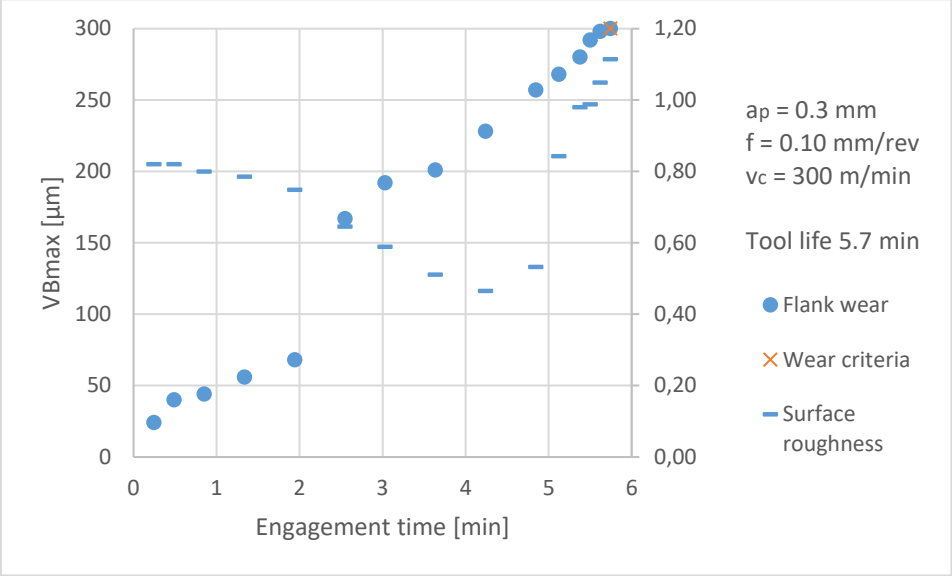

Figure 10-23. cBN 2: The flank wear and the surface roughness development as a function of the engagement time for the cutting data and tool life: a_p = 0.3 mm, f = 0.10 mm/rev, v_c = 300 m/min, T = 5.7 min.

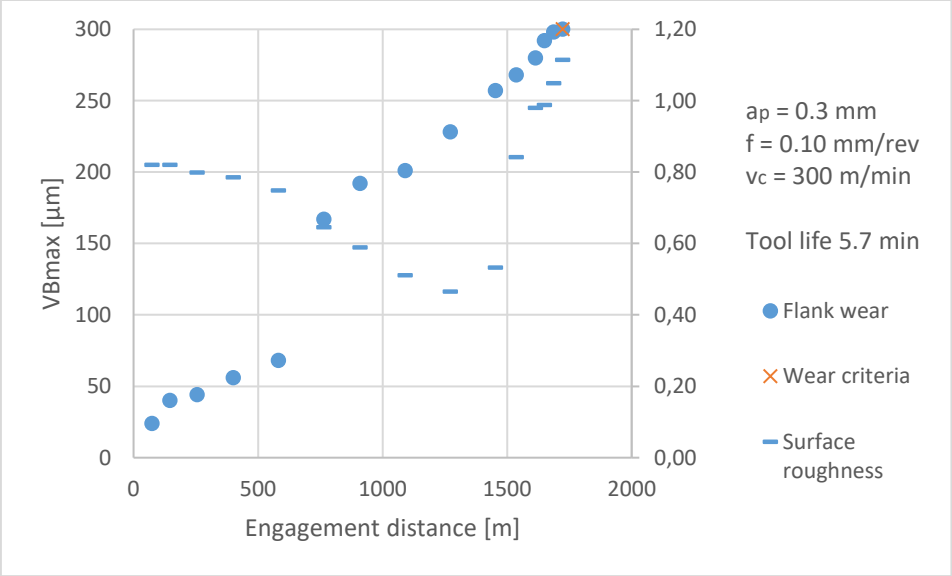

Figure 10-24. cBN 2: The flank wear and the surface roughness development as a function of the engagement distance for the cutting data and tool life: a_p = 0.3 mm, f = 0.10 mm/rev, v_c = 300 m/min, T = 5.7 min.

10.5 cBN 3

Figure 10-25 presents the flank wear development as a function of the engagement time.

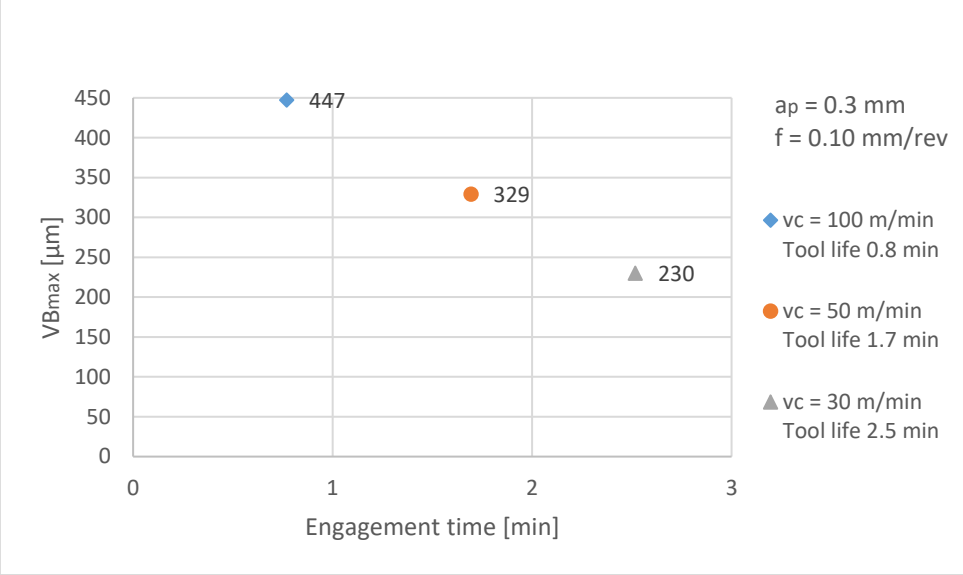

Figure 10-25. cBN 3: The flank wear and the surface roughness development as a function of the engagement time for the cutting data and tool life: a_p = 0.3 mm, f = 0.10 mm/rev, v_c = 100//50//30 m/min, T = 0.8//1.7//2.5 min.

11 Appendix C – Cutting forces

This appendix presents the mean cutting forces acquired for each passing for a certain cutting tool, cutting data and tool life. The last passing continuous force measurement is also presented to show how the wear development affects the cutting forces. In these figures it can be observed where the limits are set for calculating the mean cutting forces.

11.1 UCC 2

Figure 11-1, Figure 11-3, Figure 11-5 and Figure 11-7 presents the mean cutting forces development plotted for the engagement time.

Figure 11-2, Figure 11-4, Figure 11-6 and Figure 11-8 presents the last passing continuous force measurement plotted for the engagement time.

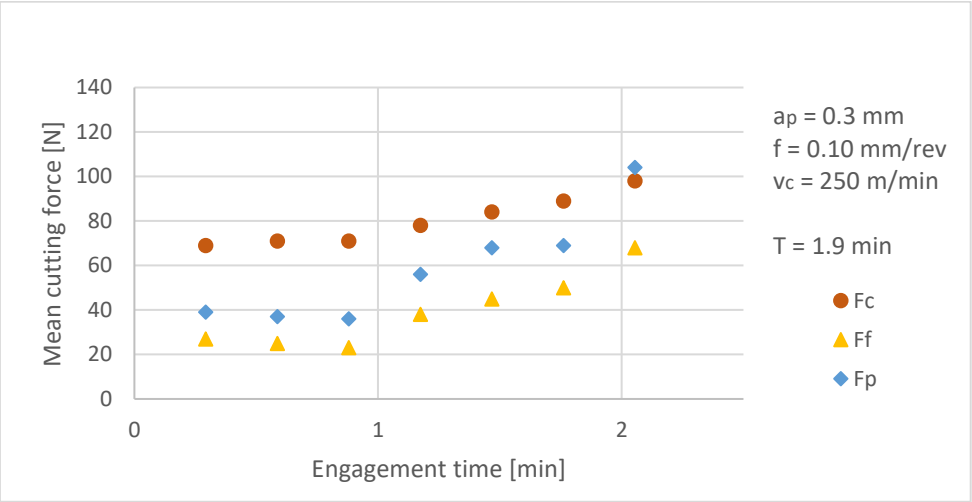

Figure 11-1. UCC 2: The mean cutting forces development during the engagement time for the cutting data and tool life: a_p = 0.3 mm, f = 0.10 mm/rev, v_c = 250 m/min, T = 1.9 min.

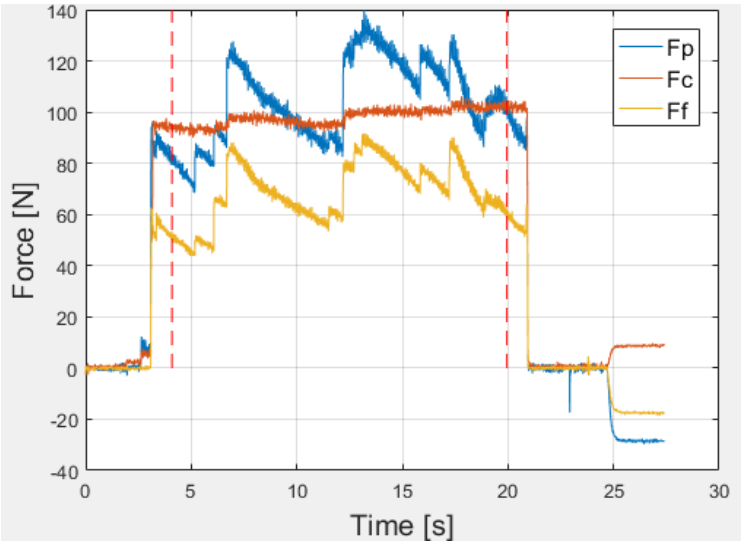

Figure 11-2. UCC 2: The last passing continuous force measurement for the cutting data and tool life: a_p = 0.3 mm, f = 0.10 mm/rev, v_c = 250 m/min, T = 1.9 min.

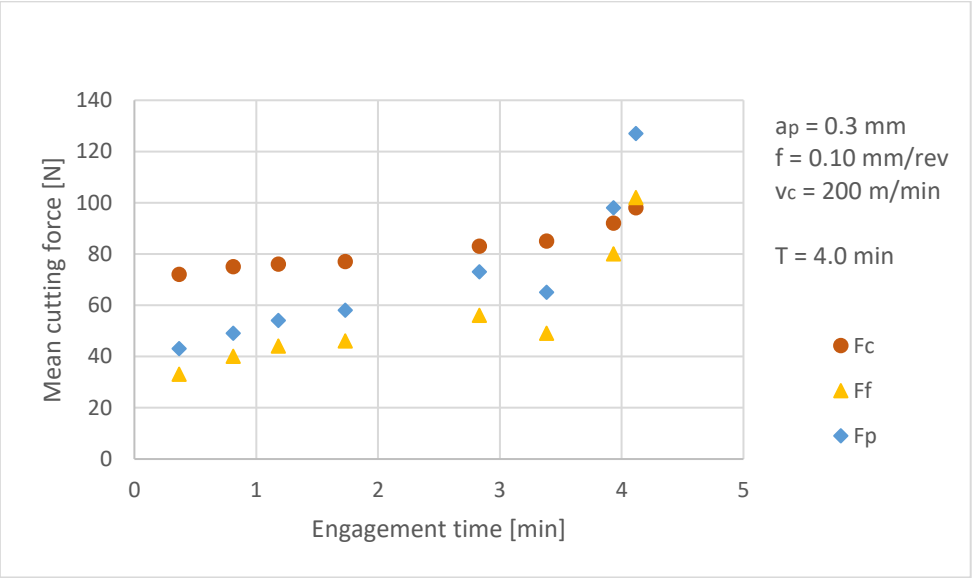

Figure 11-3. UCC 2: The mean cutting forces development during the engagement time for the cutting data and tool life: a_p = 0.3 mm, f = 0.10 mm/rev, v_c = 200 m/min, T = 4.0 min.

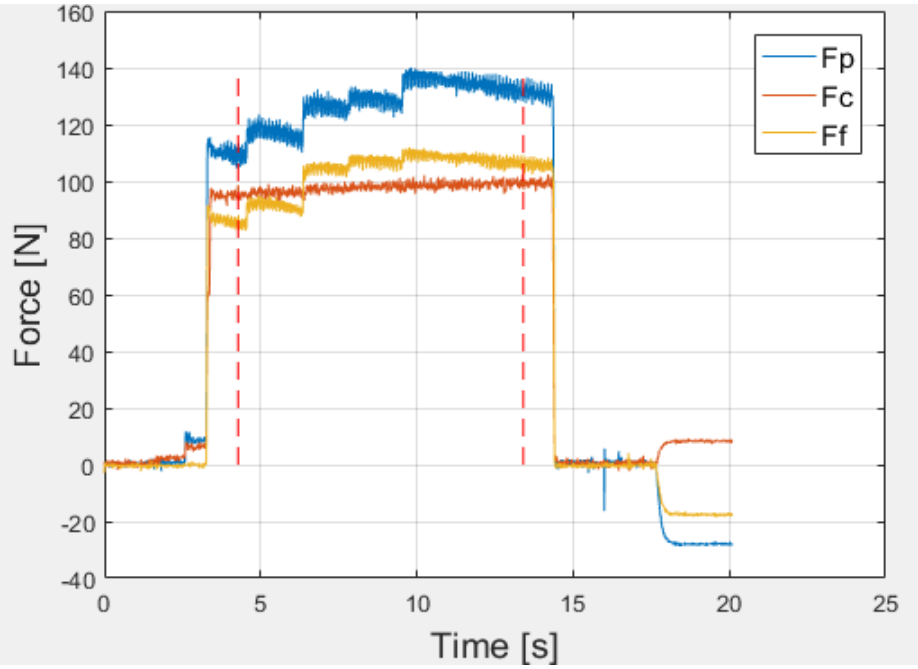

Figure 11-4. UCC 2: The last passing continuous force measurement for the cutting data and tool life: a_p = 0.3 mm, f = 0.10 mm/rev, v_c = 200 m/min, T = 4.0 min.

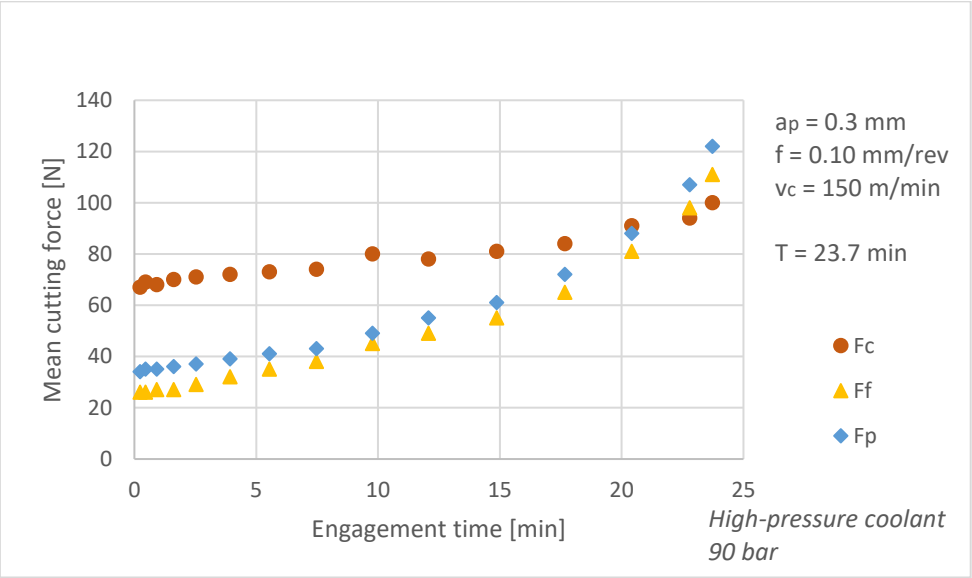

Figure 11-5. UCC 2: The mean cutting forces development during the engagement time for the cutting data and tool life: a_p = 0.3 mm, f = 0.10 mm/rev, v_c = 150 m/min, T = 23.7 min. Coolant pressure = 90 bar.

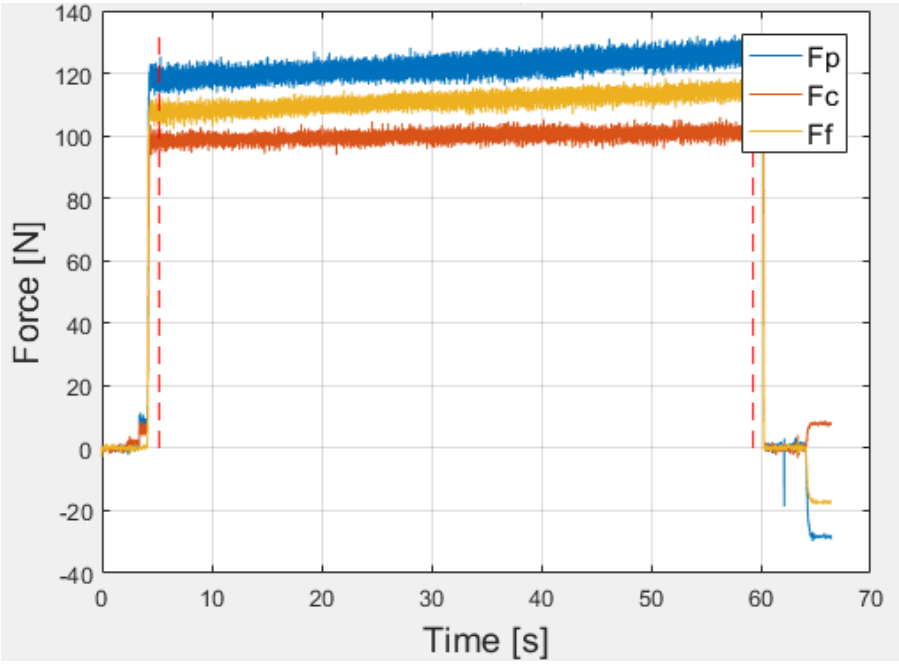

Figure 11-6. UCC 2: The last passing continuous force measurement for the cutting data and tool life: a_p = 0.3 mm, f = 0.10 mm/rev, v_c = 150 m/min, T = 23.7 min. Coolant pressure = 90 bar.

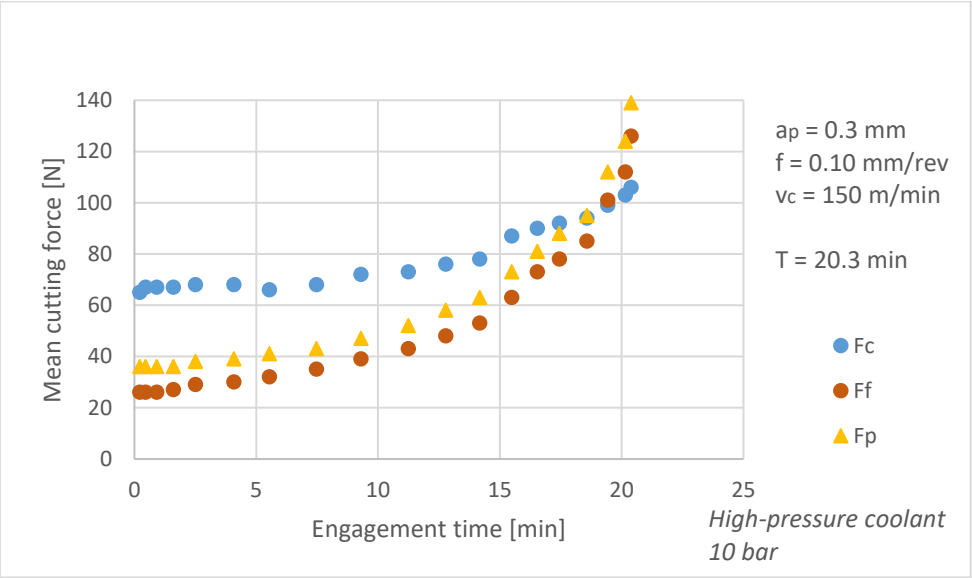

Figure 11-7. UCC 2: The mean cutting forces development during the engagement time for the cutting data and tool life: a_p = 0.3 mm, f = 0.10 mm/rev, v_c = 150 m/min, T = 20.3 min. Coolant pressure = 10 bar.

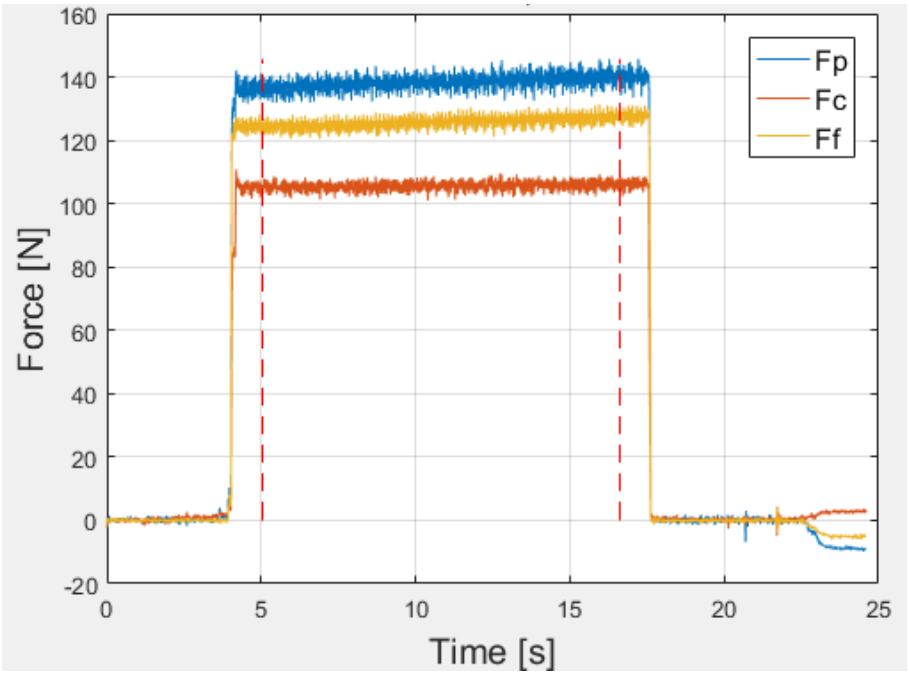

Figure 11-8. UCC 2: The last passing continuous force measurement for the cutting data and tool life: a_p = 0.3 mm, f = 0.10 mm/rev, v_c = 150 m/min, T = 20.3 min. Coolant pressure = 10 bar.

11.2 CCC 1

Figure 11-9 and Figure 11-11 presents the mean cutting forces development plotted for the engagement time.

Figure 11-10 and Figure 11-12 presents the last passing continuous force measurement plotted for the engagement time.

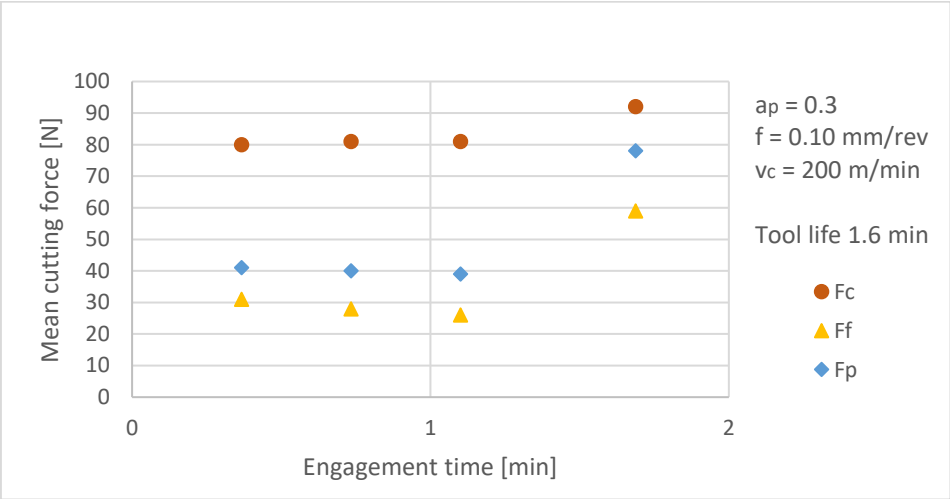

Figure 11-9. CCC 1: The mean cutting forces development during the engagement time for the cutting data and tool life: a_p = 0.3 mm, f = 0.10 mm/rev, v_c = 200 m/min, T = 1.6 min.

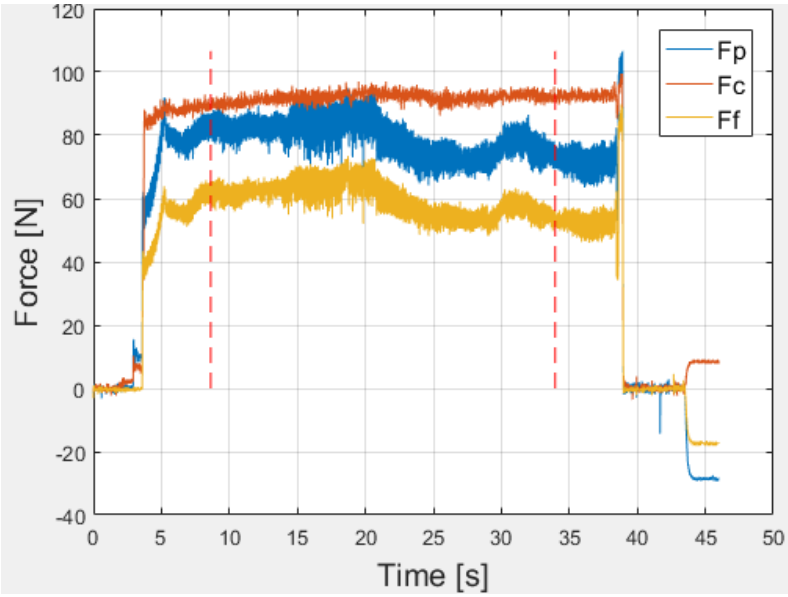

Figure 11-10. CCC 1: The last passing continuous force measurement for the cutting data and tool life: a_p = 0.3 mm, f = 0.10 mm/rev, v_c = 200 m/min, T = 1.6 min.

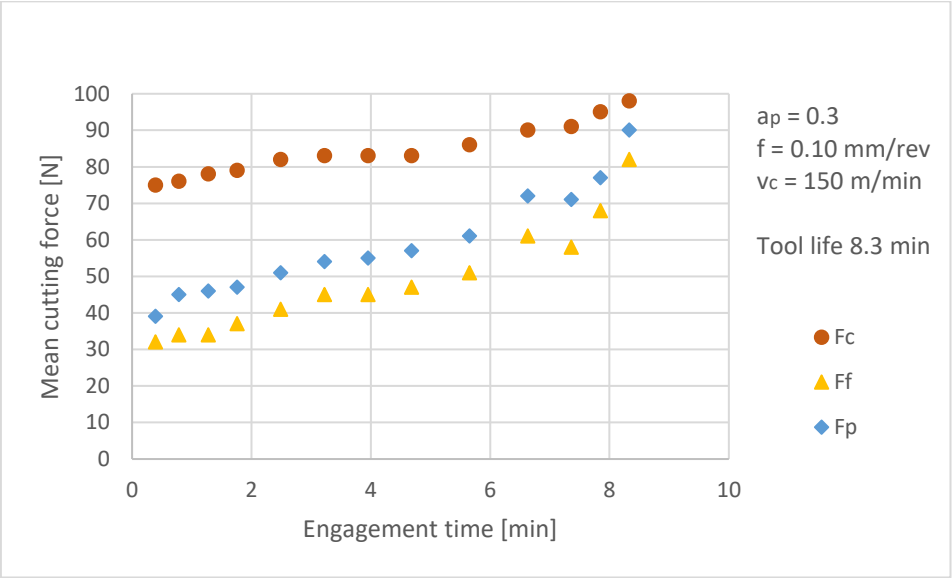

Figure 11-11. CCC 1: The mean cutting forces development during the engagement time for the cutting data and tool life: a_p = 0.3 mm, f = 0.10 mm/rev, v_c = 150 m/min, T = 8.3 min.

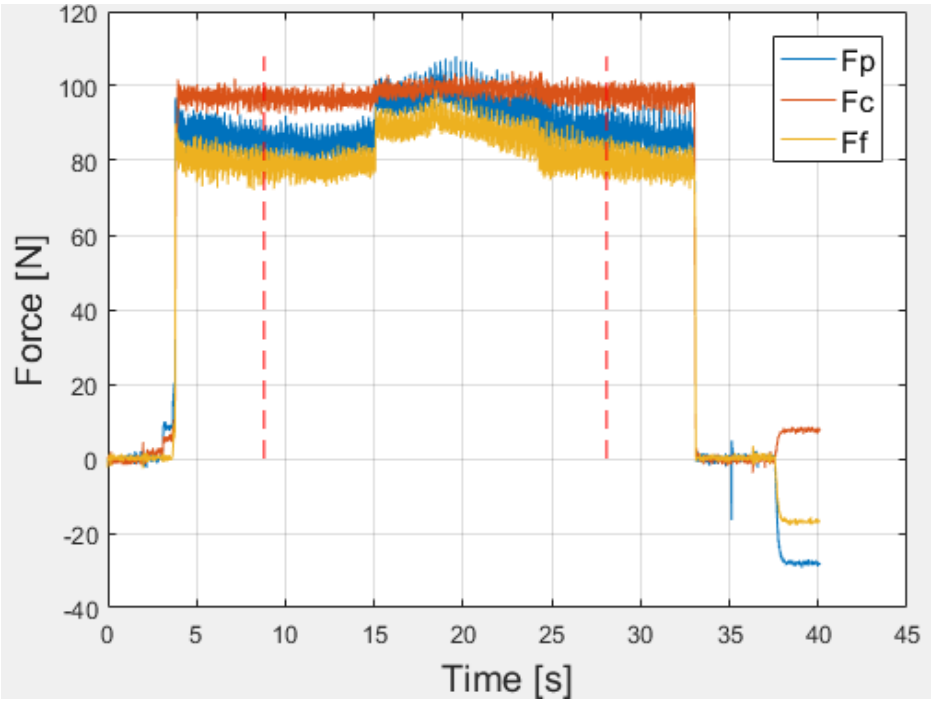

Figure 11-12. CCC 1: The last passing continuous force measurement for the cutting data and tool life: a_p = 0.3 mm, f = 0.10 mm/rev, v_c = 150 m/min, T = 8.3 min.

11.3 PCD 8

Figure 11-13 and Figure 11-15 presents the mean cutting forces development plotted for the engagement time.

Figure 11-14 and Figure 11-16 presents the last passing continuous force measurement plotted for the engagement time.

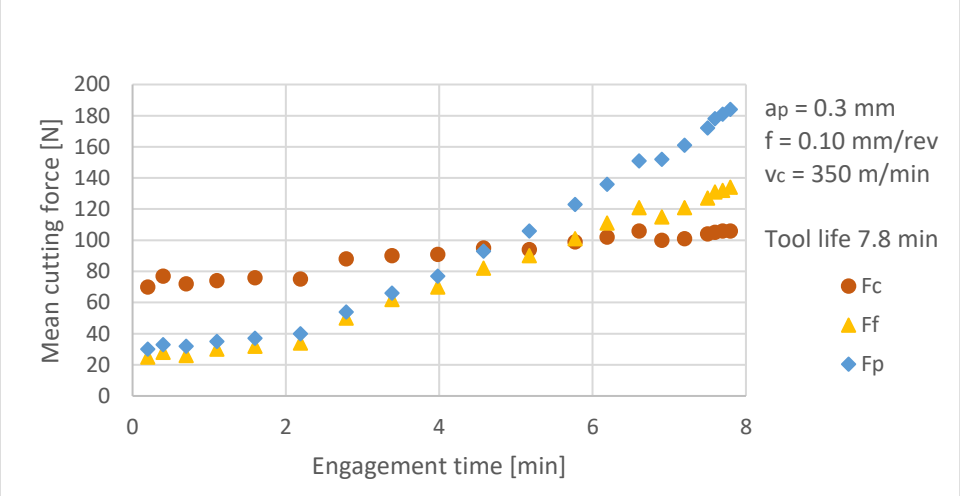

Figure 11-13. PCD 8: The mean cutting forces development during the engagement time for the cutting data and tool life: a_p = 0.3 mm, f = 0.10 mm/rev, v_c = 350 m/min, T = 7.8 min.

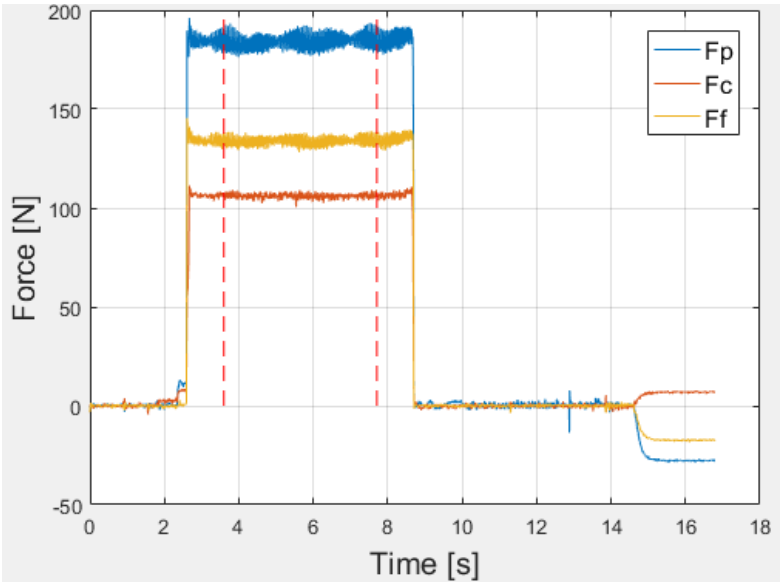

Figure 11-14. PCD 8: The last passing continuous force measurement for the cutting data and tool life: a_p = 0.3 mm, f = 0.10 mm/rev, v_c = 350 m/min, T = 7.8 min.

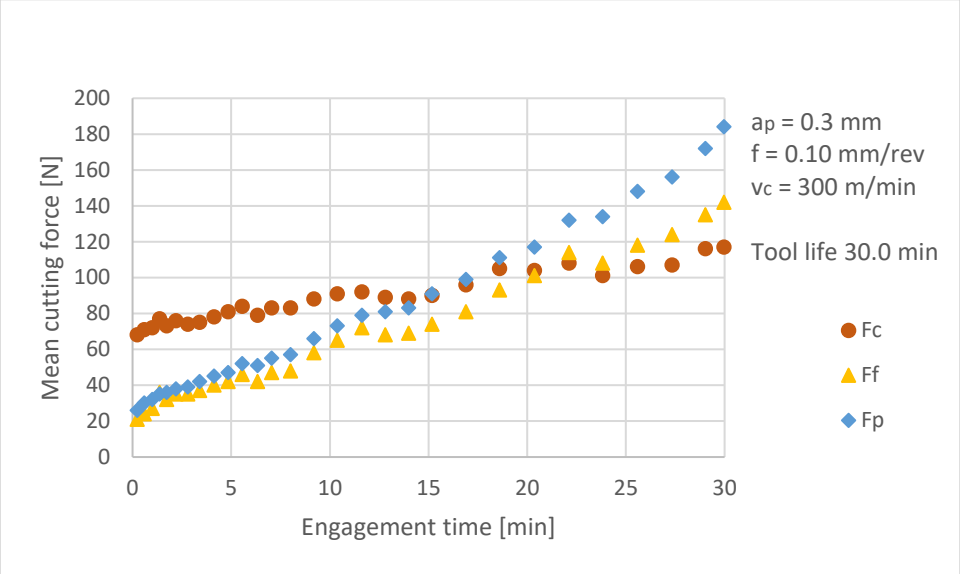

Figure 11-15. PCD 8: The mean cutting forces development during the engagement time for the cutting data and tool life: a_p = 0.3 mm, f = 0.10 mm/rev, v_c = 300 m/min, T = 30.0 min.

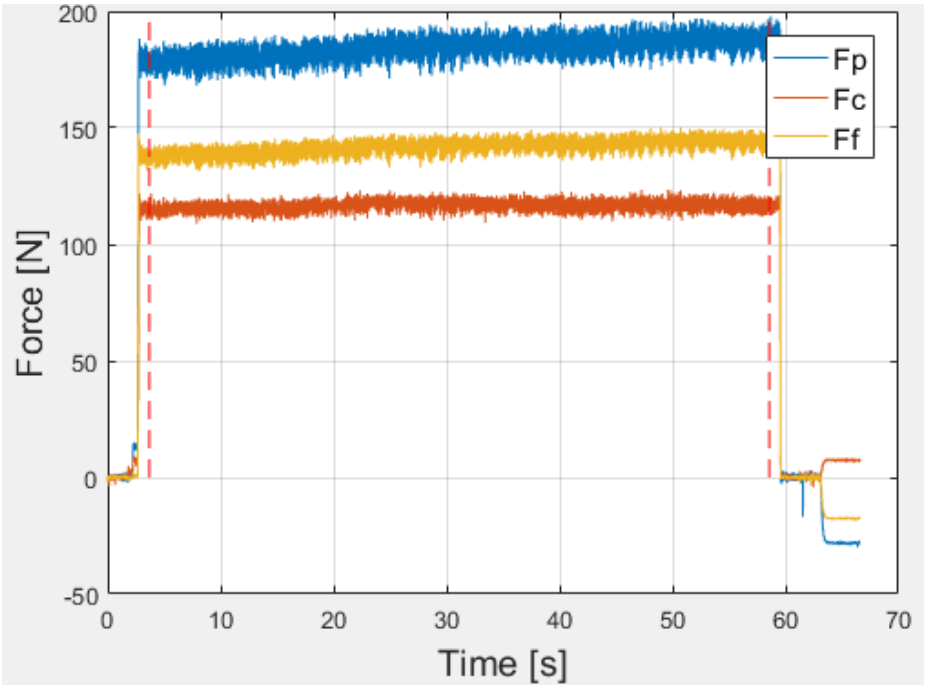

Figure 11-16. PCD 8: The last passing continuous force measurement for the cutting data and tool life: a_p = 0.3 mm, f = 0.10 mm/rev, v_c = 300 m/min, T = 30.0 min.

11.4 cBN 2

Figure 11-17 and Figure 11-19 presents the mean cutting forces development plotted for the engagement time.

Figure 11-18 and Figure 11-20 presents the last passing continuous force measurement plotted for the engagement time.

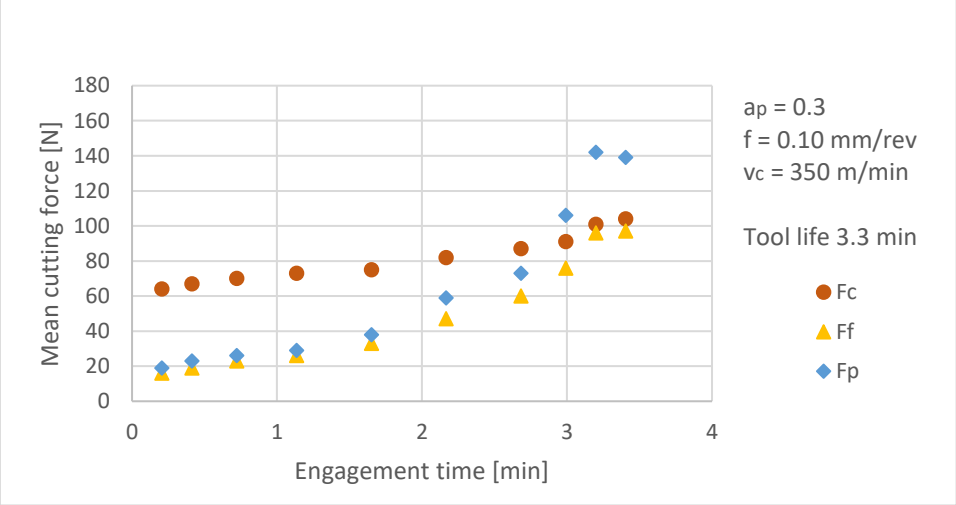

Figure 11-17. cBN 2: The mean cutting forces development during the engagement time for the cutting data and tool life: a_p = 0.3 mm, f = 0.10 mm/rev, v_c = 350 m/min, T = 3.3 min.

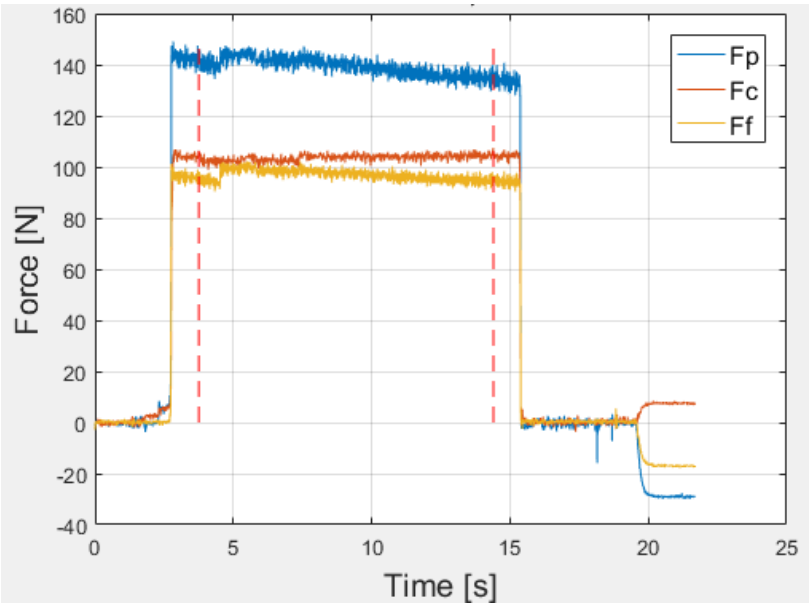

Figure 11-18. cBN 2: The last passing continuous force measurement for the cutting data and tool life: a_p = 0.3 mm, f = 0.10 mm/rev, v_c = 350 m/min, T = 3.3 min.

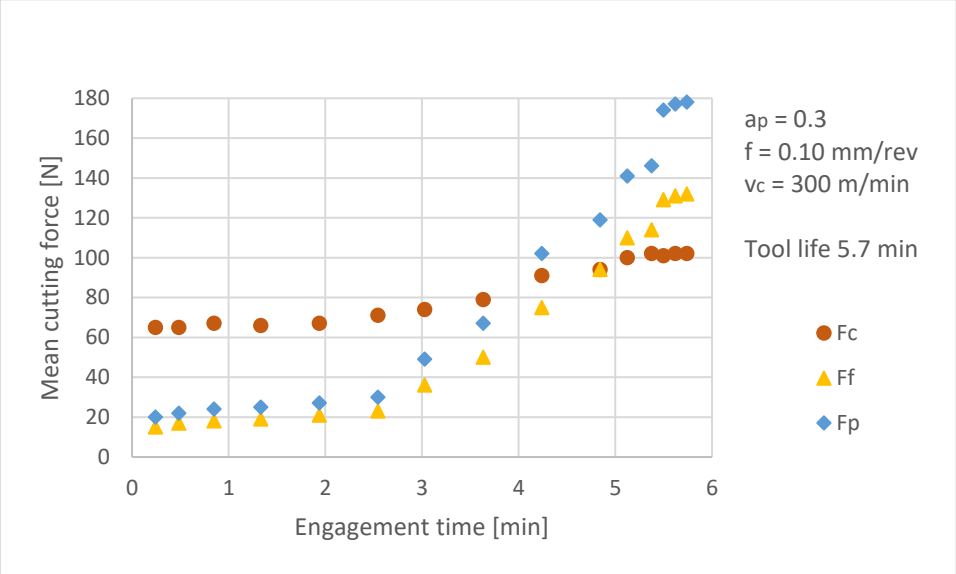

Figure 11-19. cBN 2: The mean cutting forces development during the engagement time for the cutting data and tool life: a_p = 0.3 mm, f = 0.10 mm/rev, v_c = 300 m/min, T = 5.7 min.

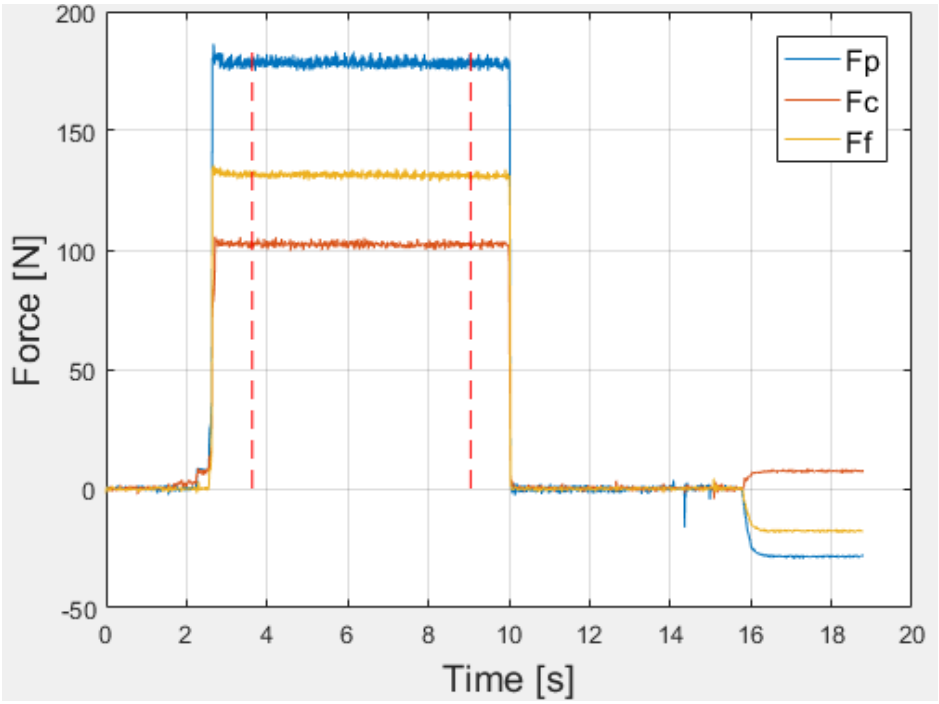

Figure 11-20. cBN 2: The last passing continuous force measurement for the cutting data and tool life: a_p = 0.3 mm, f = 0.10 mm/rev, v_c = 300 m/min, T = 5.7 min.

11.5 cBN 3

Figure 11-21, Figure 11-23 and Figure 11-25 presents the mean cutting forces development plotted for the engagement time.

Figure 11-22, Figure 11-24 and Figure 11-26 presents the last passing continuous force measurement plotted for the engagement time.

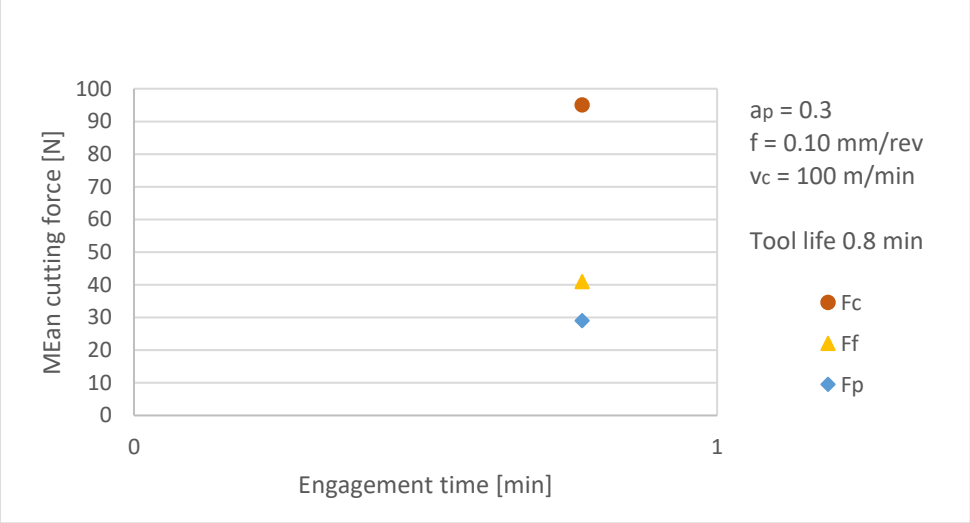

Figure 11-21. cBN 3: The mean cutting forces development during the engagement time for the cutting data and tool life: a_p = 0.3 mm, f = 0.10 mm/rev, v_c = 100 m/min, T = 0.8 min.

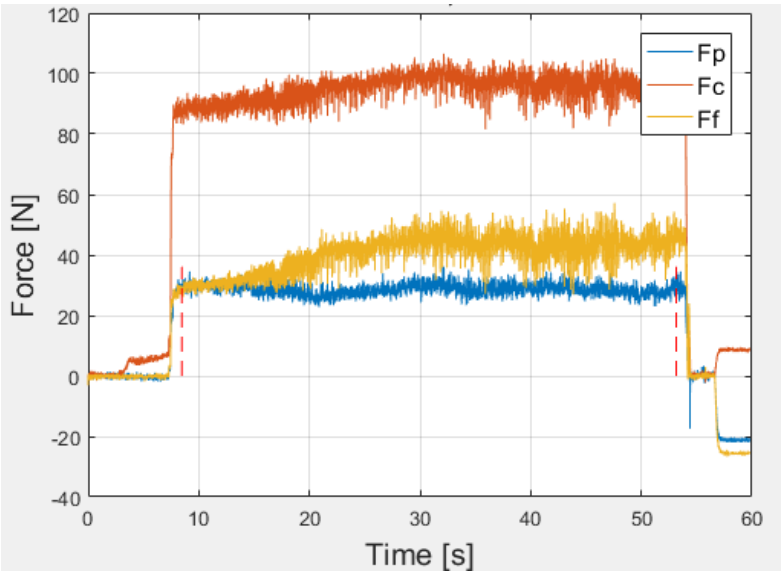

Figure 11-22. cBN 3: The last passing continuous force measurement for the cutting data and tool life: a_p = 0.3 mm, f = 0.10 mm/rev, v_c = 100 m/min, T = 0.8 min.

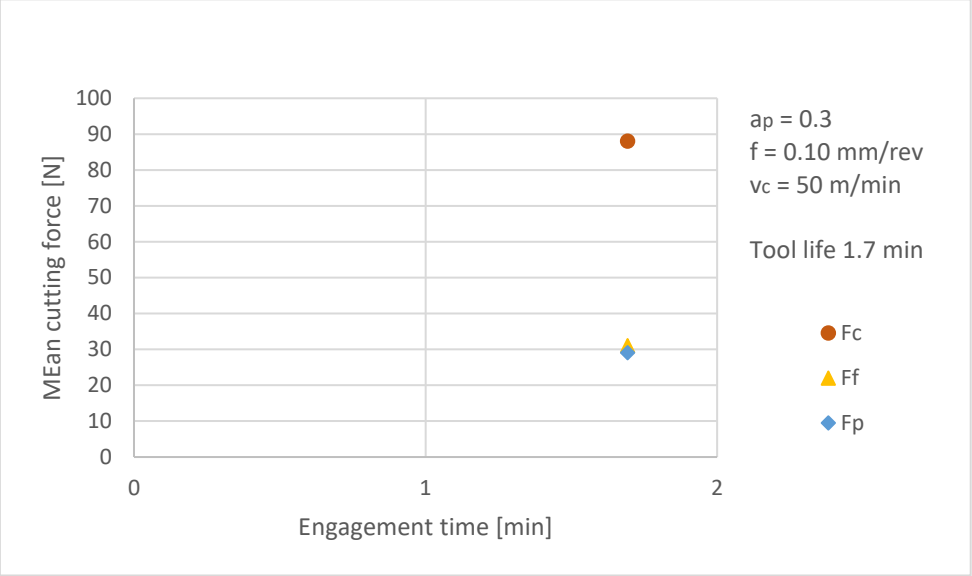

Figure 11-23. cBN 3: The mean cutting forces development during the engagement time for the cutting data and tool life: a_p = 0.3 mm, f = 0.10 mm/rev, v_c = 50 m/min, T = 1.7 min.

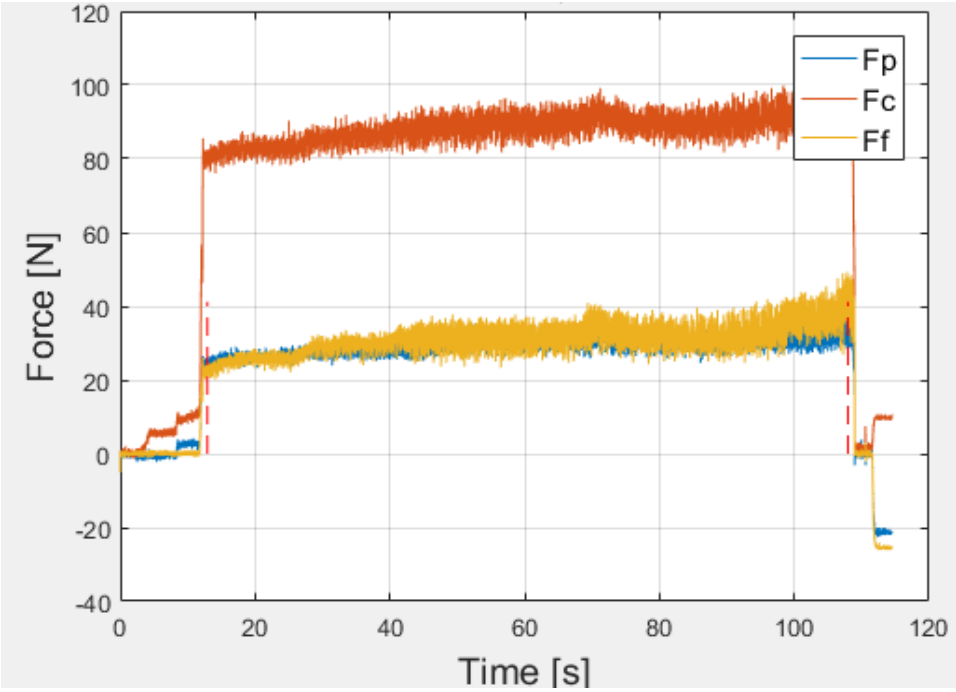

Figure 11-24. cBN 3: The last passing continuous force measurement for the cutting data and tool life: a_p = 0.3 mm, f = 0.10 mm/rev, v_c = 50 m/min, T = 1.7 min.

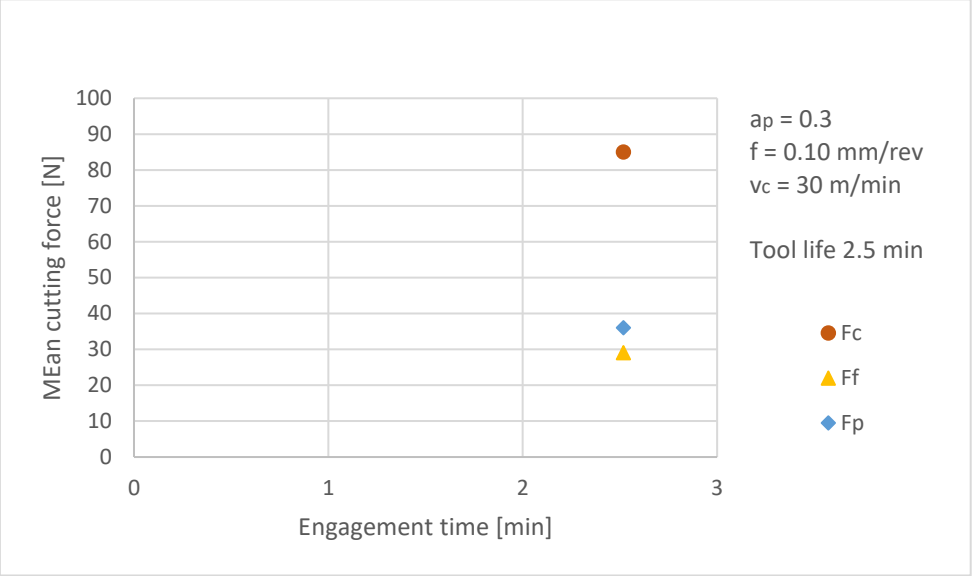

Figure 11-25. cBN 3: The mean cutting forces development during the engagement time for the cutting data and tool life: a_p = 0.3 mm, f = 0.10 mm/rev, v_c = 30 m/min, T = 2.5 min.

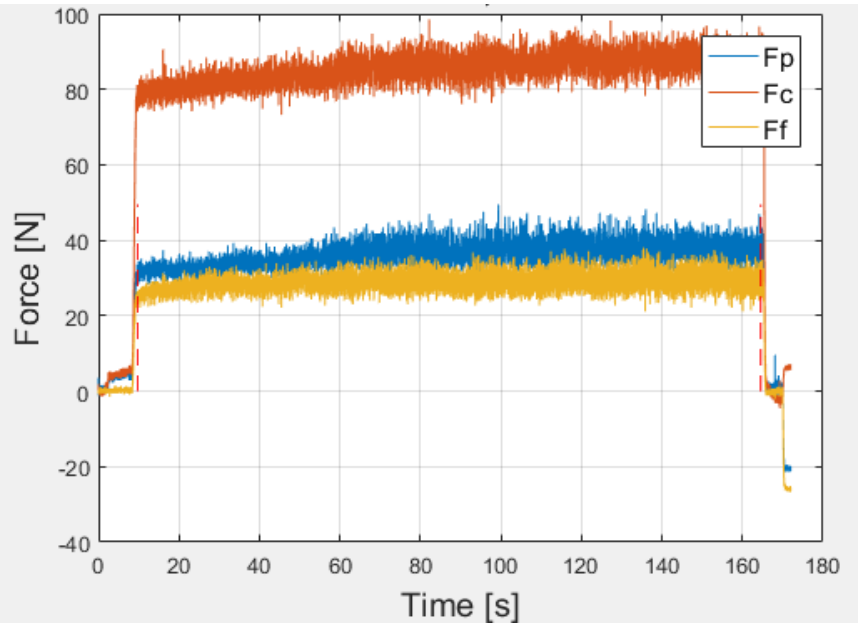

Figure 11-26. cBN 3: The last passing continuous force measurement for the cutting data and tool life: a_p = 0.3 mm, f = 0.10 mm/rev, v_c = 30 m/min, T = 2.5 min.